# IDENTIFICATION OF FRONTAL PLANE STANCE CONTROL MECHANISMS IN HUMANS

**By**

**Adam D. Goodworth**

A DISSERTATION

Presented to the Division of Biomedical Engineering within
The Department of Science & Engineering
and the Oregon Health & Science University
School of Medicine
in partial fulfillment of
the requirements for the degree of

Doctor of Philosophy
in
Biomedical Engineering

March 2010

School of Medicine

Oregon Health & Science University

---

CERTIFICATE OF APPROVAL

---

This is certify that the Ph.D. dissertation of
Adam D. Goodworth
has been approved

---

Dr. Robert J. Peterka, Dissertation Advisor
Associate Scientist

---

Dr. Fay Horak
Professor

---

Dr. Tamara Hayes,
Assistant Professor

---

Dr. Misha Pavel,
Professor

---

Dr. Deniz Erdogmus
Assistant Professor, Northeastern University

## ACKNOWLEDGMENTS

My Ph.D. program was primarily a success because of the support I received from my invested and dedicated advisor, Dr. Robert Peterka. In addition, I would like to thank Dr. Fay Horak, Dr. Tamara Hayes, and Dr. Deniz Erdogmus for serving on my committee and offering advice on this dissertation. Finally, I want to thank Dr. Misha Pavel for serving as an additional advisory member. This research was supported under the National Institutes of Health Grant AG-17960 and Grant T32DC005945.

## PREFACE

Because large portions of chapters two through five were written for separate publications in scientific journals, some repetition occurs across these chapters. The personal pronoun “we” refers to the authors of these articles and manuscripts, Adam D. Goodworth and Robert J. Peterka. Unless stated otherwise, data are from healthy control subjects. Only chapter three specifically compares healthy control subjects (abbreviated as “Cs”) and subjects with bilateral vestibular loss (abbreviated as “BVLs”).

## TABLE OF CONTENTS

## LIST OF FIGURES

## LIST OF TABLES

**ABSTRACT**

**Identification of Frontal Plane Stance Control Mechanisms in Humans**

Adam Goodworth

Doctor of Philosophy
Division of Biomedical Engineering within
The Department of Science & Engineering
and the Oregon Health & Science University
School of Medicine

March 2010
Thesis Advisor: Robert J. Peterka

The human balance control system stabilizes an inherently unstable body through torque generation around the numerous joints of the body via mechanisms that include intrinsic musculoskeletal properties and neural activation of muscles based upon reflexes and sensory integration. It is largely unknown how these mechanisms interact and contribute to balance control during sway in the frontal plane. This dissertation identifies mechanisms of frontal plane balance control using systems identification techniques including frequency-response functions, impulse-response functions, and mathematical modeling.

Chapters two and three identify frontal plane control mechanisms of the upper body (UB) while lateral sway of the lower body (LB) is prevented in healthy control and bilateral vestibular loss subjects. Continuous tilts of the pelvis and visual surround were used to evoke UB sway. Results suggest that the major contributions to UB system damping came through inter-segmental proprioceptive cues, and major contributions to UB system stiffness came through intrinsic mechanical properties and sensory integration of inter-segmental proprioceptive and pelvis-orienting proprioceptive cues. Vestibular

cues contribute to spinal stability in controls but visual cues made only minor contributions in both subject groups.

Chapters four and five identify frontal plane control mechanisms of both the UB and LB during freestanding sway in healthy control subjects using various frontal plane stance widths. Continuous rotations of a surface and visual surround were used to evoke body sway. Results showed that in narrower stance conditions, the LB and UB control system was nonlinear across stimulus amplitude in both eyes open and eyes closed conditions. This LB nonlinearity was consistent with a sensory reweighting mechanism whereby subjects shifted away from reliance on proprioceptive information and shifted toward reliance on visual/vestibular information to control their LB as stimulus amplitude increased. In contrast, the UB nonlinearity was primarily due to a decrease in stiffness contributions from all sensory systems as stimulus amplitude increased. In wider stances, intrinsic stiffness of the LB increased and active control of the LB became more linear (i.e., sensory and mechanical contributions to LB control remained relatively fixed across stimulus amplitude).

# BACKGROUND

*Introduction*

All bipedal activities require a balance control system to counteract destabilizing gravitational forces. Most people have little problem standing upright and do so with little or no cognitive awareness of the stabilizing task. This ease, however, masks the inherent complexities of human bipedal stance. These complexities arise from both the physics of upright stance and the mechanisms available to humans for maintaining balance control.

The physics of human bipedal stance involve controlling an inherently unstable body. A small deviation from a perfect upright position results in gravitational forces that further accelerate the body away from the upright position. In addition, interaction torques arise when one body segment moves relative to another (Fig. 1.1A). A simple solution to this problem could conceivably come from the intrinsic mechanical properties of the musculoskeletal system (Fig. 1.1B). The intrinsic mechanical properties of muscles, tendons, and ligaments generate force with no time delay in proportion to stretch (muscle/tendon/ligament stiffness) and in proportion to the velocity of stretch (muscle/tendon/ligament damping). Thus, intrinsic mechanical properties resist body segment motion and if stiffness and damping were large enough, then gravitational forces could be counteracted without any muscle activations. However, previous estimates of intrinsic ankle joint stiffness indicate that intrinsic mechanisms alone are insufficient to stabilize the body (Loram and Lakie 2002; Casadio et al. 2005; Qu and Nussbaum 2009; Peterka 2002). Therefore, additional control is required via neural activation of muscles.

Control mechanisms based on intrinsic mechanical properties and neural activation of muscles can be distinguished in terms of function and time delay. With respect to time delays, intrinsic mechanisms generate torque with no time delay but neural activation of muscles is based on sensorimotor transformations and contains

inherent time delays. Time is required to process sensory information, transmit signals through axons, synapses, and neuromuscular junctions, and generate muscle contractions. Muscle activations in balance control are based on reflexes and the integration of sensory information (Nashner 1977). For example, a transient backward surface translation results in instantaneous torque generation from intrinsic stiffness and damping of the muscle-tendon complex that spans the ankle joints and time-delayed torque generation from stretch reflexes and sensory integration responses, all of which orients the body upright in space (Fig. 1.2.A).

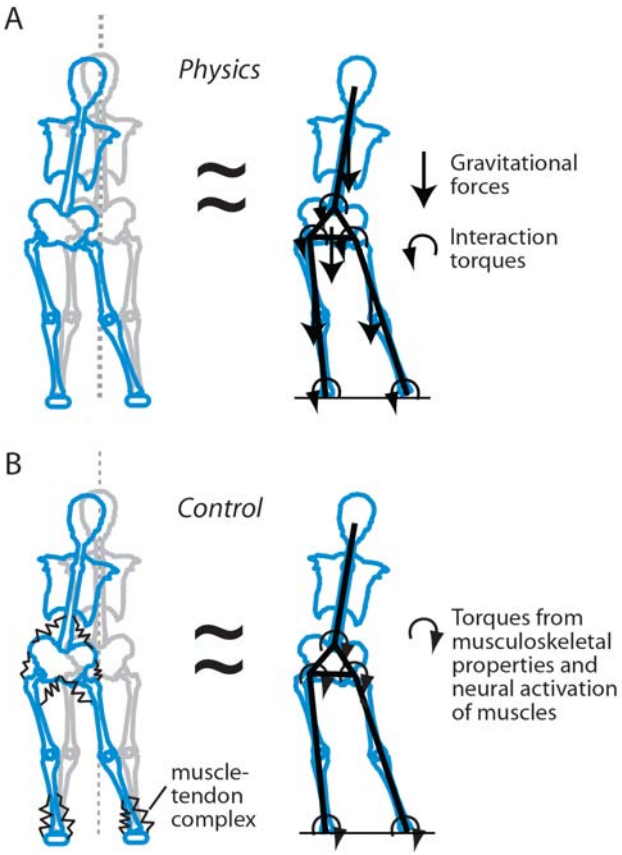


**Fig. 1.1.** *Schematic of bipedal stance. A) Physics of frontal plane stance includes vertical gravitational forces and interaction torques that arise when one body segment moves relative to another. B) Control of body segments come from intrinsic mechanical properties in the musculoskeletal system and from neural activation of muscles.*

Control mechanisms are also distinguished based on function. Intrinsic mechanisms and stretch reflexes resist muscle stretch and stretch velocity whereas muscle activation based on sensory integration can be more functionally appropriate to the balancing task. For example, a transient toe-up surface rotation results in similar torque generation about the ankle joint from intrinsic stiffness/damping and stretch reflexes compared to the backward surface translation because the toe-up surface rotation

results in similar muscle-tendon stretch as the backward surface translation. This torque orients the body toward the surface and away from upright. However, the sensory integration response is in the muscle on the opposite side of the ankle joint so that the sensory integration response orients the body more upright in space.

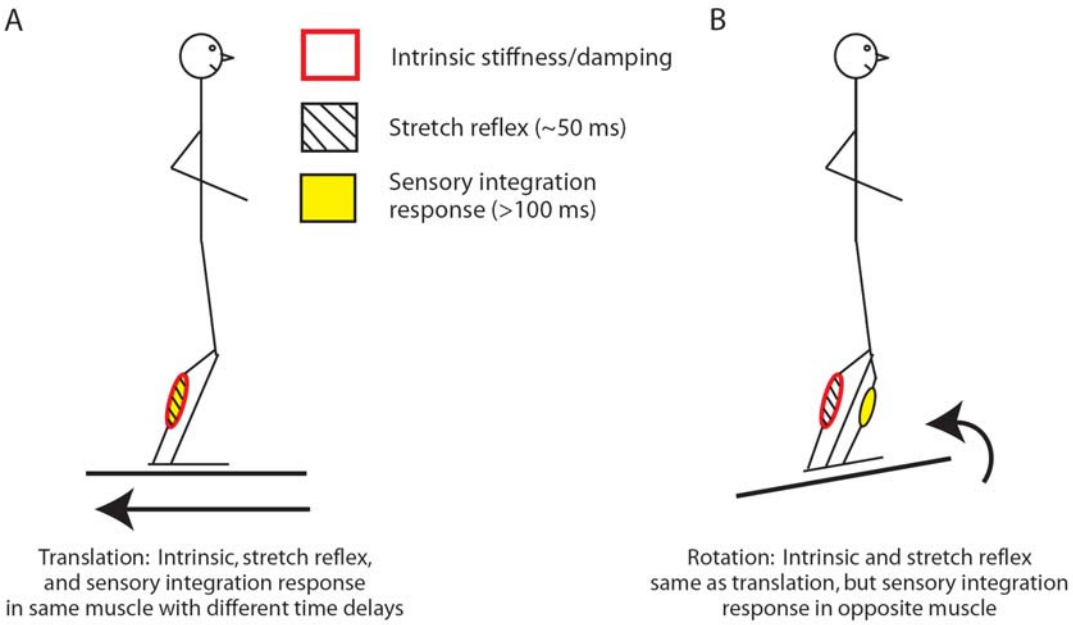


**Fig. 1.2.** *Distinguishing control mechanisms based on A) time delay and B) time delay and function. Figure modified from Nashner 1977.*

The sensory systems that contribute to balance control include vision, proprioception, and vestibular. It is widely accepted that these sensory systems contribute to balance control because stimulation of visual (Berthoz et al. 1979; Bronstein 1986; Kiemel et al. 2008; Lee and Lishman 1975; Oie et al. 2002; Peterka 2002), proprioceptive (Allum 1983; Jeka et al. 1998; Johansson et al. 1988; Oie et al. 2002) and vestibular (Day et al. 1997; Nashner and Wolfson 1974) systems evoke body sway. The challenge for researchers is to understand how information from these sensory systems is processed and integrated (Mergner et al. 1997) to generate appropriate muscle activations that are combined with intrinsic mechanisms to produce torques across body segments. The incentive for researchers to better understand balance control is to decrease the morbidity and mortality associated with falls (Horak 2006). Better knowledge of balance control

mechanisms will lead to enhanced therapeutic strategies for people with motor coordination deficits and sensory deficits (Horak et al. 1997) and will aid the design and implementation of neuroprostheses (Crago 2000; Goodworth et al. 2009, Kim et al. 2006).

*Experimental methods and principles of balance control*

Balance control has been investigated using a number of experimental techniques. At one end of the spectrum, are numerous studies investigating "quiet stance" where subjects simply stand in place (with no external perturbation) while spontaneous motion of body segments and ground reaction forces are measured. The advantage of quiet stance tests is that relatively little equipment is needed and the experimental protocol is simple. In addition, if underlying control mechanisms can be deduced from quiet stance tests, then these tests may be useful as a diagnostic tool to predict the likelihood falling (Piirtola and Era 2006; Maki et al. 1990). At the other end of the spectrum are studies investigating conditions which potentially cause humans to fall. These test conditions evoke a "change in base of support" response where subjects must step or reach and grab onto an object to maintain stability in response to a large external perturbation (Maki et al. 2003; Pai et al. 2000). These studies have identified some factors contributing to the change in support response and are a critical first step in understanding everyday falls. However, our current understanding of balance control is not yet at the level where these complex and individualized stepping and reaching responses can be incorporated into a predictive sensorimotor integration model.

In-between quiet stance (no external perturbations) and change of support tests (large external perturbations) are fixed base of support tests with moderate external perturbations that do not evoke stepping or reaching responses. Examples of external perturbations include vibration of muscles (Lackner and Levine 1979; Roll et al. 1989), galvanic vestibular stimulation (Day et al. 1997; Nashner and Wolfson 1974), external forces applied to the body (Maurer et al. 2006), tactile stimulation (Jeka et al. 1998; Oie et al. 2002), visual surround motion (Berthoz et al. 1979; Bronstein 1986; Kiemel et al. 2008; Lee and Lishman 1975; Oie et al. 2002; Peterka 2002), and surface motion (Gurfinkel 1995; Nashner 1977; Horak and Nashner 1986; Peterka 2002). These external perturbations enable researchers to characterize stimulus-response behavior over a wide

range of conditions and to compare between normal and patient populations (Horak et al. 1990; Horak et al. 1996; Kim et al. 2009; Kung et al. 2009).

Many investigators have used short-duration transient external perturbations to study balance control. In these studies, it is common for time domain measures, such as electromyograms of muscles involved in the corrective response, position and velocity of body motion, or ground reaction forces, to be the output variables under investigation. One important principle that has emerged from sudden perturbation studies is the use of "ankle" and "hip" strategies (Horak and Nashner 1986). In the ankle strategy, corrective torque is generated about the ankle to move the lower body while the upper body orients toward the lower body resulting in body motion that resembles a single link. The ankle strategy is associated with relatively small perturbations. In the hip strategy, corrective torque is first generated about the hip and the upper and lower body segments move counter-phase with each other. This strategy is associated with situations where rapid corrections are necessary (Kuo 1995), such as when subjects maintain a very narrow base of support (Horak and Nashner 1986).

Although it is convenient to describe the hip strategy separate from the ankle strategy, in fact both are present simultaneously during quiet stance (Creath et al. 2005; Horlings et al. 2009; Zhang et al. 2007) and when subjects respond to external surface (Alexandrov et al. 2005; Creath et al. 2008) or visual (Kiemel et al. 2008) perturbations. That is, at low frequencies (below ~1 Hz), the upper and lower body are nearly aligned and "in-phase" resembling the ankle strategy; however, at frequencies above about ~1 Hz, the upper and lower body move in opposite directions and exhibit an "out-of-phase" hip strategy. Although there is evidence this co-existing in-phase/out-of-phase behavior is a result of musculoskeletal system dynamics (Kiemel et al. 2008), there are still many unanswered questions surrounding this phase behavior.

Long-duration continuous perturbations have also been used to study balance control. After a transient period, balance responses to continuous perturbations can be considered steady-state. Steady-state balance responses are determined by the postural "set" (Prochazka 1989) adopted by the subjects' nervous system in order to optimally compensate for the perturbation. Thus, with continuous perturbations, the postural set is typically considered constant throughout the steady-state response period and the set can be altered to accommodate the external stimulus (such as stimulus amplitude or stimulus

type). In contrast, with sudden perturbations, the postural set is considered to be altered by initial conditions such as prior expectation (Nashner 1976; Horak and Nashner 1986) or biomechanics (Horak and Nashner 1986; Kuo 1995; Park 2002) and it remains unknown whether the stimulus itself triggers a preprogrammed response or if the transient stimulus-response is under continuous feedback control (Kuo 1995; Park et al. 2004).

One important finding from continuous perturbation studies is that subjects exhibit nonlinear stimulus-response behavior whereby the influence of larger amplitude perturbations are reduced. This reduction in responsiveness to large perturbations has been attributed to a sensory reweighting phenomenon whereby subjects shift away from reliance on sensory systems that tend to orient the body toward the stimuli and shift toward reliance on sensory systems that tend to orient the body toward upright. The sensory reweighting phenomenon has been demonstrated for continuous visual tilt (Peterka 2002), surface tilt (Peterka 2002; Maurer et al. 2006), and external force (Maurer et al. 2006) perturbations that evoke sagittal plane sway, and for surface tilt (Cenciarini and Peterka 2006), visual translation (Oie et al. 2002), and tactile (Oie et al. 2002) perturbations that evoke frontal plane sway.

Without sensory reweighting, upright stance would be severely compromised. For example, when eyes-closed healthy subjects respond to low amplitude sagittal plane surface tilts, they rely heavily on proprioceptive cues that orient their body toward the surface; however, as surface tilts increase, healthy subjects become less responsive to the surface tilt stimuli by shifting away from reliance on proprioceptive cues and toward reliance on vestibular cues. By comparison, eyes-closed subjects with a bilateral vestibular loss cannot shift toward reliance on vestibular cues and when surface tilt amplitude increases, these subjects' exhibit instability and falls (Peterka 2002).

*Mathematical modeling*

Many balance control studies have utilized mathematical model-based interpretations of experimental results. Mathematical models represent a quantitative hypothesis about how the physiological system is organized and these models can be used to generate falsifiable hypotheses (Platt 1964). However, trade-offs must be made between physiologically accurate and mathematically tractable models. In balance

control, modeling primarily involves two components: physics of motion and neural control. In the modeling literature, a general trade-off is found where simple physical models (Fig. 1.3A) include complex representations of neural control while complex physical models (Fig. 1.3B and C) tend to include more simplistic representations of neural control.

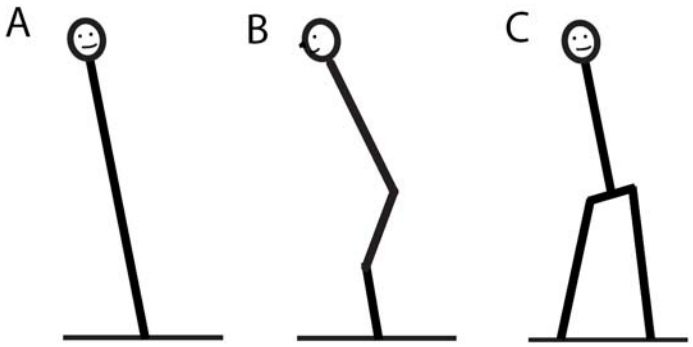


**Fig. 1.3.** *Schematic of commonly used physical representations of the body in balance control studies include A) single-link, B) open-chain multi-link, and C) closed-chain lower body multi-link models.*

A commonly used simple physical model represents the body as a single-link inverted-pendulum (Ishida and Imai 1980; Johansson et al. 1988; van der Kooij et al. 2001; Welch and Ting 2008; Qu and Nussbaum 2009; Peterka 2002; Oie et al. 2002). These models have included representations of sensory systems, time delays, passive mechanisms, sensory noise, and optimal control. Many of these models have described the phenomena of sensory reweighting through systematic changes in model parameters that represent the contributions of sensory systems to balance control (Allison et al. 2006; Cenciarini and Peterka 2006; Peterka 2002; Maurer et al. 2006; Oie et al. 2002; van der Kooij et al. 2001).

One example of a single-link model that has been used to describe sensory reweighting is shown in Fig. 1.4 (modified from Peterka 2002). In this model, foot-in-space (*FS*) is equal to support surface (*SS*) rotations. Internal estimates of body-in-space sway (*BS*) are obtained with vestibular and visual information (assuming a stationary visual field) and reliance on this vestibular and visual information is represented by the "weight" $W_V$. Internal estimates of *BS* relative to *FS* are obtained with proprioceptive information and reliance on this proprioceptive information is represented by $W_P$. The weighted sum of orientation estimates from all sensory systems is the input to the neural controller which generates time-delayed torque ($T_C$) in proportion ($K_P$) to and in

proportion to the derivative ($K_D$) of the weighted sum of sensory inputs. This model showed that $W_P$ monotonically decreases and $W_V$ monotonically increases as *FS* increases in amplitude; indicating that subjects shift away from reliance on proprioceptive information and shift toward reliance on vestibular and/or visual information as *FS* increases in amplitude.

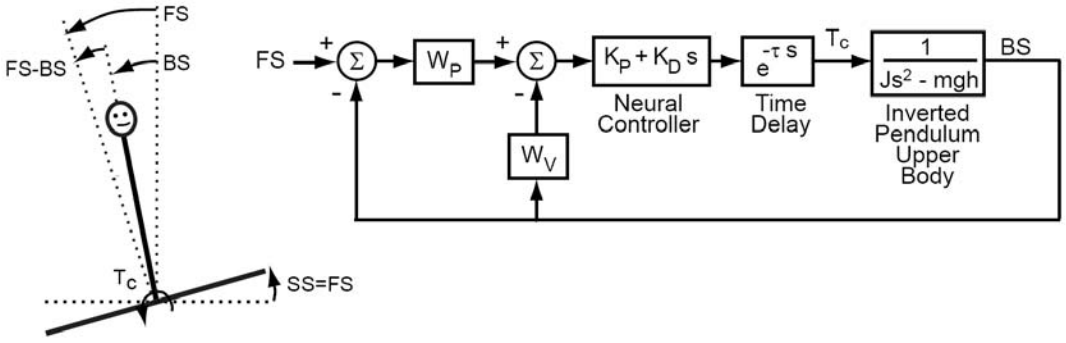


**Fig. 1.4.** *Diagram of a simple sensorimotor control model for balance control. Reliance on proprioceptive and visual/vestibular information is represented as $W_P$ and $W_V$, respectively, and s is the Laplace variable. Figure modified from Peterka 2002.*

More complex physical models have been developed that represent the body as a multi-linkage system connected in series as an open-chain (Fig. 1.3B) (Alexandrov et al. 2005; Barin 1989; Johansson and Magnusson 1991; Kuo 1995; Koozekanani 1983; Park et al. 2004; van der Kooij et al. 1999). Control of the multi-link system is typically based on feedback from state-space representations of body dynamics. Results from these multi-link studies indicate that feedback from segments across the entire body contribute to torque generation at each joint (Alexandrov et al. 2005; Barin 1989, Kuo 1995; Park et al. 2004; van der Kooij et al. 1999). Furthermore, results indicate the gain between segment kinematics and torque generation changes with stimulus amplitude and biomechanical constraints (Kuo 1995; Park 2002; Park et al. 2004). Because of the complexity surrounding multi-link physical models, only a few studies have investigated the effects of time delays (Alexandrov et al. 2005; Kuo 1995; van der Kooij et al. 1999), only one study has attempted to represent particular sensory systems (van der Kooij et al. 1999), and no studies of whole body multi-link balance control have attempted to

represent the combined effects of intrinsic and active (time-delayed) control mechanisms in a mathematical model.

Despite the presence of nonlinear neural and mechanical systems involved in balance, most models used a linear, time-invariant control system to account for experimental sway patterns at each particular test condition. Linear control models provide a linear approximation to nonlinear system behavior (Pintelon and Schoukens 2001) and the ability of these models to account for experimental data can be attributed in part to the large influence of body dynamics, which behave approximately linearly about the operating point of upright standing (Park et al. 2004; Kuo and Zajac 1993).

In addition to mathematical models, humanoid robots can also exemplify a type of model. Humanoid robots have been constructed to maintain bipedal stance and these robots have the potential to provide additional insights into mechanisms of balance control (Kajita et al. 2001; Mahboobin et al. 2008; Mergner et al. 2006; Scrivens et al. 2008). One particularly relevant robot to the current dissertation was developed by Scrivens et al. 2008. This robot mimicked frontal plane cat responses to transient surface translations with a control system that included both intrinsic and active mechanisms. This robot demonstrated that changes in stance width must be coordinated with changes in control mechanisms to maintain a stable system.

*Motivation behind the dissertation*

It is critical to maintain balance control in all planes of motion. However, sway in the sagittal plane has received much more attention than sway in the frontal plane. One reason frontal plane sway has received less attention than sagittal plane sway is because body segments moving in the sagittal plane can be modeled as an open-chain (Fig. 1.3B) whereas this model is rarely justified in the frontal plane. In the frontal plane, the lower body forms a closed-chain (Fig. 1.3C). The equations of motion describing this closed-chain differ from those used to describe open-chain sagittal plane sway. Furthermore, because lower body biomechanics are dependent on frontal plane stance width, mechanisms of frontal plane balance control are potentially dependent upon frontal plane stance width. The extent to which mechanisms of sagittal plane balance control are applicable to frontal plane control are largely unknown.

For example, the frontal plane studies that demonstrated a similar sensory reweighting mechanism to sagittal plane were only performed in narrow stance conditions (Oie et al. 2002 and Cenciarini and Peterka 2006). In both studies, interpretation was based on center-of-mass results; but a more complete understanding of sensory reweighting could be found if control mechanisms underlying multi-link control were known and characterized over changes in frontal plane stance width. In addition, simultaneous in-phase and out-of-phase upper and lower body sway behavior has only been described in the frontal plane for quiet stance where subjects maintained a narrow stance (Horlings 2009; Zhang 2007). Characterizing this phase behavior over a range of perturbations and stance widths would provide insight into the origin of this potentially important feature of balance control. Finally, there are no mathematical models of frontal plane balance control where the lower body closed-chain dynamics are represented or where contributions of sensory systems to balance control are represented.

The overall goal of this dissertation is to fill the gap in our understanding of frontal plane balance control by identifying mechanisms of control used during sway in the frontal plane. Experiments consisted of continuous external perturbations used to evoke steady-state sway responses. Continuous perturbations contained wide bandwidth stimuli so that engineering-based system identification methods could characterize system dynamics over a range of frequencies. Non-parametric system identification was based on measured experimental stimulus-response relationships expressed as frequency-response functions and impulse-response functions. Parametric system identification was based on experimentally-validated mathematical models. Both single-link and multi-link models were developed for this dissertation.

Chapters two and three of this dissertation focus on the identification of control mechanisms underlying frontal plane upper body orientation relative to the pelvis, which is synonymous with frontal plane spinal stability. In order to eliminate the complexity of interaction torques associated with motion of a multi-segment body (Zajac and Gordon 1989), previous spinal stabilization studies have found it useful to investigate upper body control in simplified conditions where various transient short-duration perturbations were applied to the upper body while the lower limbs and pelvis were held in a fixed position. Responses to these perturbations have been analyzed assuming that rapid-acting stretch reflexes and/or intrinsic biomechanical mechanisms are the primary contributors to upper

body control (Brown and McGill 2009; Cholewicki et al. 1999; Cholewicki et al. 2000b; Granata et al. 2004; Moorhouse and Granata 2007). However, it is generally recognized that sensory integration also plays a role in upper body control (Ebenbichler et al. 2001). Qualitative evidence for a sensory integration contribution includes vision-dependent changes in behavior (Radebold et al. 2001; Reeves et al. 2006) and upper body sway in seated subjects evoked by galvanic vestibular stimulation (Ali et al. 2003; Day et al. 1997). Therefore, in chapters two and three, a quantitative assessment of the contributions of intrinsic biomechanical, reflex, and sensory integration mechanisms to spinal stability is provided through an experimentally-validated mathematical model.

Chapters four and five of this dissertation identify control mechanisms underlying frontal plane balance control in freestanding conditions as a function of stance width. A few studies have investigated the role of stance width in the frontal plane. Increasing stance width has been shown to be associated with reductions in frontal plane spontaneous body sway (Day et al. 1993; Kirby et al. 1987), reductions in responses to galvanic stimulation of the vestibular nerve (Day et al. 1997; Welgampola 2001), and reductions in center of pressure motion, trunk motion, and muscle activation levels during transient surface translations (Henry et al. 2001). Although these reductions in balance related measures seem to be consistent across previous studies, the underlying cause of these reductions is unclear because the complex interaction between stance width in the frontal plane and neural control strategies for balance is still poorly understood. Stance width in the frontal plane plays an important role by directly affecting the allowable range over which the center-of-mass can move (Horak and Macpherson 1996), by changing the mechanics of the LB, and by modifying the proprioceptive sensory information available for balance control. In addition, stance width alters the intrinsic mechanical properties of the LB by changing the length of muscle/tendons spanning the hip joints and by altering the stretch of muscle/tendons per unit displacement of the LB (Scrivens et al. 2008; Day et al. 1993). Finally, changes in stance width dramatically affect the relationship between LB sway and the pelvis orientation in space. Therefore, in chapters four and five, the influence of stance width on system linearity and coordination of lower and upper body sway are characterized. Further insights are provided with a proposed multi-link model of frontal plane balance control that includes representations of time-delayed feedback from sensory systems along with intrinsic mechanisms.

# CHAPTER II.
# CONTRIBUTION OF SENSORIMOTOR INTEGRATION TO SPINAL STABILITY


## ABSTRACT

The control of upper body (UB) orientation relative to the pelvis in the frontal plane was characterized by analyzing responses to external perturbations consisting of continuous pelvis tilts (eyes open and eyes closed) and visual surround tilts (eyes open) at various amplitudes. Lateral sway of the lower body was prevented on all tests. UB sway was analyzed by calculating impulse-response functions (IRFs) and frequency-response functions (FRFs) from 0.023 to 10.3 Hz for pelvis tilt tests and FRFs from 0.43 to 1.5 Hz for visual tests. For pelvis tilt tests, differences between FRFs were limited to frequencies below 3 Hz and were dependent on stimulus amplitude. IRFs were nearly identical across all pelvis tilt tests for the first 0.2 s, but showed amplitude-dependent changes in their time course at longer time lags. The availability of visual orientation cues (eyes open compared to eyes closed) had only a small effect on the UB sway during pelvis tilt tests. This small effect of vision was consistent with the small UB sway evoked on visual tilt tests. Experimental results were interpreted using a feedback model of UB orientation control that included time-delayed sensory integration, short-latency reflexive mechanisms, and intrinsic biomechanical properties of the UB. Variation in model parameters indicated that subjects shifted toward reliance on sensory cues that oriented the UB toward upright and away from sensory cues that oriented the UB toward the stimulus (pelvis tilt or visual surround tilt) as stimulus amplitudes increased.



Goodworth AD and Peterka RJ. Contribution of sensorimotor integration to spinal stabilization in humans. *J Neurophysiol* 102: 496-512, 2009, used with permission.

## INTRODUCTION

Bipedal human stance is inherently unstable because any small deviation in the body from a perfect upright position results in the generation of a torque due to gravity that further accelerates the body away from upright. Most studies have focused on understanding the mechanisms contributing to the generation of corrective torques in order to maintain the whole body's center-of-mass position over the base of support (i.e., the feet) (Ishida and Imai 1980; Johansson et al. 1988; van der Kooij et al. 2001; Welch and Ting 2008). The physical problem of controlling an inherently unstable mass relative to a support base also applies to the stabilization of the upper body (UB) segment relative to the lower body. For sway in the frontal plane, the UB segment consists of the body mass above the pelvis. Rotational motion of the UB segment relative to the pelvis is often considered to occur primarily about the L4/L5 spinal joint (Brown and McGill 2009; Cholewicki et al. 2000b; McGill et al. 1994). Therefore, the investigation of the control of UB orientation relative to the pelvis is related to the general topic of spinal stabilization.

In order to eliminate the complexity of interaction torques associated with motions of a multi-segment body (Zajac and Gordon 1989), previous spinal stabilization studies have found it useful to investigate UB control in simplified conditions where various transient perturbations were applied to the UB while the lower limbs and pelvis were held in a fixed position. Responses to these perturbations have been analyzed assuming that rapid-acting stretch reflexes and/or intrinsic biomechanical mechanisms are the primary contributors to UB control (Brown and McGill 2009; Cholewicki et al. 1999; Cholewicki et al. 2000b; Granata et al. 2004; Moorhouse and Granata 2007). Biomechanical mechanisms include passive or intrinsic stiffness and damping from joints, spinal ligaments, and muscles/tendons (Brown and McGill 2009; Cholewicki et al. 2000b; Granata et al. 2004; McGill et al. 1994; Moorhouse and Granata 2007) and influences of intra-abdominal pressure (Cholewicki et al. 1999; Cresswell et al. 1994; McGill et al. 1994). Rapid-acting stretch reflexes have been shown to contribute to spinal stability in several studies (Granata et al. 2004; Skotte 2001; Solomonow et al. 1998).

However, it is generally recognized that sensory integration also plays a role in UB control (Ebenbichler et al. 2001). Qualitative evidence for a sensory integration

contribution includes vision-dependent changes in behavior (Radebold et al. 2001; Reeves et al. 2006) and UB sway in seated subjects evoked by galvanic vestibular stimulation (Ali et al. 2003; Day et al. 1997). A goal of the current study is to provide a quantitative assessment of the contributions of intrinsic biomechanical, reflex, and sensory integration mechanisms to UB control.

Our approach was to evoke medial-lateral sway of the UB using external perturbations that produced continuous pelvis rotations (eyes open and eyes closed) and visual field rotations in standing subjects while lateral displacement of the pelvis was prevented by a mechanical constraint. Dynamic behavior of evoked UB rotations was characterized using frequency domain analysis methods (frequency-response function gains and phases and coherence functions) and time domain analysis methods (impulse-response functions). Finally, underlying control mechanisms were investigated by developing a mathematical feedback control model of UB orientation that accounted for the experimental results. The model included simplified representations of sensory systems, sensory integration mechanisms, reflex mechanisms, and intrinsic mechanical properties. Model parameters were identified in order to quantify the contributions of the various mechanisms to UB control and to characterize changes in control as a function of stimulus conditions. The model effectively represents a hypothesis for the organization of the UB control system.

Our modeling results were then compared with two alternative hypotheses of UB control. One alternative hypothesis is that the frontal plane control of UB orientation is accomplished using the same mechanisms as used for whole body stance control. Previous studies that used continuous perturbations to characterize the dynamic behavior of stance control have shown that whole body stance control in the sagittal plane is dominated by sensory integration mechanisms that generate corrective torque based on a combination of sensory orientation information from proprioceptive, visual, and vestibular systems and with relatively long feedback delays (150-200 ms) (Maurer et al. 2006; Peterka 2002). A similar sensory integration mechanism was also demonstrated for frontal plane whole body control (Cenciarini and Peterka 2006). These studies have also demonstrated the phenomenon of sensory reweighting whereby the stance control system can shift its reliance from one sensory system to another depending on the postural task. Although there is evidence that the UB and whole body share some similar control

mechanisms (Cholewicki et al. 2000a; Genthon and Rougier 2006; Kiemel et al. 2008), it is unknown to what extent UB postural control is similarly characterized by sensory integration and sensory reweighting.

A second alternative hypothesis is that the control of UB orientation is accomplished using intrinsic biomechanical mechanisms and/or rapid-acting stretch reflexes as previously described. These mechanisms would tend to orient the UB to the pelvis and would act with either zero time delay or with shorter delays than the delay associated with a sensory integration mechanism which requires a greater amount of central processing.

Results from the current study fill gaps in our understanding of the contribution of sensory integration to UB control and provide a valuable starting point for understanding the more complex multi-segment orientation control problem of freestanding bipedal stance in the frontal plane.

## METHODS

### *Subjects*

Fourteen healthy subjects (7 male, 7 female, mean age 31 years ± 6 SD) with no history of balance disorders participated in this experiment. All subjects gave their informed consent prior to being tested using a protocol approved by the Institutional Review Board at Oregon Health & Science University.

Because the experimental protocol required subjects to maintain straight knees during testing, knee displacement was monitored throughout all tests. Data are presented for eight subjects whom we were certain were able to maintain straight knees throughout all tests (3 male, 5 female, mean age 31 ± 5 SD, mean height 169 cm ± 6 SD, mean mass 70.6 kg ± 11 SD).

### *Stimuli and data collection*

Frontal plane perturbations of the UB were evoked through pelvis tilts and visual field tilts. Pelvis tilts were elicited by rotating the support surface that subjects stood on while simultaneously preventing lateral displacement of the pelvis and lower body using a rigid frame with two roller carriages that pressed against the greater trochanters (Figs.

2.1 A, B, C). The roller systems permitted vertical motions of the hips but prevented lateral movement. The support surface rotation angle was controlled by a servo motor and the support surface axis of rotation was halfway between the subjects' heels and was at ankle height. We set the distance between the middle of each subject's heels (mean of 17.1 cm ± 1.3 SD) to be equal to the distance between his/her hip joint centers as estimated using a regression equation relating hip-joint distance to inter-ASIS distance (Seidel et al. 1995), so that the lower body formed an approximate parallelogram. Throughout the paper we refer to these tests as pelvis tilt tests.

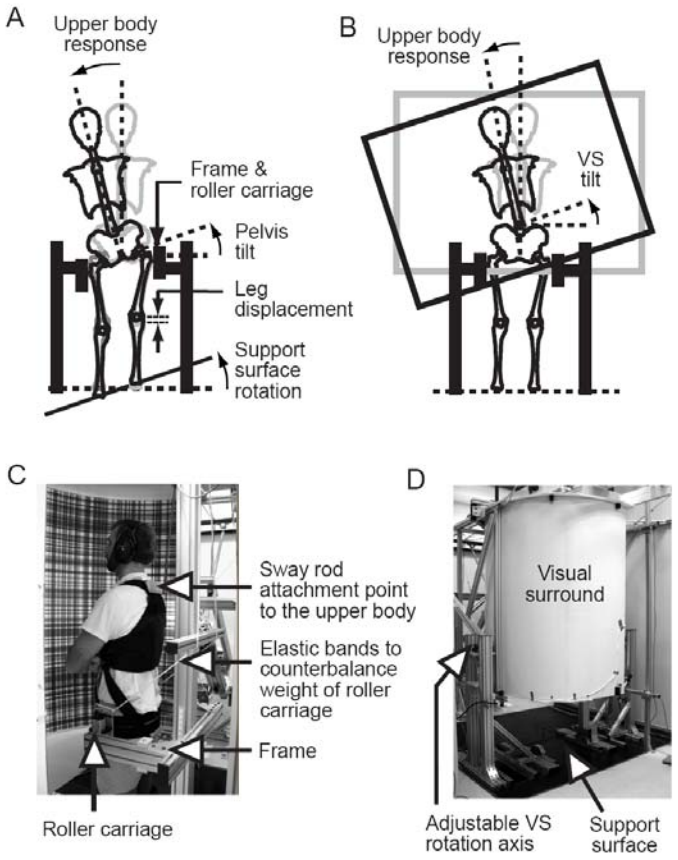


**FIG. 2.1**. *Experimental setup and definition of stimulus and response variables. A: Support surface rotations produced pelvis tilts that evoked upper body sway while the lower body was prevented from moving laterally. B: Visual tilts about axis aligned with L4/L5 joint evoked upper body sway. C: Photograph of subject viewing the illuminated checkered visual surround patterns with lower body stabilized by the frame and roller system. D: Photograph of the support surface that subjects stood on and the visual surround with rotation axis height individually set to each subject's L4/L5 joint height.*

Support surface rotations vertically displaced both legs equally, one leg up and the other leg down. The lower body parallelogram mechanics enabled these vertical leg displacements to produce pelvis rotations that equaled the support surface rotations assuming no knee-joint motion.

Visual stimuli were delivered using a servomotor to rotate a visual field which the subjects faced. The visual surround had a half-cylinder shape (70-cm radius) and was

lined with a complex checkerboard pattern of white, black, and three gray levels (Fig. 2.1B, C, and D). The visual surround was illuminated by fluorescent lights attached to the right and left edges of the surround. The rotation axis was horizontal and perpendicular to the subjects' frontal plane at the L4/L5 level (estimated as the iliac crest height (Skotte 2001)). Throughout the paper we refer to these tests as visual tilt tests.

In all experiments, stimulus delivery and data sampling occurred at 200 Hz. Pelvis and visual tilt stimuli were presented continuously according to a pseudorandom stimulus based on a pseudorandom ternary sequence (PRTS) of numbers (Davies 1970; Peterka 2002). Each number was assigned an angular velocity value of either +a, 0, or –a that was maintained constant for a specified state duration of $\Delta t$ s. The angular velocity waveform was mathematically integrated to derive the angular position waveform. The angular position waveform was scaled to a specific peak-to-peak value for each test condition and was used to drive either the support surface or the visual surround rotation.

Pelvis tilt stimuli were created from a 2186-length PRTS with 0.02 s state duration and cycle length of 43.72 s, giving a power spectrum of stimulus velocity with approximately equal amplitude spectral components ranging from 0.023 Hz to about 16.7 Hz. Eight PRTS cycles were presented in the lowest amplitude pelvis tilt test and seven cycles were presented in the higher amplitude tests. Visual tilt stimuli were created from a 242-length PRTS with 0.1 s state duration and cycle length of 24.2 s, giving a velocity power spectrum bandwidth of 0.041 Hz to 3.3 Hz. Twelve PRTS cycles were presented in each visual tilt test. A stimulus based on a PRTS was used because there are advantages to using periodic wide-bandwidth stimuli compared to random white-noise type stimuli for obtaining lower variance estimates of stimulus-response functions (Pintelon and Schoukens 2001).

Sampled data included the actual support surface angular position, visual surround angular position, UB displacements in the frontal plane, and vertical leg displacements at knee level. The UB and vertical knee displacement data were collected with rods that rested on small lightweight metal hooks that were fixed to the upper back between the C6 and T3 vertebrae (Fig. 2.1C) and the back of the knee, respectively. Rotational motion of each rod was recorded by a potentiometer and appropriate trigonometric conversions were used to calculate linear vertical displacements of the leg and linear lateral displacements of the upper trunk. The vertical leg displacements were

analyzed to ensure that subjects maintained straight knees on all tests and that the support surface rotational motions were accurately transmitted to produce leg displacements. We assumed that leg displacement motion was accurately transmitted to produce pelvis rotations. The upper trunk displacements were used to calculate the angular UB tilt with respect to earth-vertical (Fig. 2.1A and B). The angular UB tilt was considered to be the response variable that was compared to the stimulus.

*Protocol*

Subjects performed a total of 12 tests in a single test session lasting about 2½ hours. The tests included 2 quiet stance tests with either eyes open (EO) or eyes closed (EC) where no stimulus was given, 6 pelvis tilt tests with 1, 2, or 4º peak-to-peak amplitudes with either EO or EC, and 4 visual tilt tests with 0.5, 1, 2, or 4º peak-to-peak amplitudes with EO. These 12 tests were randomized to offset potential biases due to fatigue and learning. Each test lasted approximately 5½ minutes and subjects were given the opportunity to rest after every test.

Subjects were informed that there was no danger of falling and were instructed to maintain straight knees throughout the test and allow their UB to respond naturally. Subjects wore headphones and listened to their choice of novels or short stories to mask environmental equipment sounds and to maintain alertness.

*Analysis*

Experimental data were analyzed by calculating frequency-response functions, coherence functions, and impulse-response functions. For linear systems, these analyses provide complete characterizations of the dynamic properties of the system and can be used to derive the response of any transient or sustained stimulus. For nonlinear systems, these analyses provide a linear approximation to the system dynamics under the given test conditions. One possible interpretation for the variation of system dynamics as a function of test condition is that these variations represent changes in the postural system's "set" whereby neural control is altered to accommodate stimulus conditions (Prochazka 1989).

FREQUENCY-RESPONSE FUNCTION (FRF). An FRF is a non-parametric representation of the relation of a response signal to a stimulus signal through the decomposition of these stimulus-response signals into frequency components (Bendat and Piersol 2000). Each FRF was expressed as a set of gain and phase values that vary with frequency (Peterka 2002). Each gain value indicates the ratio of the response to the stimulus signal at its particular frequency and each phase value indicates the relative timing of the response compared to the stimulus (expressed in degrees). The phase values were "unwrapped" using the function "phase" from the Matlab Signal Processing Toolbox (The MathWorks, Natick, MA) so that phase lags exceeding -180º could be displayed.

The stimulus signal was either the pelvis tilt angle (determined to be equal to the surface rotation angle) or the visual surround tilt angle. The response signal was always defined as the UB sway angle with respect to earth vertical (Fig. 2.1A and B). For pelvis tilt stimuli, the UB sway angle was calculated using a trigonometric conversion of the measured linear displacement of the UB from a mid-line position with respect to the mid-point of the two hip joints (Fig. 2.1A). Use of this angular measure effectively normalizes the response measure across subjects such that calculated FRF gains (ratio of UB sway angle to pelvis tilt angle) indicate the extent to which the UB aligned to the pelvis. That is, a gain of one and phase of zero indicates alignment of the UB with the pelvis. For visual tilt stimuli, the UB sway angle calculation was based on the measured linear displacement of the UB from a midline position with respect to a presumed anatomic rotation joint at the L4/L5 level (Fig. 2.1B). Use of this angular measure allows FRF gain measures to indicate the extent to which the UB aligned to the tilted visual surround.

Using these stimulus-response signals, we estimated FRFs through the equation

$$H(f_k) = \frac{Y(f_k)}{X(f_k)} \tag{2.1}$$

where $X(f_k)$ is the discrete Fourier transform of the stimulus angle, $Y(f_k)$ is the discrete Fourier transform of the UB sway response angle, $H(f_k)$ is the estimated FRF, and $f_k$ are the frequencies were the FRF is calculated. This method for FRF estimation is the recommended approach when stimuli are periodic (Pintelon and Schoukens 2001). The fundamental frequencies, $f_1$, of the PRTS stimuli were 0.023 Hz for the support surface stimuli and 0.041 Hz for the visual tilt stimuli. The highest frequency, $f_{max}$ was limited by

the signal-to-noise ratio of the experimental data (10.3 Hz for pelvis tilt stimuli and 1.5 Hz for visual tilt stimuli).

$H(f_k)$ was calculated for each stimulus cycle (except the first cycle in order to avoid transient behavior) and was then smoothed by first averaging $H(f_k)$ over the stimulus cycles, and then averaging $H(f_k)$ across adjacent frequency points. The number of adjacent points included in the frequency smoothing were selected to provide a final set of FRF points that were approximately equally spaced on a logarithmic frequency scale while maintaining adequate frequency resolution (Otnes and Enochson 1972).

COHERENCE FUNCTIONS. Coherence functions are a frequency-domain equivalent of linear correlation coefficients. Coherence function values vary from 0 to 1, with values of 1 indicating a perfect linear relationship between stimulus and postural response with no noise in the system or measurements (Bendat and Piersol 2000). We estimated coherence functions via cross power spectral calculations, as previously described (Peterka 2002).

IMPULSE RESPONSE FUNCTIONS (IRF). The IRF of a linear system is the time domain equivalent of the frequency domain FRF (Davies 1970; Westwick and Kearney 2003). Although the IRF and FRF representation of the system dynamics are equivalent, system properties are often easier to appreciate in one representation compared to another. For example, a time delay is easier to recognize in an IRF than a FRF where its effects are distributed.

Because the PRTS stimulus velocity waveform is an approximate white-noise stimulus, an IRF can be calculated using an appropriately scaled cross correlation between the ideal PRTS velocity waveform and the response waveform:

$$g(i) = \frac{3N}{2a^2(N+1)} \sum_{j=1}^{N} x(j)\, y(j+i), \quad \text{for } i = 0, \ldots M \tag{2.2}$$

where $x$ is the sampled ideal PRTS velocity waveform, $y$ is 2 repeated cycles of the mean UB sway velocity waveform with the mean UB sway velocity calculated by averaging over the stimulus cycles (but not including the first cycle to avoid transient responses), $a$ is the velocity amplitude of the PRTS stimulus, $N$ is the length of the PRTS (2186 for pelvis tilt tests), and $M$ is the maximum time lag index (Davies 1970). IRFs calculated

from eqn. (2.2) are unitless when $x$ and $y$ have units of angular velocity. The IRFs displayed in Figs. 2.4 and 2.8 are shown having units of angular velocity. These IRFs represent the convolution between the IRFs calculated using eqn. (2.2) and a unit impulse of stimulus velocity.

Note that the IRFs include the dynamics of the actuator as well as the physiological system. Because of the high bandwidth of the support surface actuator (~25 Hz), the effective filtering/smoothing of the IRF by the actuator dynamics is minimal. IRFs for responses to visual stimuli were not calculated because the lower bandwidth of the visual surround actuator as well as the generally low signal-to-noise of responses to visual stimuli did not permit accurate estimates of IRFs.

MODEL OF UPPER BODY CONTROL. To help understand the underlying mechanisms behind the experimental results, we developed a mathematical model of the UB postural control system. The model can be thought of as representing a quantitative hypothesis about how the UB control system is organized. Numerous model structures were explored; however, this paper focuses on the simplest model we were able to identify that was physiologically plausible and was able to account for the detailed features of experimental FRFs and IRFs. This model was contrasted with two alternative models that previously have been used to account for whole body stance control or UB responses to transient perturbations.

UB control mechanisms were represented as model parameters and were estimated from experimental results using a constrained nonlinear optimization routine 'fmincon' (Matlab Optimization Toolbox, The MathWorks, Natick, MA) to minimize the total mean-squared-error (*MSE*) of the normalized difference between model FRFs and experimental FRFs (Peterka 2002). To further validate the model and understand the UB control system, model IRFs were calculated from simulated UB sway angles using Simulink (The MathWorks, Natick, MA). Simulated UB sway was evoked from pelvis tilt stimuli that were identical to the pseudorandom pelvis tilts during the experiments and the simulated UB response was analyzed in a manner identical to the experimental data.

STATISTICS. To test if stimulus amplitude and visual availability (EO compared to EC) had a statistically significant effect on UB root-mean-square (RMS) sway and

parameters in the UB postural control model, we used repeated measures ANOVAs with two experimental factors: stimulus amplitude and visual availability. Stimulus amplitude was a continuous variable in the statistical model and we tested for significant linear trends in UB control parameters with stimulus amplitude. Null hypothesis rejection was set to $p < 0.05$ for all tests. In addition, mean FRFs include 95% confidence intervals that were determined using the percentile bootstrap method with 5000 bootstrap samples (Zoubir and Boashash 1998).

## RESULTS

*Upper body sway evoked by pelvis rotations*

Pelvis tilt stimuli and the UB responses for the three stimulus amplitudes, EO and EC, are shown in Fig. 2.2A. The UB sway response waveforms (averaged over all subjects) generally followed the pelvis tilt stimulus meaning that subjects tended to align their UB to their pelvis. Fig. 2.2A shows that UB responses in EO conditions were qualitatively similar to EC responses. A statistical comparison of EO to EC RMS sway measures did not reveal any significant effect of vision (Fig. 2.2C), suggesting that subjects made very little use of visual information to control their UB orientation. Increasing stimulus amplitude produced a statistically significant increase on RMS sway responses.

FRF GAINS. The variation across frequency of FRF gains was similar across stimulus amplitudes and EO/EC conditions (Fig. 2.3A and B upper plots). Gains in the 0.02 to 0.6 Hz range increased with increasing frequency to reach a peak value around 0.6 to 0.9 Hz. For all test conditions, the gain in the frequency region of this peak was always greater than 1.0 indicating that the UB sway amplitude was greater than the pelvis tilt amplitude. Gains decreased rapidly above 1 Hz, showed a minor peak around 2 Hz, deceased rapidly again for frequencies greater than 3 Hz, and then showed another minor peak at about 8 Hz.

Subjects exhibited amplitude dependent changes in FRF gains. At low- and mid-frequencies (<1.3 Hz), gains generally decreased with increasing pelvis tilt amplitude. However, in the region of the second peak (1.3-3 Hz), gains generally increased with

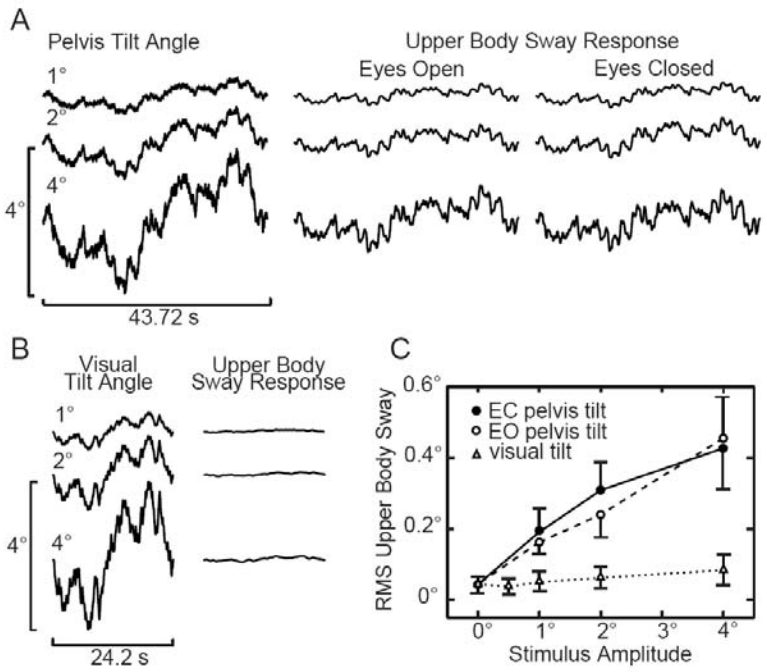


**FIG. 2.2.** *Stimulus waveform and mean upper body sway responses averaged across subjects and stimulus cycles. A: Pelvis tilts evoked UB sway that generally followed the stimulus with little differences between eyes open and eyes closed conditions. B: Visual tilts evoked small UB sway. C: Root-mean-square (RMS) upper body sway as a function stimulus amplitude (mean ± 1 SD).*

increasing pelvis tilt amplitude. At the highest frequencies (>3 Hz), there was little change in gain with changing pelvis tilt amplitudes.

Vision had a limited effect on FRF gains, and these effects occurred primarily at lower frequencies. The 1° and 2° stimuli EO gains were slightly lower than the EC gains below frequencies of 0.3 Hz and 1.0 Hz, respectively. Conversely, the 4° stimulus resulted in EO gains that were slightly larger than EC gains below frequencies of 0.1 Hz.

FRF PHASES. Subjects' FRF phase curves generally showed decreasing values (more phase lag) with increasing frequency (Fig. 2.3A and B middle plots). At frequencies below about 0.2-0.4 Hz, pelvis tilt stimuli resulted in UB phase leads, while at mid- and high-frequencies (>0.4 Hz) all stimuli resulted in UB phase lags. At 4 Hz, phases reached a low value of about -180° before increasing to about -120° around 6 Hz and then decreasing again to about -180° at 10.3 Hz.

There were small but systematic amplitude dependent changes in phase curves between 0.1-2 Hz with increasing stimulus amplitudes resulting in more phase lead and/or less phase lag values for both the EO and EC conditions.

Comparison of EO and EC phase curves at a given stimulus amplitude showed that vision had a limited effect.

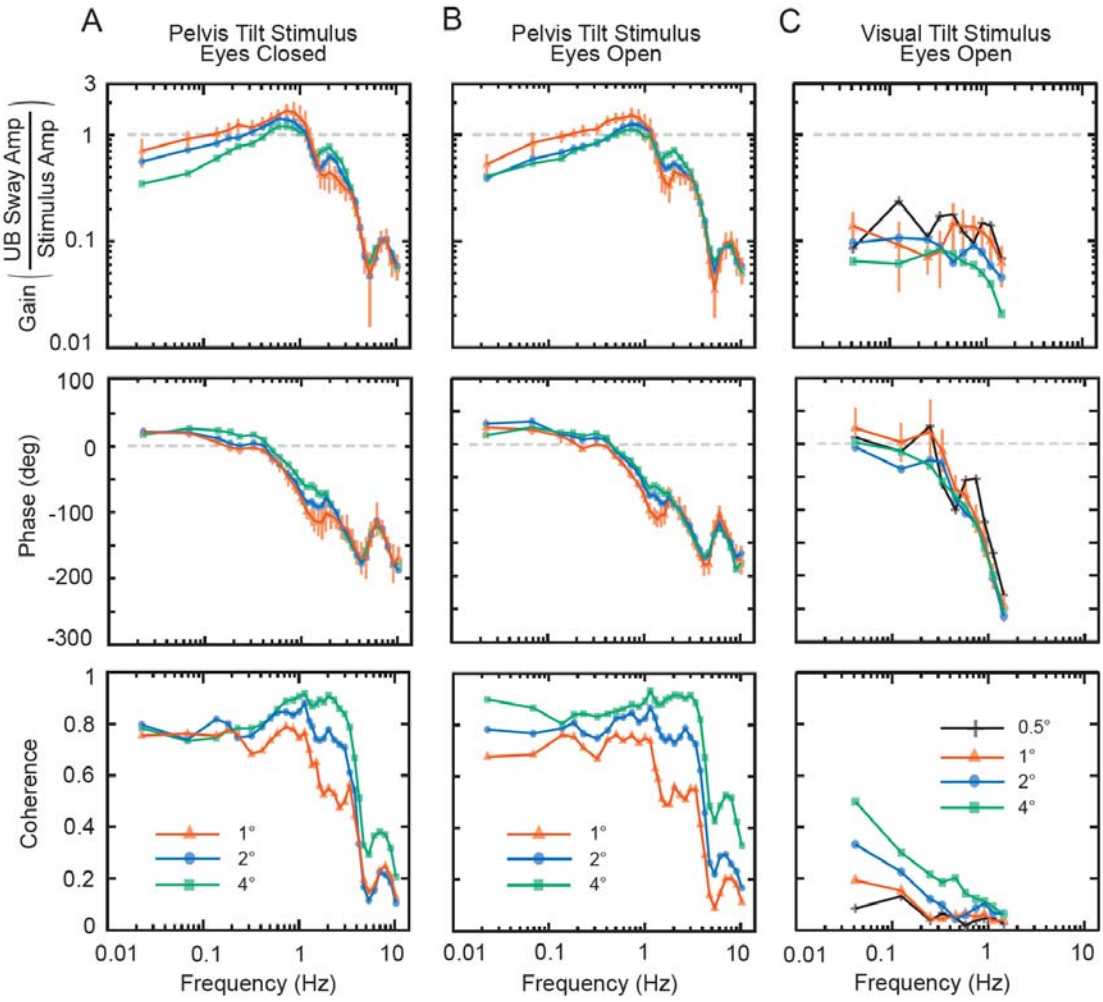


**FIG. 2.3.** *Experimental frequency-response and coherence functions averaged across subjects. A: Eyes closed (EC) pelvis tilt stimuli. B: Eyes open (EO) pelvis tilt stimuli. C: Visual tilt stimuli. Error bars on pelvis and visual tilt frequency-response functions show 95% confidence intervals on mean gain and phase at each frequency based on 5,000 bootstrap samples (Zoubir and Boashash 1998).*

COHERENCE FUNCTIONS. All pelvis tilt stimuli resulted in coherences between 0.6 and 0.9 at frequencies below 1 Hz and coherences decreased sharply at frequencies above 3 Hz (Fig. 2.3A and B lower plots). Increasing stimulus amplitudes resulted in higher coherences above about 0.2 Hz for EC conditions and across all measured frequencies for EO conditions. The higher coherences at larger stimulus amplitudes are consistent with increased signal-to-noise ratios in the experimental data.

IMPULSE RESPONSE FUNCTIONS. Although continuous rotations were used to estimate IRFs, an IRF can be intuitively thought of as the time course of a subject's UB rotational sway velocity evoked by a sudden pelvis tilt of 1° (i.e. a velocity impulse). A change in the IRF time course with changing stimulus conditions is indicative of a change in the dynamic characteristics of the UB control system as a function of stimulus conditions.

Three time epochs of the IRFs (Fig. 2.4) showed specific features related to stimulus conditions. In the first epoch (0.0-0.2 s), subjects' UB IRFs were very similar (Fig. 2.4B, C, and D). Independent of stimulus amplitude or visual conditions, the IRFs exhibited a short delay (0.025 s) before a sharp increase to about 3.5°/s at 0.04 s and then

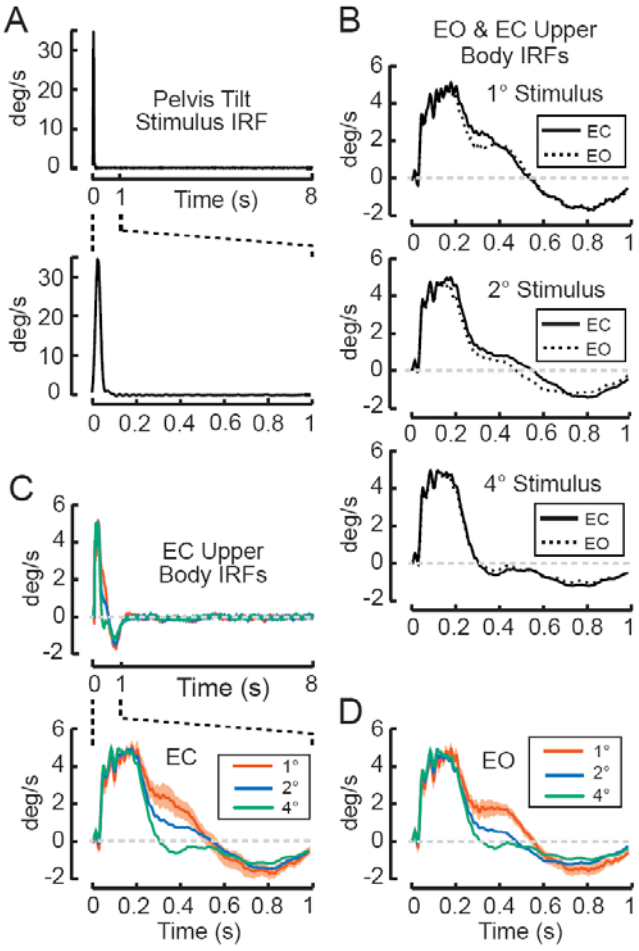


**FIG. 2.4.** *Experimental impulse-response functions (IRFs) from pelvis tilt tests. A: Pelvis tilt stimulus IRF calculated from eqn. 2 between the ideal PRTS velocity and the actual support surface velocity. B: Comparison of eyes open (EO) to eyes closed (EC) upper body (UB) IRFs. C: EC UB IRFs derived from three different pseudorandom pelvis tilt stimulus amplitudes. D: EO UB IRFs derived from the three amplitudes of pelvis tilt stimuli. Across-subject mean with ± 1 SE shown for the 1° stimulus.*

a more gradual increase to about 4.6°/s at 0.2 s. This early time course means that, after a short time delay following a sudden pelvis tilt, the UB begins to rotate toward alignment with the tilted pelvis.

During the second epoch (0.2-1.0 s), subjects' UB IRFs decreased from the peak positive value at 0.2 s to a peak negative value of -1 to -1.7°/s at about 0.8 s. The time course of the IRFs in this time epoch depended on the amplitude of the PRTS pelvis tilt stimulus from which the IRF was derived. For both the EC and EO conditions, the IRF time courses showed systematic differences as a function of stimulus amplitude between about 0.2 s and 0.5 s with the IRF decreasing toward zero most rapidly for the 4° amplitude (Fig. 2.4C and D). The peak negative value that occurred at about 0.8 s was also less negative for the 4° amplitudes. A comparison of EO and EC IRFs in this epoch showed similar or slightly lower IRF values for EO for the 1° and 2° pelvis tilt amplitudes, and very slightly larger EO IRF values on the 4° pelvis tilt amplitude.

During the third epoch (1.0-8.0 s), subjects' UB IRFs had on average small negative values between 1.7 and 8 s on all pelvis tilt test conditions. The mean sway velocities from 1.7 to 8.0 s were -0.05, -0.03, and -0.01°/s for the 1°, 2°, and 4° EC stimulus amplitudes and -0.05, -0.04, and -0.02°/s for the 1°, 2°, and 4° EO stimulus amplitudes. After about 8 s (not shown in figures), sway velocities for all test conditions were essentially zero.

*Upper body sway evoked by visual field rotations*

UB responses to visual tilt rotations were small compared to pelvis tilts (Fig. 2.2B). There was a small, but statistically significant increase in RMS sway with increasing stimulus amplitude (Fig. 2.2C).

FRF gain and phase curves (Fig. 2.3C) were quite variable due to the low UB signal-to-noise ratio during visual tilt tests. For all stimulus amplitudes, at low- and mid-frequencies (<0.8 Hz), gain curves were relatively constant, with most gain values between 0.05 and 0.2. These gains are about 10 times smaller than the gains for pelvis tilt stimuli over corresponding frequency ranges. At higher frequencies (>0.8 Hz), all gain curves decreased with increasing frequency. Although FRF gains were quite variable, there was a trend for FRF gains to decline with increasing stimulus amplitude.

Phase curves generally decreased (more phase lag) with increasing frequency (Fig. 2.3C). At lower frequencies (<0.3 Hz), phase values were close to zero (in phase with the stimulus), and at the highest frequency (1.5 Hz) phase lags exceeded 200°. Phase curves showed no systematic changes across the 4 visual tilt amplitudes.

Coherence function values were low compared with coherences from pelvis tilt stimuli, consistent with the low responses to visual stimuli and subsequent poor signal-to-noise. Coherence values generally decreased with increasing frequency and increased with increasing stimulus amplitude.

*Model-based Interpretation*

A feedback control model (Fig. 2.5) of the UB postural system was developed to gain insight into the underlying mechanisms that might account for the experimental results. This model was able to account for the detailed features of the experimental FRFs and IRFs. Below we 1) describe the model, 2) characterize how model parameters vary with test conditions, 3) show that the model provides a detailed prediction of FRF and IRFs, 4) quantify the corrective torque contributions of different control mechanisms of the model, and 5) consider versions of the model that represent alternative hypotheses related to the mechanisms contributing to UB control.

MODEL DESCRIPTION. Each block in the model represents a sensory, neural, neuromuscular, or mechanical system. The UB is assumed to sway as a single-link inverted pendulum about a joint that corresponds to L4/L5 (Brown and McGill (in press); Cholewicki et al. 2000b; McGill et al. 1994). The system output is upper body-in-space (*UBS*) tilt angle with respect to earth vertical. The UB block includes the UB moment of inertia ($J$) about the L4/L5 joint, the UB mass ($m$), and the UB center-of-mass height ($h$) above the L4/L5 joint. The values of $J$, $m$, and $h$ were estimated for each subject using anthropometric methods (Erdmann 1997; Winter 2005). The mean values of these parameters were 3.2 $kg \cdot m^2$, 40.2 kg, 0.22 m, respectively. Note that the model does not account for the inertial torque that would be generated by the small lateral displacement of the L4/L5 joint as the pelvis tilts about an axis located midway between the two hip joints. The justification for this simplification and other modeling assumptions are addressed in the Discussion.

The stimulus to the UB block is a corrective torque ($T_c$) generated based on four types of mechanisms that are distinguished from one another based on the time delay of torque generation. These mechanisms are 1) intrinsic stiffness, 2) short-latency phasic

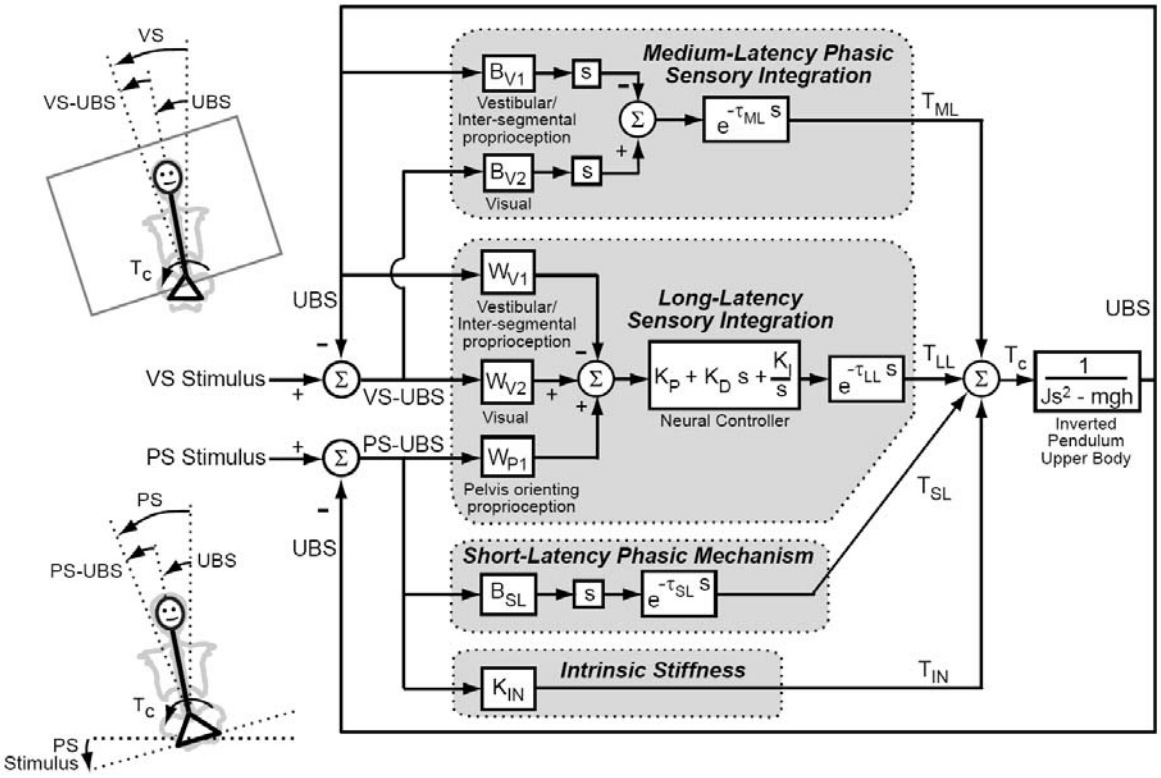


**FIG. 2.5.** *Model of upper body control includes feedback from 4 mechanisms. Upper body-in-space (UBS) tilt angle is the model output. The model input is either pelvis tilt-in-space (PS) or visual tilt-in-space (VS) angle.*

reflex, 3) medium-latency phasic sensory integration, and 4) long-latency sensory integration.

The intrinsic stiffness mechanism tends to orient the UB perpendicular to the pelvis by generating instantaneous torque in proportion to the difference between the pelvis-in-space angle (*PS*) and *UBS*. The proportionality constant $K_{IN}$ represents the intrinsic stiffness of tendons, joints, spinal ligaments, and muscles.

The short-latency phasic mechanism generates a torque proportional to the tilt velocity of the *UBS* relative to *PS* with a short-latency time delay ($\tau_{SL}$). The proportionality constant is $B_{SL}$. This mechanism may represent the contribution of stretch reflex pathways.

The medium-latency phasic sensory integration mechanism generates angular velocity-related torque from sensory systems with a medium-latency time delay ($\tau_{ML}$). $B_{VI}$ represents the sensory systems that generate a torque proportional to *UBS* velocity

and could potentially come from inter-segmental proprioceptive cues (i.e., sensory cues that orient the UB to the stationary lower body) and/or vestibular cues. $B_{V2}$ represents the visual contribution that generates a torque proportional to the difference between the visual surround-in-space angle (*VS*) and *UBS*. In the EC condition, $B_{V2} = 0$. For the EO conditions with a stationary visual surround ($VS = 0$), the $B_{V1}$ and $B_{V2}$ components both generate torque proportional to *UBS* velocity. For EO conditions with a moving visual surround, the $B_{V2}$ contribution tends to move the UB into alignment with visual tilt while the $B_{V1}$ contribution tends to move the UB toward an upright orientation.

The long-latency sensory integration mechanism generates angular position-related, angular velocity-related, and time integrated angular position-related torques via a "neural controller" in relation to a summation of sensory orientation signals with a long-latency time delay ($\tau_{LL}$). The sensory weights $W_{P1}$, $W_{V1}$, and $W_{V2}$ represent the relative contribution of the pelvis-orienting proprioceptive, the combined inter-segmental proprioceptive and vestibular, and the visual systems, respectively, and are constrained to sum to unity ($W_{P1} + W_{V1} = 1$ in EC conditions, $W_{P1} + W_{V1} + W_{V2} = 1$ in EO conditions). This long-latency sensory integration mechanism corresponds to the mechanism that was previously shown to make the dominant contribution to ankle corrective torque during experiments that evoked whole body sway (Peterka 2002).

The Laplace transform representation of the differential equation relating *UBS* to *PS* is

$$\frac{UBS}{PS} = \frac{K_{IN} + SL + W_{P1}LL}{Js^2 - mgh + K_{IN} + SL + ML + LL} \tag{2.3}$$

where $s$ is the Laplace variable, $SL = B_{SL}\, s\, e^{-\tau_{SL} s}$, $ML = (B_{V1} + B_{V2})\, s\, e^{-\tau_{ML} s}$, and $LL = (K_P + K_D s + K_I / s)\, e^{-\tau_{LL} s}$. The Laplace equation of the UB model with visual tilt stimuli is given by

$$\frac{UBS}{VS} = \frac{W_{V2}LL + B_{V2}\, s\, e^{-\tau_{ML} s}}{Js^2 - mgh + K_{IN} + SL + ML + LL} \tag{2.4}$$

MODEL PARAMETERS. All identified model parameters are given in Table 2.1 Only certain model parameters needed to vary across test conditions to accurately describe the observed changes in experimental FRFs and IRFs, while other parameters

**TABLE 2.1** *Model Parameters*

| Parameter | Pelvis tilt Stimulus | | Visual tilt Stimulus |
|---|---|---|---|
| | EC | EO | |
| $K_{IN}$ /mh | 7.8 +/- 2.7 * | 7.8 +/- 2.7 * | 7.8 † |
| $B_{SL}$ /mh | 1.25 +/- 0.36 * | 1.25 +/- 0.36 * | 1.25 † |
| $\tau_{SL}$ | 25.1 +/- 6.1 * | 25.1 +/- 6.1 * | 25.1 † |
| $B_{V1}$ /mh | 3.7 § | - | 2.16 ‡ |
| $(B_{V1} + B_{V2})$/mh | - | 4.0 § | - |
| $B_{V2}$ /mh | 0 | - | 0.018 ‡ |
| $\tau_{ML}$ | 135 +/- 18 * | 135 +/- 18 * | 135 † |
| $K_P$ /mh | 16.6 § | 18.7 § | 8.44 ‡ |
| $K_D$ /mh | 0.70 § | 0.77 § | 0.670 ‡ |
| $K_I$ /mh | 9.2 § | 12.1 § | 2.00 ‡ |
| $W_{P1}$ | 0.40 § | 0.43 § | - |
| $W_{V1}$ | 0.60 § | - | - |
| $W_{V1} + W_{V2}$ | - | 0.57 § | - |
| $W_{V2}$ | 0 | - | 0.089 § |
| $W_{V1} + W_{P1}$ | 1 | - | 0.91 § |
| $\tau_{LL}$ | 281 +/ 24 * | 281 +/ 24 * | 281 † |

** Parameters that were fixed across stimulus amplitudes, across-subject mean ± 1 standard deviation.*
*§ Parameters that varied across stimulus amplitudes, mean value across subjects and stimulus amplitudes.*
*† Parameters fixed to the across-subject mean.*
*‡ Parameters that were fixed across visual tilt tests.*
*Standard deviations were not available on visual tilt tests because parameters were estimated from fits to the across-subject mean FRFs. Units on $K_{IN}$ and $K_P$ are N·m/rad, units on $B_{SL}$ , $B_{V1}$ , $B_{V2}$ , and $K_D$ are (N·m·s)/rad, units on $K_I$ are N·m/(rad·s), units on $\tau_{SL}$, $\tau_{ML}$, and $\tau_{LL}$ are ms, and $W_{P1}$, $W_{V2}$, and $W_{V1}$ are unitless. Mean value of m·h is 9.1 kg m.*

could be fixed across test conditions. Fixed parameters included intrinsic stiffness, short-latency phasic gain, and the short-, medium-, and long-latency time delays. These fixed parameter values were determined from fits to the FRFs of the pelvis tilt tests because pelvis tilt stimuli excited a larger dynamic range of the UB control system than visual tilt stimuli and produced more reliable experimental FRFs compared to visual tilt stimuli.

Because of the variable UB responses to visual tilt stimuli, only the general trend in UB sway during visual tilt tests could be described. Therefore, the only parameters that varied across visual tilt amplitudes were the sensory weights.

To counteract destabilizing torques due to gravity, the overall stiffness of the UB control system must be greater than the gravitational stiffness factor $K_g = mgh$ (Peterka

2002). That is, for small UB tilts away from earth-vertical, a gravitation torque is generated in proportion to the UB tilt angle and the proportionality constant is $K_g$. To ensure stability, the UB control system must include mechanisms that generate a counterbalancing corrective torque in proportion to the UB sway angle that is at least as large in magnitude as the gravitational torque. The two model parameters that represent the stiffness factors proportional to UB sway are the intrinsic stiffness ($K_{IN}$) and the neural controller proportional gain ($K_P$). The sum of $K_{IN}$ and $K_P$, representing the "overall stiffness" factor of the UB control system, are plotted in Fig. 2.6A as a function of *mh*. The extent to which each subject's overall stiffness exceeded $K_g$ represents a safety factor of corrective torque generation (Peterka 2002). The slope of the overall stiffness regression line was 3.1 times the slope of the line representing $K_g = mgh$. Both $K_{IN}$ and $K_{IN} + K_P$ increased with *mh*. The increase in $K_{IN}$ with *mh* indicates that intrinsic stiffness scales with body size. A similar result can be seen in intrinsic stiffness measures reported by McGill et al. (1994) where lower mass female subjects had lower frontal plane intrinsic stiffness than higher mass male subjects for small UB displacements. The fact that there was a statistically significant positive correlation (R = 0.98) between each subject's mean overall stiffness ($K_{IN} + K_P$) across pelvis tilt tests and their $m \cdot h$ (Fig. 2.6A) suggests that overall stiffness is carefully regulated to achieve some behavioral goal that is the same for all subjects. In 7 of 8 subjects, $K_{IN}$ was smaller than $K_P$ and $K_{IN}$ was below $K_g$ (mean $K_{IN} / K_g = 0.80$). The fact that $K_{IN}$ was less than $K_g$ in most subjects underscores the importance of torque generation originating from neural activation of muscles to achieve UB stability.

The "overall damping" factor was defined as the summation of the parameters that generate torque in proportion to a velocity signal. This overall damping factor is equal to $K_D + B_{V1} + B_{V2} + B_{SL}$ and is plotted in Fig. 2.6B as a function of *mh*. A statistically significant positive correlation (R = 0.93) existed between each subject's mean overall damping across pelvis tilt tests and their *mh*. The high correlation suggests that there is careful regulation of overall damping. The largest contribution to overall damping was provided by the medium-latency phasic mechanism ($B_{V1}$ in EC and $B_{V1} + B_{V2}$ in EO). Averaged across all pelvis tilt tests, $B_{V1}$ or $B_{V1} + B_{V2}$ provided 66% of the overall damping, whereas $B_{SL}$ provided 21% and $K_D$ 13% of the overall damping.

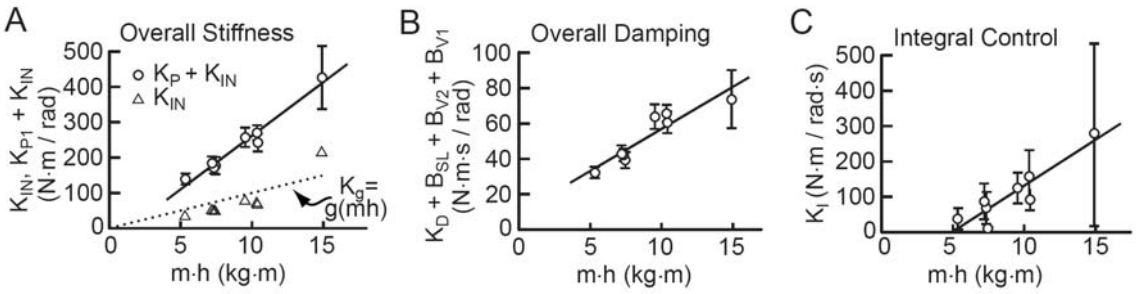


**FIG. 2.6.** *Model parameters related to overall stiffness, overall damping, and integral control as a function of m (upper body mass) times h (upper body center-of-mass height above the L4/L5 joint). Each data point represents one subject's mean value across the 6 pelvis tilt test conditions (± 1 SD).*

The integral control factor ($K_I$) was variable across test conditions, but still exhibited a statistically significant positive correlation (R = 0.92) between each subject's mean $K_I$ across pelvis tilt tests and their *mh* (Fig. 2.6C).

Figure 2.7A shows how parameters varied as a function of stimulus amplitude in EC and EO pelvis tilt tests. All parameters plotted in Fig. 2.7A except long-latency sensory weights were normalized by *mh*. Neural controller parameters $K_P$ and $K_I$ showed statistically significant increases with increasing stimulus amplitude, but $K_D$ showed no significant change. $K_P$ was significantly greater for EO compared to EC conditions, although the mean normalized $K_P$ value across all stimulus amplitudes was only 13% greater in EO compared to EC. There was no significant difference in $K_I$ or in $K_D$ between EC and EO conditions.

Medium-latency sensory integration parameters ($B_{V1}$ or $B_{V1}$+$B_{V2}$) increased significantly with increasing stimulus amplitude. The combined gain factors $B_{V1}$+$B_{V2}$ identified on EO tests were significantly larger than the gain factor $B_{V1}$ identified on the EC tests although the mean normalized $B_{V1}$+$B_{V2}$ values across all stimulus amplitudes was only 8% greater in EO compared to $B_{V1}$ in EC. Increasing stimulus amplitudes produced a statistically significant increase in the long-latency sensory integration parameters ($W_{V1}$ or $W_{V1}$+$W_{V2}$), and thus a significant decrease in $W_{P1}$. These parameter changes imply that subjects increased their reliance upon information that oriented their UB vertical as stimulus amplitudes increased, while decreasing their reliance upon pelvis-orienting proprioceptive information. The similarity in the values of the medium-latency gains and the long-latency weights in EO compared to EC test conditions imply that subjects made relatively little use of visual information to control their UB.

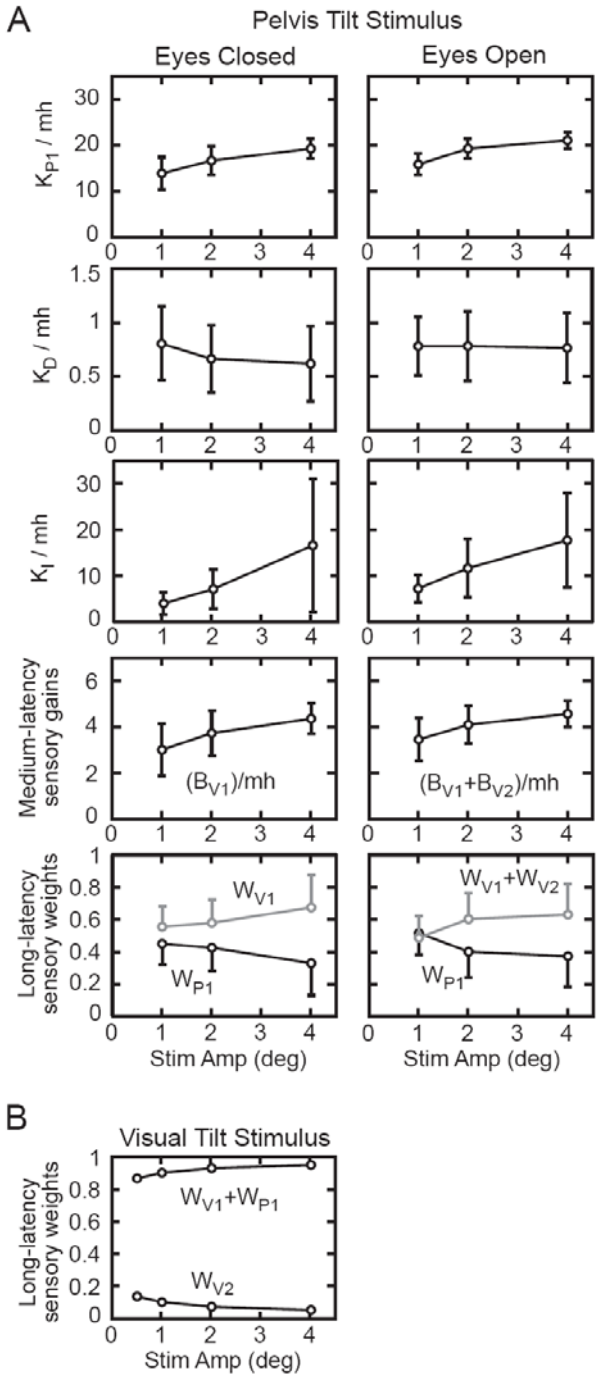


**FIG. 2.7.** *Model parameter variations as a function of A: pelvis tilt stimulus amplitude and visual availability (across-subject mean parameter values ± 1 SD) and B: visual tilt stimulus amplitude (parameters derived from fits to across-subject mean FRFs). Units on $K_P$ are N·m/rad, units on $K_I$ are N·m/(rad·s), and units on $K_D$, $B_{V1}$, and $B_{V2}$ are (N·m·s)/rad. Sensory weights $W_{P1}$, $W_{V1}$, and $W_{V2}$ are unitless. Mean subject mh was 9.1 kg·m.*

During visual tilt tests, the long-latency sensory integration parameter $W_{V2}$ was much smaller than $W_{V1}+W_{P1}$. Increasing stimulus amplitude produced a small decrease in $W_{V2}$, and thus a small increase in $W_{V1}+W_{P1}$ (Fig. 2.7B). These parameter values imply that subjects had an overall low reliance upon visual information relative to vestibular

and proprioceptive information during visual tilt tests and this low reliance on visual information decreased even further as visual surround stimulus amplitudes increased.

The mean values of neural controller parameters $K_P$ and $K_I$ were lower during visual tilt tests compared to pelvis tilt tests (Table 2.1). This is consistent with the trend seen on pelvis tilt tests for $K_P$ and $K_I$ values to be smallest on the low amplitude tests that evoked the smallest UB responses since UB responses evoked on visual tilt tests were much smaller than even the lowest amplitude pelvis tilt test (Fig. 2.2). Similarly, medium-latency sensory gains ($B_{V1}$ and $B_{V2}$) were also lower during visual tilt tests compared to pelvis tilt tests, consistent with the trend in $B_{V1}$ and $B_{V1} + B_{V2}$ parameters during pelvis tilt tests to decrease with decreasing UB responses.

MODEL PREDICTIONS OF FRFs AND IRFS. Model-predicted FRFs were able to account for the detailed shapes of the experimental gain and phase data over the entire frequency range of available data and as a function of pelvis tilt test conditions (Fig. 2.8A and B). In addition, this model was able to describe the general trend in experimental FRFs for all visual tilt tests, i.e. gain decreases with increasing stimulus amplitudes with minimal phase changes across visual tilt test conditions (Fig. 2.8C).

Model-predicted IRFs (Fig. 2.8D) closely matched the detailed time courses of the experimental IRFs (Fig. 2.4C). The early time epoch of experimental IRFs was invariant across all pelvis tilt tests. In the model, this invariance was attributable to fixed values of parameters in the intrinsic and short-latency mechanisms. Changes in the experimental IRFs with pelvis tilt test condition in later time epochs were attributable to changes in the model's medium- and long-latency sensory integration parameters across test conditions.

Note that the change in the IRF trajectory that is attributable to torque generated by the medium-latency mechanism becomes evident at about 0.2 s (Figs. 2.4 and 2.8) even though the medium-latency time delay is 0.135 s. This apparently longer onset delay occurs because a sudden pelvis tilt must first generate torque via the intrinsic and short-latency mechanisms. This torque produces an UB sway trajectory that is effectively filtered by the UB mechanics before being sensed by vestibular and/or visual systems which in turn generate torque via the medium-latency mechanism. Finally, the UB

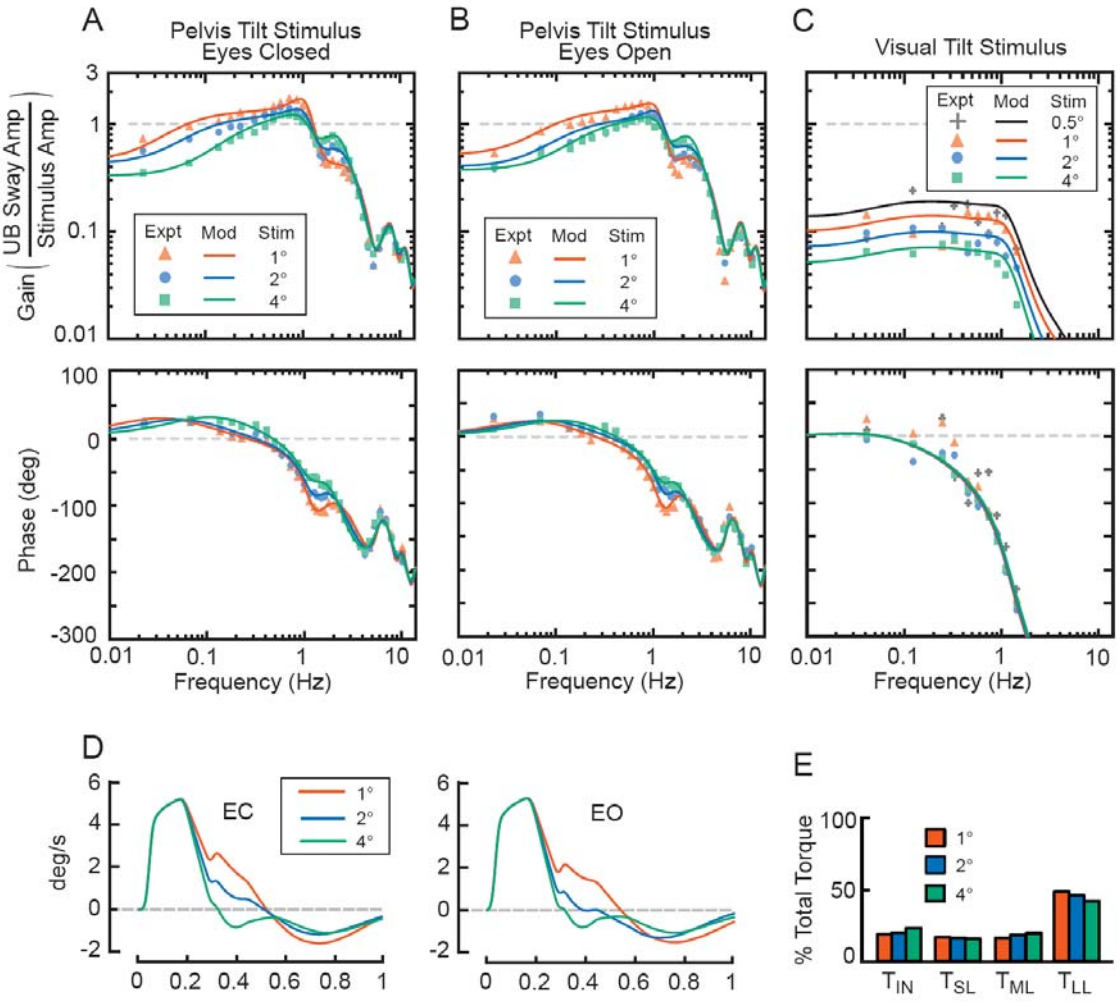


**FIG. 2.8.** *Model predictions for A: Eyes closed (EC) pelvis tilt stimuli FRFs; B: Eyes open (EO) pelvis tilt stimuli FRFs, C: visual tilt stimuli FRFs, and D: EC and EO pelvis tilt stimuli IRFs. Individual data points in A, B, and C are across-subject mean experimental data and solid lines are model predictions using equation 1.3 and mean subject parameters. E: Contributions of the 4 control mechanisms are displayed as a percent of total torque for the three different pseudorandom stimulus amplitudes. For each pelvis tilt amplitude, the total torque was defined as the summation of the RMS torque generated from each of the 4 control mechanisms over one stimulus cycle.*

mechanics once again effectively filter the corrective torque before producing the change in UB sway trajectory attributable to the medium-latency mechanism.

TORQUE CONTRIBUTIONS OF UB CONTROL MECHANISMS. To appreciate the relative contributions of the four mechanisms during continuous pelvis tilt perturbations and to see how these contributions change with changing stimulus amplitude, the RMS torque generated from $T_{IN}$, $T_{SL}$, $T_{ML}$, and $T_{LL}$ over one 43.72 s cycle

of EC pseudorandom pelvis tilts of 1°, 2°, and 4° was calculated from model simulations using the parameters previously identified. The RMS values of the four torque components were normalized by the summation of the RMS values of the four torque components calculated for each stimulus amplitude. Results are shown in Fig. 2.8E. Across all stimulus amplitudes, torque output from the long-latency sensory integration mechanism ($T_{LL}$) was about twice the torque output of any other single mechanism. There were only small changes with changing stimulus amplitudes. This result underscores the important role of the long-latency mechanism in shaping the overall UB sway characteristics during an experiment using continuous broad bandwidth perturbations.

ALTERNATIVE MODELS. We explored alternative UB models in order to test two hypotheses: 1) UB control is accomplished using a sensory integration mechanism and 2) UB control is accomplished using mechanisms that act with little or no time delay. To test the first hypothesis, we explored how well the long-latency sensory integration mechanism alone could account for the experimental FRFs. The long-latency sensory integration mechanism corresponds to a model that was previously shown to provide a good account for whole body postural control (Peterka 2002).

We found that the ability of a model which included the long-latency sensory integration mechanism alone to fit the experimental FRFs was highly dependant upon the time delay $\tau_{LL}$. When $\tau_{LL}$ was manually set to 150 ms (consistent with whole body sensory integration time delays), and the remaining model parameters were determined from the optimization routine with the constraint that the overall system was stable, the FRF of the optimized model fit was not remotely close to the experimental FRFs (Fig. 2.9A, solid curves). However, when all parameters, including $\tau_{LL}$, were free to vary, the optimization set $\tau_{LL}$ to 25 ms and the model was able to describe the general features of the experimental FRFs but not the detailed variations in the experimental gain and phase data at frequencies greater than 1 Hz (Fig. 2.9A, dotted curves). Because 25 ms is far lower than sensory integration time delays associated with whole body postural control and because time delays associated with whole body postural resulted in poor predictions of UB experimental FRFs, we rejected the notion that control of the UB is identical to whole body control. Furthermore, because a sensory integration time delay of 25 ms is

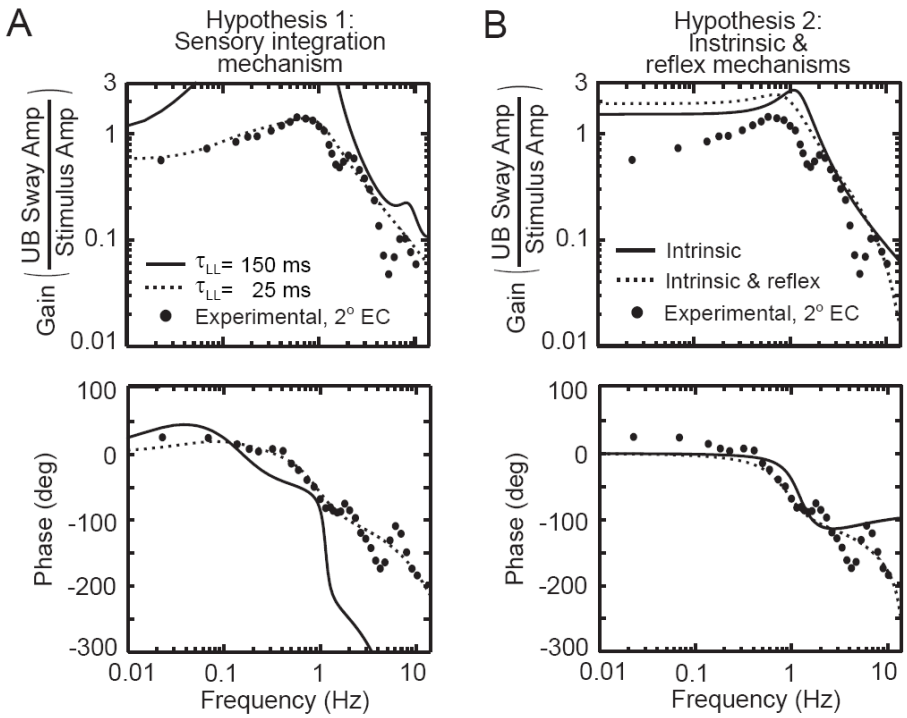


**FIG. 2.9.** *Hypothesis testing using simplified models of UB control. A: The hypothesis that UB control could be described through a single sensory integration mechanism was rejected because the model could only account for the general features in the experimental gain and phase curves with an unrealistically short time delay for sensory integration of 25 ms. B: The hypothesis that UB control could be described through only intrinsic and reflex mechanisms was rejected because the model could not account for any of the detailed features in the experimental gain or phase curves.*

outside of the physiologically range reported in literature, we rejected the hypothesis that a sensory integration mechanism alone is a reasonable explanation for UB control.

To test the hypothesis that control mechanisms used for UB postural control are dominated by mechanisms that act with little or no time delay (i.e. intrinsic stiffness and damping of joints, spinal ligaments, and muscles/tendons and local stretch reflexes), we explored two model variations. The first variation included only intrinsic stiffness and damping components that generated corrective torque with no time delay. The second variation included an additional reflex component that generated position and velocity-related torques with a finite time delay.

The equation of the model that included only intrinsic stiffness and damping components is given by

$$\frac{UBS}{PS} = \frac{B_{IN}\, s + K_{IN}}{Js^2 + B_{IN}\, s + (K_{IN} - mgh)} \tag{1.5}$$

where $B_{IN}$ is an intrinsic damping factor and all other parameters are the same as previously described. $K_{IN}$ and $B_{IN}$ were determined from the optimization routine. The intrinsic stiffness and damping mechanism provided a poor accounting for the experimental FRFs (Fig. 2.9B, solid curves). The model FRF gains for all frequencies less than 2 Hz were much larger than the experimental gains. Note that the low frequency gains predicted by Eq. 1.5 approach a value of $K_{IN}$ /( $K_{IN}$ - $mgh$) and therefore can never be less than one at low frequencies. If large values of $K_{IN}$ were selected in order to obtain low frequency model gains closer to experimental gains, the model was unable to account for the decline in gains with increasing frequency for frequencies greater than 1 Hz.

We explored the possibility that an additional short-latency reflex mechanism could improve the model prediction. The model equation for this system is

$$\frac{UBS}{PS} = \frac{B_{IN} s + K_{IN} + (B_{SL}\, s + K_{SL})\, e^{-\tau_{SL} s}}{Js^2 + B_{IN} s + K_{IN} - mgh + (B_{SL}\, s + K_{SL})\, e^{-\tau_{SL} s}} \tag{1.6}$$

where $K_{SL}$ and $B_{SL}$ are the position- and velocity-related reflex gains, respectively, and $\tau_{SL}$ is the reflex time delay. We determined $K_{IN}$, $B_{IN}$, $K_{SL}$, $B_{SL}$, and $\tau_{SL}$ from the optimization routine. Predictions of experimental FRFs were only slightly improved with the addition of the reflex mechanism but were still unable to account for overall gains or any detailed experimental FRF features (Fig. 2.9B, dotted curves). Thus, we rejected the hypothesis that UB control is accomplished using only mechanisms that act with little or no time delay.

## DISCUSSION

We evoked UB sway by applying continuous pseudorandom tilts of the pelvis (EO and EC conditions) and the visual surround at various amplitudes. UB sway from pelvis tilt tests were analyzed by calculating FRFs over a range of 0.023 to 10.3 Hz and IRFs. FRF gain and phase curves exhibited a characteristic shape with peaks at specific frequencies. Differences between FRFs obtained at different pelvis tilt amplitudes were limited to frequencies below 3 Hz (Fig. 2.3A and B). IRFs were nearly identical across all

pelvis tilt tests for the first 0.2 s, but showed changes in their time course at longer time lags that depended on the pelvis tilt amplitude. The availability of visual orientation cues (EO compared to EC) had only a small effect on the UB sway evoked by pelvis tilt stimuli. This small effect of vision was consistent with the small UB sway evoked by visual tilt stimuli. UB sway responses to visual tilts were analyzed by calculating FRFs over a frequency range of 0.43 to 1.5 Hz. These visual tilt FRFs were variable and showed overall low gains that decreased with increasing stimulus amplitude (Fig. 2.3C).

Experimental results were interpreted by developing a model that included feedback from 4 mechanisms: intrinsic stiffness (no time delay), short-latency phasic mechanism, medium-latency phasic sensory integration, and long-latency sensory integration. With appropriate selection of model parameters, the model was able to account for the detailed shapes of the FRF gain and phase curves and the time courses of the IRFs. We found that a number of parameters could be fixed across all test conditions. These included intrinsic stiffness, short-latency phasic gain, and all time delays. It was necessary to vary other parameters to account for changes in FRFs and IRFs as a function of stimulus amplitude. These parameters included medium-latency sensory gains, long-latency sensory weights, and long-latency neural controller parameters. All these variable parameters were part of what we called sensory integration mechanisms, because they affect how proprioceptive, visual, and vestibular orientation information are combined and used for UB control. Variation in model parameters indicated that subjects shifted toward reliance on sensory cues that oriented the UB vertical and away from sensory cues that oriented the UB toward the stimulus (pelvis tilt or visual surround tilt) as stimulus amplitudes increased.

The underlying cause of shifting reliance or reweighting from one sensory system to another is currently unknown, but two prominent theories exist. One theory suggests that the balance control system utilizes optimization principles to obtain the most accurate representation of body orientation in the presence of noisy sensory systems. Thus, in different environmental conditions the variability of orientation signals from different sensory systems differs and the balance control system shifts reliance toward sensory systems that would minimize ambiguity about body orientation (van der Kooij et al. 2001). The other theory suggests that sensory re-weighting is produced by thresholds involved in the central processing and fusion of signals from different sensory systems

(Maurer et al. 2006). In this theory, central threshold phenomena produce apparent gain changes without actually altering the sensitivity of central pathways.

*Experimental and modeling approximations and limitations*

The interpretation of our experimental results was aided by the development of a control system model that accounted for detailed features of the experimental data. Simplifications are necessarily required in model development. Here we discuss assumptions and limitations that were considered in the model development. We also discuss how experimental constraints may influence the general applicability of results.

In the current experiment, lateral displacement of the lower body and pelvis was prevented. This experimental setup isolated the UB and allowed for identification of UB control mechanisms. Although the modeling results showed that the experimental results could be explained by a control system that only utilized signals related to changes in orientation of the UB in space and relative to the pelvis or stationary lower body, we cannot rule out the potential contributions of additional sensory signals from the lower body. These contributions could include proprioception signaling changes in configuration of the lower body and sensory signals responding to vertical forces on the feet and horizontal forces at the hips caused by the hip restraint.

Because subjects' lower body was externally stabilized, the mechanisms of UB control identified in the current study might not be representative of UB control during freestanding where both the upper and lower body must be controlled together in a coordinated manner. It has been shown previously that the postural context can greatly affect the neural control systems contributing to postural responses (Cordo and Nashner 1982; Marsden et al. 1981). However, at the very least, our experimental results do reveal the nature of neural systems contributing to spinal stability and should be directly applicable to other situations, like seated posture.

The experimental UB sway angle was calculated with an axis of rotation located at the midpoint between the hip joints. This axis location was chosen because this is the actual axis about which the pelvis rotated and it provided an earth-fixed reference frame. However, in our experiment, support surface rotations produced translations of the L4/L5 joint and one could argue that a more accurate description of UB mechanics would be to

choose a reference frame that moved with the L4/L5 joint and to define the response variable as an UB rotation with respect to earth-vertical about the L4/L5 joint. A model describing this stimulus-response relationship would be the same as the Fig. 2.5 model, but would include an additional stimulus component representing the inertial torque evoked by translation of the L4/L5 joint. This inertial torque component would be added to the torques produced by the various feedback mechanisms at the summation point prior to the block representing the UB inverted pendulum.

The extent to which representations of our experimental data were altered by the choice of reference frame (i.e., UB sway with respect to the actual pelvis tilt axis or with respect to the L4/L5 joint axis) is illustrated in Fig. 2.10 which shows FRFs and IRFs calculated with the L4/L5 joint as the reference frame (estimate of the mean distance between the L4/L5 joint and midpoint of the hip joint centers was 12.2 cm). There are differences in FRFs across all frequencies for the different reference frames (compare Fig. 2.3A with Fig. 2.10A). However, the patterns of peaks and amplitude-dependent changes are similar. For the IRFs, the main difference is in the first 50 ms where the IRF calculated with the reference frame aligned with the L4/L5 joint axis shows an initial UB tilt velocity in a direction opposite to the pelvis tilt velocity. After about 50 ms, this oppositely directed UB tilt reverses and then follows a time course essentially identical to the time course shown for the IRFs calculated using the reference frame aligned with the actual pelvis tilt axis (Fig. 2.4). Note that for time lags greater than 50 ms, the amplitude of the IRFs in Fig. 2.4 are slightly smaller than the IRFs whose reference frame is the L4/L5 joint axis. This is simply due to fact that the distance from the mid-point between the hip joints to the UB center-of-mass is larger than the distance between L4/L5 and the UB center-of-mass. Therefore, a given UB center-of-mass displacement from upright corresponds to a larger angler tilt in the L4/L5 reference frame.

Because the medium- and long-latency mechanisms are the dominant contributors to shaping the time course of the IRFs at time lags greater than the medium-latency time delay, the fact that the time course of the IRFs calculated in the two reference frames are essentially identical indicates that the model-based identification of the medium- and long-latency mechanisms would not be influenced by the choice of reference frames.

Independent of the choice of reference frame, there is likely a greater uncertainty regarding the identification of the parameters that characterize the intrinsic and short-

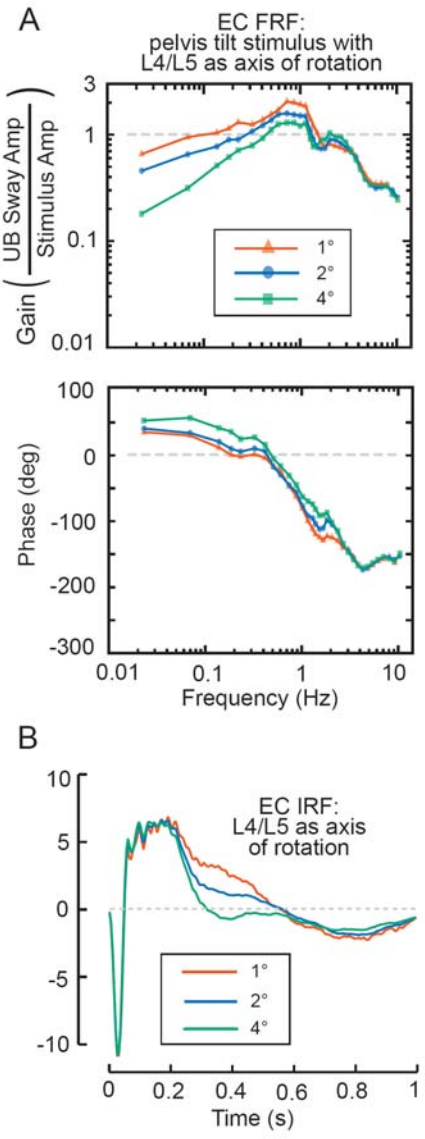


**FIG. 2.10.** *Experimental results of eyes closed pelvis tilt tests with the response variable defined as UB rotation with respect to earth-vertical about the L4/L5 joint. A: Experimental frequency-response with the L4/L5 joint as the reference frame show very similar patterns of UB sway as observed in Fig. 2.3A. B: The impulse-response function calculated with the L4/L5 joint as the reference frame only differed from the UB sway in Fig. 2.4A before the first 50 ms. After 50 ms, UB sway was essentially identical regardless of the reference frame chosen except for a slightly different scale factor due to the fact that the distance from the mid-point between the hip joints to the UB center-of-mass is larger than the distance between the L4/L5 and the UB center-of-mass.*

latency mechanisms. This is because the actual non-rigid, distributed spinal motion (causing a distributed time course of disk compression across spinal segments, stretching and relaxing muscles/tendons and evoking associated local stretch reflexes) would clearly influence the time course of corrective torque generation as spinal segmental motion played out over time in the time interval immediately following a perturbation. In particular, one could imagine that intrinsic muscle/tendon behavior would be better approximated by a combination of stiffness and damping factors. However, even though these intrinsic factors generate torque with zero time delay, the distributed spinal motion following a sudden pelvis tilt would effectively introduce a time delay as a traveling wave of motion propagates across spinal segments. One could also imagine that the short-

latency reflex could include both tonic and phasic components. But our inability to observe the detailed behavior of spinal segments limited our ability to make fine distinctions among these potential contributors to intrinsic and short-latency torque generation. Therefore, our model representation, using a single stiffness parameter $K_{IN}$ acting at zero delay and a phasic short-latency reflex acting at a single time delay, is an obvious approximation.

*Spinal stability*

INTRINSIC & SHORT-LATENCY MECHANISMS. The majority of previous studies in the field of spinal stability have focused on the role of passive or intrinsic stiffness of joints, spinal ligaments, and muscles/tendons (Brown and McGill 2009; Cholewicki et al. 2000b; Granata et al. 2004; McGill et al. 1994; Moorhouse and Granata 2007), local stretch reflexes (Granata et al. 2004; Moorhouse and Granata 2007; Skotte 2001; Solomonow et al. 1998), and muscle activations that alter intra-abdominal pressure (Cholewicki et al. 1999; Cresswell et al. 1994; McGill et al. 1994). Most of these previous studies applied a sudden external perturbation to the UB to acquire experimental measures of the UB sway, reactive force, or EMG. Mechanisms contributing to spinal stability were quantified by identifying parameters of models that were assumed to represent the biomechanics and control of UB system. Typically these models only included mechanisms consisting of intrinsic stiffness and damping terms (Brown and McGill 2009; Cholewicki et al. 2000b; Gardner-Morse and Stokes 2001) or a combination of intrinsic and reflex mechanisms (Granata et al. 2004; Moorhouse and Granata 2007). To the extent that these previous modeling studies obtained estimates of model parameters, we found poor correspondence between our results and the previous studies, and poor correspondence within the previous studies.

In one study (Cholewicki et al. 2000b), standing subjects were given a sudden torque that evoked UB sway. Intrinsic stiffness, estimated from a model fit, was found to be about 10 times larger than the current study. We cannot account for this large difference.

In a second study (Brown and McGill 2009), the UB of subjects in a supine position were perturbed by a sudden torque that evoked UB sway relative to the pelvis of about 10° in one second. Intrinsic stiffness was estimated from a model fit to the UB

sway data. The intrinsic stiffness parameter was estimated to be about 2.5 times larger than the intrinsic stiffness in the current study. One factor contributing to this larger intrinsic stiffness estimate could be the large 10° UB sway. This sway is about 5 times larger compared to the current study. Intrinsic stiffness estimates have been shown to increase exponentially with increasing UB tilt angles (McGill et al. 1994). Therefore, the value of a stiffness parameter estimated from a perturbation causing a large amplitude sway should be larger than the value estimated from a perturbation causing a small amplitude sway. Another explanation for the larger estimate of intrinsic stiffness could be that a full second of UB sway data following the perturbation was used to fit model parameters. Based on our results, sensory integration mechanisms as well as intrinsic stiffness and reflexes would have contributed to UB sway over a 1 s time course. Parameter estimates can be biased when a simplified model structure is assumed for a system that is, in fact, more complex (Perreault et al. 2000). A final factor potentially contributing to the different results could be the very different contexts of the experiments (Cordo and Nashner 1982; Marsden et al. 1981).

A third study (McGill et al. 1994) estimated $K_{IN}$ by measuring the resisting torque during slow passive rotational displacements of the UB relative to the pelvis of supine, relaxed subjects. It was found that $K_{IN}$ increased exponentially with UB displacement, but for small angle displacements that correspond to UB tilts in the current study, the measured $K_{IN}$ was about one third the value of the $K_{IN}$ parameter identified in the current study. Several factors likely account for this difference. Muscles were in a relaxed state in this previous study while trunk muscles were almost certainly activated throughout the current study. Intrinsic stiffness would be expected to be larger in activated muscles (Hogan 1990; Kandel et al. 2000). Also, subjects were supine in this previous study but were in an upright position in the current study. Gravitational loading of the spinal column will compress the spinal disks and likely change their elastic properties (Koeller et al. 1984). Finally, as previously discussed, we do not have high confidence that our methods were able to reliably distinguish between intrinsic and short-latency mechanisms. Therefore, our $K_{IN}$ parameter value may have included a contribution from a tonic short-latency stretch reflex mechanism.

Our model attributed the short-latency mechanism entirely to a phasic signal of UB sway. A likely source of this phasic signal is muscle spindles innervated by group 1a

afferents (Pierrot-Deseilligny and Burke 2005) and sensory receptors in spinal ligaments (Solomonow et al. 1998). The short-latency time delay ($\tau_{SL}$) identified in the current study is 25 ms. This time delay represents all delays in the reflex loop and would include afferent and efferent transmission, spinal synaptic delay, muscle activation delay, and the delay between muscle activation and force generation. Although one study showed EMG onset delays as short as 11 ms in paraspinal muscles of the low back following mechanical taps of these muscles (Skotte et al. 2005), other studies have shown longer EMG onset delays of 24 to 65 ms (Cresswell et al. 1994), 53 ms (Radebold et al. 2000) and 70 ms or more (Preuss and Fung 2007) in various trunk muscles following sudden UB perturbations. Because EMG onset delays do not include the added delay to force onset, our model-derived delay of 25 ms appears to be rather short. As with our estimate of $K_{IN}$, which may include a contribution from the tonic component of a stretch reflex, it is possible that the short-latency gain factor $B_{SL}$ represents contributions from both a true phasic reflex component and an intrinsic damping component arising from the force-velocity properties of skeletal muscle. This dual contribution from one component with a finite time delay and a second component without delay may account for the short 25 ms delay identified in our model.

SENSORY INTEGRATION MECHANISMS. The contribution of sensory integration to spinal stability previously has been inferred from studies that compared eyes open to eyes closed responses (Radebold et al. 2001; Reeves et al. 2006), applied galvanic vestibular stimulation (Ali et al. 2003; Blouin et al. 2007; Day et al. 1997), and demonstrated the ability of subjects to maintain UB balance while sitting on an unstable seat (Cholewicki et al. 2000a; Preuss et al. 2005; Radebold et al. 2001; Reeves et al. 2006). The current study extends previous spinal stability research by quantitatively characterizing the contribution of sensory integration mechanisms to spinal stability.

One hypothesis in the current study was that UB postural control mechanisms would be essentially identical to whole body postural control which previously had demonstrated a dominant role of a sensory integration mechanism (Cenciarini and Peterka 2006; Peterka 2002) and a relatively minor role of intrinsic mechanisms (about 10% of corrective torque). This previous work showed that the sensory integration mechanism could be represented as a negative feedback control system that generated

corrective torque in relation to a weighted combination of proprioceptive, vestibular, and visual orientation cues. There was a substantial feedback time delay of 150 to 200 ms in this control system suggesting an important role of central processing of sensory orientation information. This large feedback delay did not jeopardize the controllability of the whole body system.

The experimental UB FRF and IRF data could not be adequately explained by a sensory integration mechanism of the same form as used to explain whole body control. An optimal fit of a sensory integration model could account for the general form but not the specific shapes of FRFs and IRFs (Fig. 2.9A). However, the time delay parameter in these fits always converged to an unrealistically small value of about 25 ms. Such a short time delay is not compatible with the time needed for the complex processing of visual (Reynolds and Day 2005; Soechting and Lacquaniti 1983) and vestibular (Merfeld and Zupan 2002) orientation information, and for the spinal transmission and muscle activation required for UB control. Therefore, we concluded that UB control could not be represented by control mechanisms of the same functional form as previously shown to account for whole body postural control.

To account for the detailed shapes of UB FRFs and time courses of IRFs we found it necessary to include two mechanisms that could be defined as sensory integration mechanisms in that they both represented mechanisms that generate corrective torque in relation to combined orientation information from different sensory systems. We referred to these two mechanisms as medium- and long-latency mechanisms based on the identified value of the time delays associated with these two mechanisms, but there were other characteristics that distinguished these mechanisms from one another. Specifically, the medium-latency mechanism generated corrective torque in relation to only phasic, velocity-related UB sway whereas the long-latency mechanism generated torque in relation to position, velocity, and the time integral of position. These two sensory integration mechanisms were similar to one another in that values of the identified gain and sensory weighting factors that represented the visual contribution to both mechanisms were quite small.

The long-latency mechanism in our UB model had the same functional form as the sensory integration mechanisms used to describe whole body postural control. However, the identified long-latency time delay was about 0.28 s, which is about 0.1 s

longer than the time delay for whole body control (Cenciarini and Peterka 2006; Peterka 2002). A motor action with a time delay on the order of 0.28 s is often considered to be indicative of a voluntary control mechanism (Ghez and Krakauer 2000). However, we note that the test subjects were not given specific instructions on how to respond to the presented stimuli, and they were in fact presented with a distracting audio task of listening to a recorded story. Furthermore, the responses of all subjects were similar in that a long-latency mechanism was required to account for the experimental data of all subjects, and the relative contribution provided by this mechanism to the overall corrective torque was similar across subjects. Therefore, it seems reasonable to consider the long-latency mechanism to be a component of the overall automatic UB control system. Furthermore, the long-latency mechanism we identified appears to be consistent with results from a previous study (Day and Cole 2002) that evoked UB responses with galvanic vestibular stimulation in seated subjects. This study showed UB responses with a long onset delay of 240 ms that were modified by the availability of visual and somatosensory orientation information. Future experiments that request the subject to perform specific behaviors during testing, such as resist the perturbation, relax the UB, or align the UB to the stimulus could be used to determine whether voluntary control will simply modify the contribution of the long-latency mechanism, or whether an additional mechanism will be needed to account for voluntary behavior.

Our model-based interpretation of the experimental results indicated that all of the amplitude-dependent changes in response dynamics were attributable to changes in the medium- and long-latency sensory integration pathways and there were no contributions to these changes from the intrinsic stiffness and short-latency reflex mechanisms. However, results from previous studies have shown changes in UB response characteristics related to changes in intra-abdominal pressure (Cholewicki et al. 1999; Cresswell et al. 1994) and to voluntary changes in the activation levels of trunk muscles (Cholewicki et al. 2000b; Gardner-Morse and Stokes 2001; Granata et al. 2004; Moorhouse and Granata 2007) both of which would be expected to result in changes in intrinsic trunk stiffness. Although the current experiments showed no changes in intrinsic stiffness or reflex contributions across test conditions, it seems likely that more complex situations could evoke compensatory changes in all four mechanisms.

In the current study stimulus-related changes in the sensory integration mechanisms were represented by the changes in the medium-latency gain factors ($B_{V1}$ for EC pelvis tilt tests or $B_{V1} + B_{V2}$ for EO tests), and by changes in the long-latency sensory weights ($W_{P1}$, $W_{V1}$, $W_{V2}$). The long-latency sensory weights represented the relative contribution of the different sensory systems to UB control such that $W_{P1} + W_{V1} + W_{V2} = 1$. Independent of the specific combination of sensory weight values in a given test condition, the combined long-latency sensory signal produced a corrective torque as a function of the values of the neural controller parameters $K_P$, $K_D$, and $K_I$. The modeling results indicated that there were small increases in $K_P$ and $K_I$ with increasing pelvis tilt amplitude while $K_D$ remained nearly constant, similar to the neural controller changes seen in whole body control (Peterka 2002). Also similar to results for whole body control was the shift toward increased reliance on sensory systems that orient the body vertical with increasing stimulus amplitude. For the EC pelvis tilt stimulus, this shift was represented by an increased value of $W_{V1}$ (and a corresponding decrease in $W_{P1}$), and by an increased value of $B_{V1}$. It was not possible to distinguish between the inter-segmental proprioceptive and vestibular contributions to $W_{V1}$. For the EO pelvis tilt stimulus, a similar shift away from utilization of pelvis-orienting proprioceptive information occurred although with this stimulus it was not possible to determine whether the reduced reliance on pelvis-orienting proprioceptive information was accompanied by an increased reliance on $W_{V1}$ or a combination of $W_{V1}$ and $W_{V2}$ because visual, vestibular, and inter-segmental proprioceptive information provide equivalent orientation information in the EO condition. Finally, for the visual tilt stimulus, there was a shift away from utilization of visual information and toward increased use of vestibular and/or proprioceptive information with increasing visual tilt amplitude.

To understand which frequencies of UB sway were most impacted by the medium- and long-latency sensory integration mechanisms, we performed a sensitivity analysis of the model parameters $B_{V1} + B_{V2}$ or $W_{P1} + W_{V1} + W_{V2}$ on the pelvis tilt stimulus FRFs. Variations in these model parameters only impacted FRFs over a specific range of frequencies. In particular, the sensitivity analysis showed that the long-latency mechanism had its main influence on UB sway at frequencies below 2.5 Hz, with almost no impact at frequencies greater than 3 Hz. The medium-latency mechanism influenced UB sway between 0.5-2.5 Hz, with no impact on UB sway at frequencies less than 0.25

Hz or greater than 3 Hz. The fact that the sensory integration mechanisms did not impact UB sway at frequencies greater than 3 Hz is not surprising because the experimental FRFs (Fig. 2.3A and B) did not vary across pelvis tilt test condition above 3 Hz. The result that the medium-latency sensory integration mechanism did not impact UB sway at frequencies below 0.25 Hz implies that the gain reductions with increasing pelvis tilt at frequencies below 0.25 Hz are entirely attributable to the long-latency sensory re-weighting mechanism.

The medium-latency phasic sensory integration mechanism in the UB control model had no counterpart in previous models of whole body postural control (Cenciarini and Peterka 2006; Peterka 2002). Our model-based interpretation of the current results indicated that the vertical orienting contribution ($B_{V1}$) to the medium-latency mechanism was by far the largest, there was only a small visual contribution, and no pelvis-orienting proprioceptive contribution. Specifically, during visual tilt tests, the estimated value of an average subject's $B_{V1}$ parameter was 120 times larger $B_{V2}$. In EO pelvis tilt tests, the estimated value of $B_{V1}+B_{V2}$ was only 8% larger than the $B_{V1}$ value estimated from EC pelvis tilt tests.

A postural control system requires both position-related and velocity-related feedback in order to have good dynamic properties and to avoid resonant behavior and instability. Velocity-related feedback provides system damping. Our model-based analysis indicated that the medium-latency mechanism provided a large portion of the overall damping. The overall damping can be represented by the sum of all velocity-related feedback gain factors from long-, medium-, and short-latency mechanisms ($K_D+B_{V1}+B_{V2}+B_{SL}$ for visual tilt and EO pelvis tilt tests, and $K_D+B_{V1}+B_{SL}$ for EC pelvis tilt tests). Based on the average of model parameters across subjects, the medium-latency mechanism contributed between 53% (on visual tilt tests) to 70% (on EC 4° amplitude pelvis tilt tests) of the overall UB damping.

The relative contribution of inter-segmental and vestibular inputs to spinal stability could have important implications for subjects with bilateral vestibular loss. If inter-segmental proprioceptive signals only have a limited contribution to spinal stability in comparison to the vestibular contribution, then vestibular loss should have a large impact on spinal stability. Alternatively, if inter-segmental proprioception provides the dominant contribution or its contribution was enhanced to compensate for vestibular loss,

then a vestibular loss would have little or no effect on spinal stability. We used our UB model to investigate the effects of a total bilateral vestibular loss (BVL) on spinal stability in an EC condition under the assumption that contributions to $B_{VI}$ and $W_{VI}$ were entirely vestibular. Specifically, BVL was represented in the model by setting the parameters $W_{VI}$ and $B_{VI}$ to zero, thus resulting in a model that included only intrinsic stiffness, short-latency, and long-latency mechanisms. Furthermore, the sensory weights in the long-latency mechanism were set to values that indicated total reliance on pelvis-orienting proprioceptive information ($W_{PI}$=1, $W_{VI}$ = $W_{V2}$ =0). All remaining EC BVL model parameters were set to those of the average normal subject.

Results from the EC BVL model predicted that the UB control system is unstable. This instability was mainly due to the loss of system damping from the medium-latency mechanism. Given that BVL subjects are not obviously disabled to the extent that their UB collapses, then either 1) the medium-latency mechanism is not completely dependent on vestibular inputs, but rather receives both vestibular and inter-segmental proprioceptive inputs or only inter-segmental proprioceptive inputs or 2) BVL subjects are able to compensate for their vestibular loss by adjusting the remaining control mechanisms. We explored this later possibility to determine if stability could be regained by alteration of available control parameters.

Various combinations of increases in $B_{SL}$, $K_D$, and $K_{IN}$ were found that restored stability or contributed to improved control behavior once stability was restored. Given that the model predicted that BVL would cause a loss of system damping, it was not surprising that an increase in $B_{SL}$ alone could restore stability. It was necessary to increase $B_{SL}$ by a factor of 2.9 to restore stability. However, with this increase alone the FRF showed severe resonant behavior. A further increase of $B_{SL}$ to a factor of 6 times the mean value shown in Table 2.1 reduced the resonant properties of the FRF (Fig. 2.11, solid lines). If $K_{IN}$ was also allowed to increase, an FRF with similar characteristics could be found with a slightly lower $B_{SL}$ value ($B_{SL}$ x 5 and $K_{IN}$ x 2.5 the mean values shown in Table 2.1, Fig. 2.11, dotted lines). Adjustments in $K_D$ provided no benefit even though $K_D$ is also a damping factor. This is likely due to the long time delay of motor action via the long-latency mechanism.

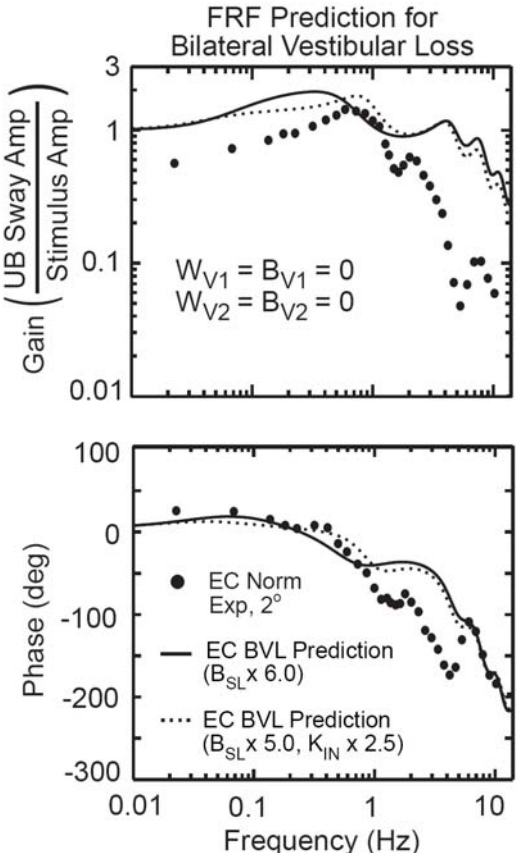


**FIG. 2.11.** *Two predictions of pelvis tilt frequency-response functions in eyes closed (EC) condition following bilateral vestibular loss. Predictions assumed contributions to $W_{V1}$ and $B_{V1}$ are entirely of vestibular origin and therefore $W_{V1} = B_{V1} = 0$; and in EC conditions, $W_{V2} = B_{V2} = 0$. Presumed compensation occurred by either increasing short-latency phasic gain ($B_{SL}$) by 6 times the mean value in Table 1.1 or by a combination of increased $B_{SL}$ by 5 times and intrinsic stiffness ($K_{IN}$) by 2.5 times the mean values in Table 2.1.*

Our manipulations of the EC BVL model imply if contributions to $B_{V1}$ were entirely vestibular, then BVL subjects could achieve stable UB control by increasing the contribution of the short-latency phasic mechanim, potentially by enhancing stretch reflex gain, and by increasing intrinsic stiffness, potentially by co-contraction of trunk muscles or by activation of muscles that can elevate intra-abdominal pressure. In an EO condition, enhancement of the normally small visual medium-latency contribution to UB control would obviously provide an effective compensation for BVL. These predictions are specifically tested in chapter three of this dissertation.

# CHAPTER III.
# INFLUENCE OF BILATERAL VESTIBULAR LOSS ON SPINAL STABILIZATION IN HUMANS


## ABSTRACT

The control of upper body (UB) orientation relative to the pelvis in the frontal plane was characterized in bilateral vestibular loss subjects (BVLs) and compared to healthy control subjects (Cs). UB responses to external perturbations were evoked using continuous pelvis tilts (eyes open and eyes closed) at various amplitudes. Lateral sway of the lower body was prevented on all tests. UB sway was characterized with frequency-response functions (FRFs) from 0.023 to 10.3 Hz. Both subject groups had similar FRF variations across stimulus frequency and were relatively unaffected by visual availability, indicating that visual cues contributed little to UB control. BVLs had larger UB sway at frequencies below ~1 Hz compared to Cs. A feedback model of UB control was used to identify contributions to spinal stability and differences between subject groups. The model-based interpretation indicated that a phasic proprioceptive signal encoding the angular velocity of UB relative to lower body motion was a major contributor to overall system damping. Parametric system identification showed that BVLs used proprioceptive information that oriented the UB toward the pelvis to a greater extent compared to Cs. Both subject groups used sensory information that oriented the UB vertical in space to a greater extent as pelvis tilt amplitudes increased. In BVLs, proprioceptive information signaling the UB orientation relative to the fixed lower body provided the vertical reference while in Cs, vestibular information also contributed to the vertical reference.



Goodworth AD and Peterka RJ. Influence of bilateral vestibular loss on spinal stabilization in humans. *J Neurophysiol*, in press, 2010, used with permission.

## INTRODUCTION

Control of upper body (UB) segment orientation is essential to everyday behaviors such as stabilizing the trunk during sitting (Reeves et al. 2007) and bipedal stance. Poor bipedal stance control is often accompanied by poor UB control (Carpenter et al. 2001; Creath et al. 2008) and improper stabilization of the UB may be associated with chronic back pain (Radebold et al. 2001; Reeves et al. 2007). Stabilization of the UB with respect to the pelvis in the frontal plane is synonymous with spinal stabilization because rotational motion of the UB is often considered to occur about the L4/L5 spinal joint (Brown and McGill 2009; Cholewicki et al. 2000b; McGill et al. 1994; Zhao et al. 2008). There is evidence that sensory integration of proprioceptive, visual, and vestibular information contribute to spinal stability (Day et al. 1997; Goodworth and Peterka 2009; Radebold et al. 2001; Reeves et al. 2006). It is also recognized that reflexive and biomechanical mechanisms (i.e., intrinsic mechanical stiffness and damping inherent in joints, spinal ligaments, and muscles/tendons in the trunk-pelvis musculoskeletal system which can be altered by cocontraction and intraabdominal pressure) contribute to spinal stability (Brown and McGill 2009; Cholewicki et al. 1999; Cresswell et al. 1994; Goodworth and Peterka 2009; Moorhouse and Granata 2007; Solomonow et al. 1998).

However, to our knowledge, only one recent study has attempted to understand the combined influences of these interacting mechanisms (Goodworth and Peterka 2009; Chapter 2). In this previous study, frontal plane UB sway was evoked using continuous tilts of the pelvis and tilts of a visual surround which subjects faced, while lower body sway was prevented. Experimental results were accounted for with a model that included time-delayed medium- and long-latency sensory integration mechanisms, a short-latency reflexive mechanism, and intrinsic biomechanical properties of the UB.

One important prediction made by the model was that a major contribution to overall system damping was attributable mainly to a mechanism we referred to as a medium-latency phasic sensory integration mechanism. Sensory inputs to this mechanism included vestibular and/or inter-segmental proprioception. Furthermore, the model predicted that removal of this mechanism would result in instability without major compensatory changes in other mechanisms contributing to spinal stability. Specifically, we postulated that some combination of increased intrinsic stiffness and an enhanced

contribution of a short-latency phasic reflex mechanism would be necessary to compensate for loss of the vestibular contribution to UB control. Because both of these mechanisms tend to orient the UB toward the pelvis, an enhancement of intrinsic stiffness and reflex contributions would make the UB more responsive to pelvis tilt stimuli over a wide bandwidth of input stimulus frequencies. Therefore, if the medium-latency mechanism was primarily composed of vestibular inputs as originally postulated (Goodworth and Peterka 2009), the dynamic characteristics of UB control in bilateral vestibular loss subjects (BVLs) would differ considerably from subjects with normal vestibular function.

Therefore, the first goal of the present study was to test our predictions regarding the vestibular contributions to spinal stability by investigating the dynamic characteristics of UB control in BVLs. We tested BVLs in an experimental setup identical to the previous study (Goodworth and Peterka 2009; Chapter 2). If the medium-latency mechanism is primarily attributable to a vestibular source, then we expected BVLs to exhibit altered UB control dynamics due to compensation provided by increased intrinsic stiffness and short-latency reflex gains (Fig. 2.11 in Chapter 2). Alternatively, if the medium-latency mechanism is primarily attributable to an inter-segmental proprioceptive source or if the inter-segmental proprioceptive contribution was enhanced to compensate for vestibular loss, then UB sway behavior would not differ between BVLs and healthy control subjects (Cs).

The second goal of the current study was to characterize the nature of compensatory mechanisms adopted by BVLs using parametric system identification techniques. Parametric system identification involves the determination of model parameters based upon experimental data where model parameters represent specific neural or biomechanical systems. By comparing parameter values between BVLs and Cs, we can quantify differences in the underlying mechanisms of spinal stability between subject groups. By analogy to results in whole body sway, we predicted that BVLs would have a heightened reliance upon proprioceptive information in eyes closed (EC) conditions and would make greater use of visual information in eyes open (EO) conditions (Nashner et al. 1982; Peterka 2002; Horak 2009). More specifically, we expected that in EC conditions the parameters which characterize the contributions of sensory orientation information in the sensory integration mechanism (i.e. sensory

weights) would show that BVLs rely exclusively on proprioceptive signals that encode UB sway with respect to the pelvis, and that this proprioceptive weighting factor would not change with changing pelvis tilt amplitude. Parametric system identification results could also identify other possible compensation mechanisms such as heightened intrinsic stiffness and/or reflexive gains.

## METHODS

*Subjects*

Three BVLs (mean height 175 cm ± 14 SD, mean mass 77 kg ± 10 SD, additional details in Table 3.1) participated in this experiment. Experimental data from eight Cs (3 male, 5 female, mean age 31 ± 5 SD, mean height 169 cm ± 6 SD, mean mass 70.6 kg ± 11 SD) with no history of balance disorders were collected for our previous study (Goodworth and Peterka 2009). A subset of these previous results was used to compare with results obtained from BVLs in the current study. All subjects gave their informed consent prior to being tested using a protocol approved by the Institutional Review Board at Oregon Health & Science University.

**TABLE 3.1.** *Bilateral vestibular loss (BVL) subject information*

| **Subject** | BVL1 | BVL2 | BVL3 |
|---|---|---|---|
| **Gender** | M | F | M |
| **Age** | 36 | 44 | 53 |
| **Duration of loss (yrs)** | 4 | 13 | 5 |
| **Cause of loss** | unknown | unknown | unknown |
| **HVOR gain (0.05 Hz)** | 0.01 | 0.00 | 0.01 |
| **HVOR gain (0.2 Hz)** | 0.02 | 0.00 | 0.04 |
| **HVOR gain (0.8 Hz)** | 0.10 | 0.06 | 0.12 |
| **Eyes closed surface Sway referencing** | fell | fell | not tested |

*Normal horizontal vestibular ocular reflex (HVOR) range is 0.39-1.02 for 0.05 Hz, 0.40-1.02 for 0.2 Hz, and 0.59-1.07 for 0.8 Hz (Peterka et al. 1990). Surface sway-referencing is a balance test whereby the surface rotates in direct proportion to the body sway angle. This test greatly reduces the contribution of proprioceptive information to balance control.*

*Stimulus and data collection*

Stimuli and data collection were previously described in detail (Goodworth and Peterka 2009) and is briefly described below. Frontal plane perturbations of the UB were

evoked using continuous pelvis tilts elicited by rotating the surface that subjects stood on. Lateral displacement of the pelvis and lower body was prevented using a rigid frame with two roller carriages that pressed against the greater trochanters (Fig. 3.1A). The roller carriages permitted vertical motion of the hips but prevented lateral movement. The visual surround was stationary on all tests and was lined with a complex checkerboard pattern of white, black, and three gray levels.

The surface rotation angle was controlled by a servo motor and the surface axis of rotation was halfway between the subjects' heels and was at ankle height. The distance between the middle of each subject's heels (mean of 17.9 cm ± 1.3 SD for BVLs and 17.1 cm ± 1.3 SD for Cs) was set to be equal to the distance between his/her hip joint centers as estimated using a regression equation relating hip-joint distance to inter-ASIS distance (Seidel et al. 1995), so that the lower body formed an approximate parallelogram. The lower body parallelogram mechanics enabled pelvis rotations to equal the surface rotations assuming no knee-joint motion.

In all experiments, stimulus delivery and data sampling occurred at 200 Hz. Pelvis stimuli were presented continuously according to a pseudorandom stimulus which had a power spectrum of stimulus velocity with approximately equal amplitude spectral components ranging from 0.023 Hz to about 16.7 Hz. The angular position waveform of pelvis stimuli was scaled to a specific peak-to-peak value for each stimulus condition and was used to drive the surface rotation. The stimulus waveform consisted of eight repeating cycles on the lowest stimulus amplitude test and seven repeating cycles on the remaining tests. Each stimulus cycle lasted 42.72 s.

Sampled data included the actual surface angular position, UB displacements in the frontal plane, and vertical leg displacements at knee level. The UB and vertical knee displacement data were collected with rods that were fixed to the upper back between the C6 and T3 vertebrae and the back of the knee, respectively. Rotational motion of each rod was recorded by a potentiometer. The vertical leg displacements were analyzed to ensure that subjects maintained straight knees on all tests and that the surface rotational motions were accurately transmitted to produce vertical leg displacements. We assumed that leg displacement motion was accurately transmitted to produce pelvis rotations. The upper trunk displacements were used to calculate the angular UB tilt with respect to

earth-vertical. The angular UB tilt was considered to be the response variable that was compared to the pelvis tilt stimulus.

*Protocol*

BVLs performed a total of 8 tests in a single test session lasting about 2 hours. The test session included 2 quiet stance tests with either eyes open (EO) or eyes closed (EC) where no stimulus was given and 6 pelvis tilt tests with 1, 2, or 4º peak-to-peak amplitudes with either EO or EC. These 8 tests were randomized to offset potential biases due to fatigue and learning. Each test lasted approximately 5½ minutes and subjects were given the opportunity to rest after every test. Prior to beginning the test session, subjects "warmed-up" with an EC 2º stimulus amplitude test to become acquainted with the stimulus conditions.

Subjects were informed that there was no danger of falling and were instructed to maintain straight knees throughout the test and allow their UB to respond naturally. Subjects wore headphones and listened to their choice of novels or short stories to mask environmental equipment sounds and to maintain alertness.

*Frequency domain analysis*

Frequency domain analyses were previously described in detail (Goodworth and Peterka 2009) and are briefly described below. Frequency-response functions (FRFs) were determined for each subject and test condition and were defined as the ratio of the discrete Fourier transform of the UB sway response to the discrete Fourier transform of the pelvis tilt stimulus (Pintelon and Schoukens 2001). FRFs were calculated for each stimulus cycle (except the first cycle in order to avoid transient behavior) and were then smoothed by first averaging FRFs over the stimulus cycles, and then averaging FRFs across adjacent frequency points. An increasing number of adjacent points were averaged with increasing frequency (no averaging at the lowest two frequencies and 30 points averaged at the highest frequency) to reduce the variance of estimates at higher frequencies while maintaining adequate frequency resolution (Otnes and Enochson 1972). The final FRF estimates were approximately equally spaced on a logarithmic frequency scale ranging from 0.023 to 10.3 Hz (the upper frequency range was limited by the signal-to-noise ratio of the experimental data).

Each FRF was expressed as a set of gain and phase values that varied with frequency. Each gain value indicated the ratio of the UB response amplitude to the stimulus amplitude at its particular frequency and each phase value indicated the relative timing of the response compared to the stimulus expressed in degrees. A gain of one and phase of zero at a particular frequency indicated perfect alignment of the UB to the pelvis tilt stimuli with no lead or lag in timing. Mean gain and phase curves were computed by first averaging the real components and imaginary components of FRFs across subjects and then calculating gains and phases. Mean FRFs for Cs include 95% confidence intervals that were determined using the percentile bootstrap method with 1000 bootstrap samples at each stimulus frequency (Zoubir and Boashash 1998).

Coherence functions measured the extent to which the UB sway response was linearly related to the pelvis tilt stimulus. Coherence function values varied from 0 to 1, with values of 1 indicating a perfect linear relationship between stimulus and response with no noise in the system or measurements (Bendat and Piersol 2000). We estimated coherence functions via power spectra and cross-power spectral calculations, as previously described (Peterka 2002).

*Modeling and parameter estimation*

To quantify differences in the underlying UB control system between BVLs and Cs, parametric system identification techniques were carried out based on an existing model of frontal plane spinal stability (Goodworth and Peterka 2009). Model parameters representing biomechanical properties of the trunk-pelvis system and neural control mechanisms were estimated from experimental results using a constrained nonlinear optimization routine 'fmincon' (Matlab Optimization Toolbox, The MathWorks, Natick, MA) to minimize the total mean-squared-error (*MSE*) of the normalized difference between model FRFs and experimental FRFs (Peterka 2002). Because only three BVLs were tested, the highest frequency FRF data contained too much noise, consistent with lower coherences, to confidently include in the model fits. Therefore, FRF data above 5.75 Hz were not included in model fits to both Cs and BVLs. Consistent with parameter estimation procedures previously described (Goodworth and Peterka 2009), we found that it was necessary to allow the neural controller parameters, medium-latency inter-segmental gain, and long-latency weights to vary across test conditions. Intrinsic

stiffness, short-latency phasic gain, and all time delays were not allowed to vary across test conditions. The rationale behind fixing these model parameters across test conditions was based upon impulse response function analyses (see Goodworth and Peterka 2009 for detailed description). The time course of impulse response functions at latencies prior to a fixed time delay did not show changes across test conditions, consistent with a fixed contribution of intrinsic stiffness and short-latency reflexes. Mean model parameters for Cs include 95% confidence intervals determined from model fits to 1000 FRF bootstrap samples (Zoubir and Boashash 1998).

*ANOVA statistics*

Repeated-measures ANOVAs were used to determine if stimulus amplitude, visual availability (EO compared to EC), and subject group (BVLs compared to Cs) had statistically significant effects. Stimulus amplitude was a continuous variable in the statistical model and null hypothesis rejection was set to $p < 0.05$ for all tests. Data from Cs were obtained from our previous study (Goodworth and Peterka 2009).

## RESULTS

*Upper body sway evoked by pelvis tilt stimuli*

Pelvis tilt stimuli and the UB responses for one exemplary BVL subject are shown in Fig. 3.1B. The UB sway response waveforms generally followed the pelvis tilt stimulus (similar to Cs (Goodworth and Peterka 2009)), meaning that subjects tended to align their UB to their pelvis, and root-mean-square (RMS) sway significantly increased with increasing tilt amplitude. There was minimal qualitative difference between EO and EC sway responses consistent with the finding that visual availability did not have a significant effect on RMS sway in either subject group (Fig. 3.1C). RMS sway was significantly different between subject groups with BVLs having larger RMS sway compared to Cs. There was also a significant interaction effect between subject group and stimulus amplitude related to the fact that increasing stimulus amplitude resulted in larger increases in RMS sway in BVLs compared to Cs.

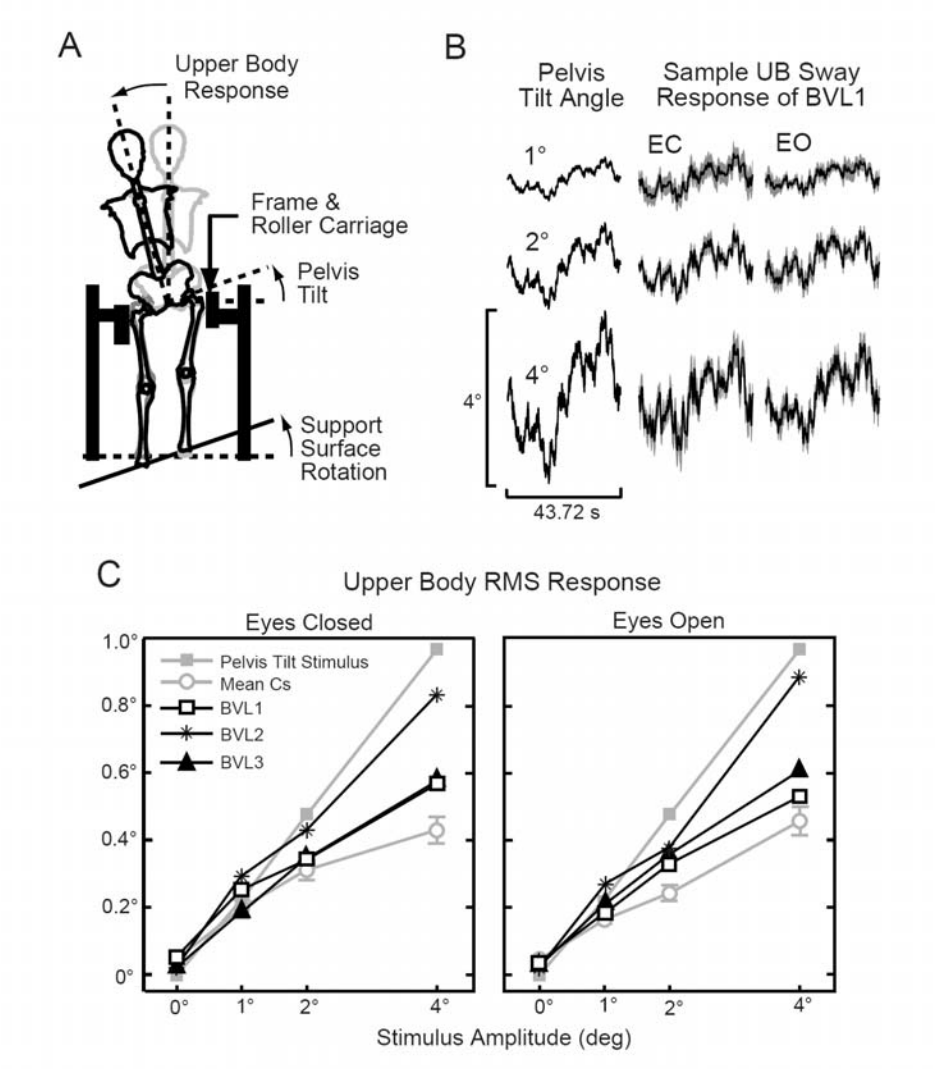


**FIG. 3.1.** *Upper body (UB) sway responses to pelvis tilt stimuli. A: Surface rotations produced pelvis tilts that evoked UB sway while the lower body was prevented from moving laterally. B: Mean (± 95% confidence intervals) UB sway from one bilateral vestibular loss (BVL) subject. C: Root-mean-square (RMS) UB sway as a function of stimulus amplitude for individual BVLs and the mean (± 1 SE) of control subjects (Cs).*

*Dynamic UB sway behavior*

FRF GAINS. The variation across frequency of FRF gains was similar across stimulus amplitudes and EO/EC conditions for both BVLs and Cs (Fig. 3.2, top row). Gains in the 0.02 to 0.6 Hz range increased with increasing frequency to reach a peak value around 0.6 to 0.9 Hz. Gains decreased rapidly above 1 Hz, showed a minor peak around 2-2.5 Hz, deceased rapidly again for frequencies greater than 3 Hz, and then showed another minor peak at about 8 Hz.

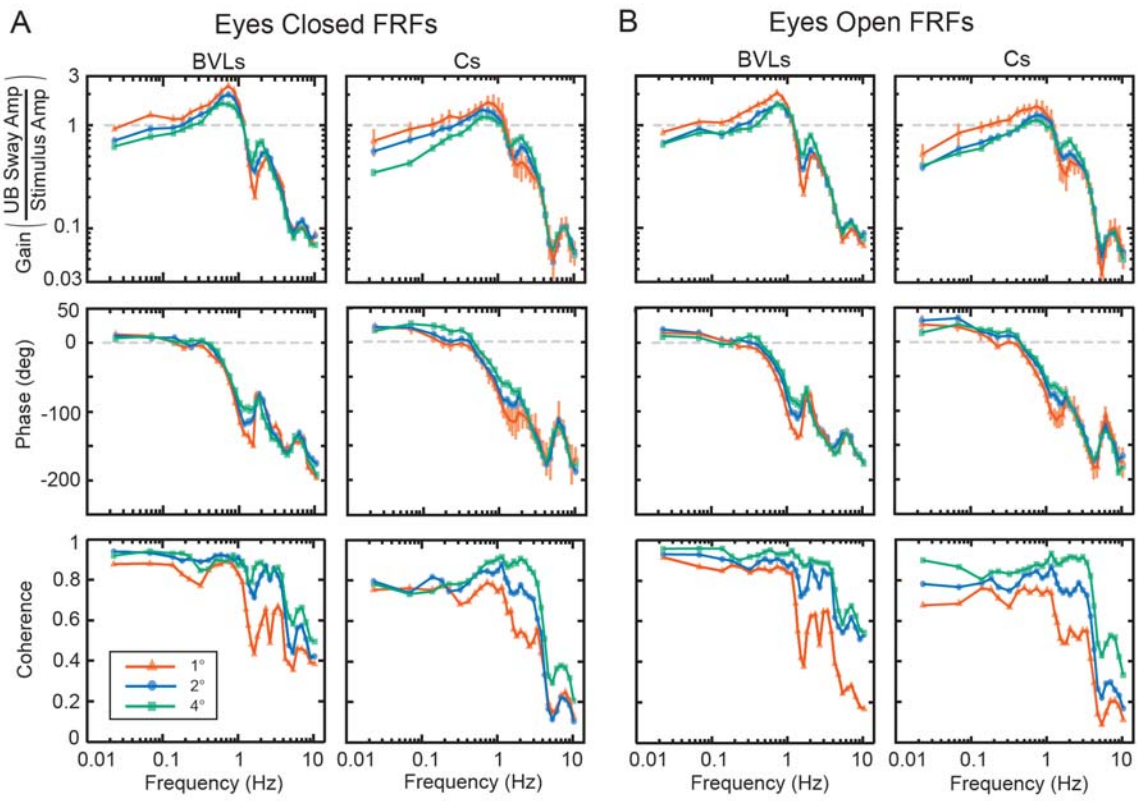


**FIG. 3.2.** *Mean experimental frequency-response functions (FRFs) and coherence functions in bilateral vestibular loss subjects (BVLs) and control subjects (Cs) for A) eyes closed and B) eyes open conditions. Error bars on FRFs in Cs for the 1° stimulus amplitude represent 95% confidence intervals on mean gain and phase.*

Both Cs and BVLs exhibited amplitude-dependent changes in FRF gains. At low- and mid-frequencies (<~1.1-1.3 Hz), gains generally decreased with increasing pelvis tilt amplitude. However, between ~1.3-2.5 Hz, gains generally increased with increasing pelvis tilt amplitude. At the highest frequencies (>~3 Hz), there was little change in gain with changing pelvis tilt amplitudes.

Visual availability had a limited effect on FRF gains. In both Cs and BVLs, vision influenced gains at low frequencies where EO gains were slightly lower than EC during the 1° and 2° stimulus amplitudes below ~0.3-1 Hz and were slightly larger than EC during the 4° stimulus amplitude below ~0.1 Hz.

Gains in BVLs and Cs differed in several ways. First, gains in BVLs averaged across low stimulus frequencies (<1 Hz) were 1.3-1.4 times larger than gains in Cs. Second, the apparent resonant peak around 0.8 Hz was more pronounced in BVLs compared to Cs and this peak was more pronounced in EC compared to EO conditions

for BVLs. Third, gains in BVLs were lower than gains in Cs at ~1.6 Hz (1.3-2.2 times lower). Finally, at the highest frequencies (>4 Hz), gains in BVLs were larger than gains in Cs.

FRF PHASES. Across all test conditions and in both BVLs and Cs, FRF phase curves generally showed decreasing values (more phase lag) with increasing frequency (Fig. 3.2, middle row). At frequencies below about 0.2-0.4 Hz, pelvis tilt stimuli resulted in UB phase leads, while at mid- and high-frequencies (>0.4 Hz) all stimuli resulted in UB phase lags.

In both BVLs and Cs, there were small but systematic amplitude-dependent changes in phase curves between 0.2-2 Hz with increasing stimulus amplitudes resulting in more phase lead and/or less phase lag values. Visual availability had only a limited effect on phase curves.

Phase curves in BVLs showed less phase lead compared to Cs at frequencies below 0.14 Hz. Also, phase values showed more severe decline in BVLs compared to Cs between 0.6-1.2 Hz, resulting in more phase lag at 1.2 Hz (~80-150° lag in BVLs and ~60-120° lag Cs). At frequencies above ~3 Hz, phases in BVLs exhibited smaller peaks and valleys compared to Cs.

COHERENCE FUNCTIONS. Across all test conditions, coherences were between 0.6 and 0.9 at frequencies below 1 Hz and coherences decreased at frequencies above 3 Hz (Fig. 3.2, bottom row). Increases in stimulus amplitude were associated with higher coherences. BVLs had higher coherences than Cs at frequencies below 1 Hz and above 4 Hz.

*Model of spinal stability*

MODEL DESCRIPTION. A mathematical model (Fig. 3.3) was used to understand and quantify neural and mechanical mechanisms contributing to UB control. To explain our experimental results, we began with an existing model (Fig. 2.5) and updated some previous model assumptions about what sensory information contributed to UB control mechanisms. Each block represents a sensory, neural, neuromuscular, or mechanical system. The UB is assumed to sway as a single-link inverted pendulum about

a joint that corresponds to L4/L5. The system output is upper body-in-space (*UBS*) tilt angle with respect to earth vertical. The UB block includes the UB moment of inertia (*J*) about the L4/L5 joint, the UB mass (*m*), and the UB center-of-mass height (*h*) above the L4/L5 joint. The values of *J*, *m*, and *h* were estimated for each subject using

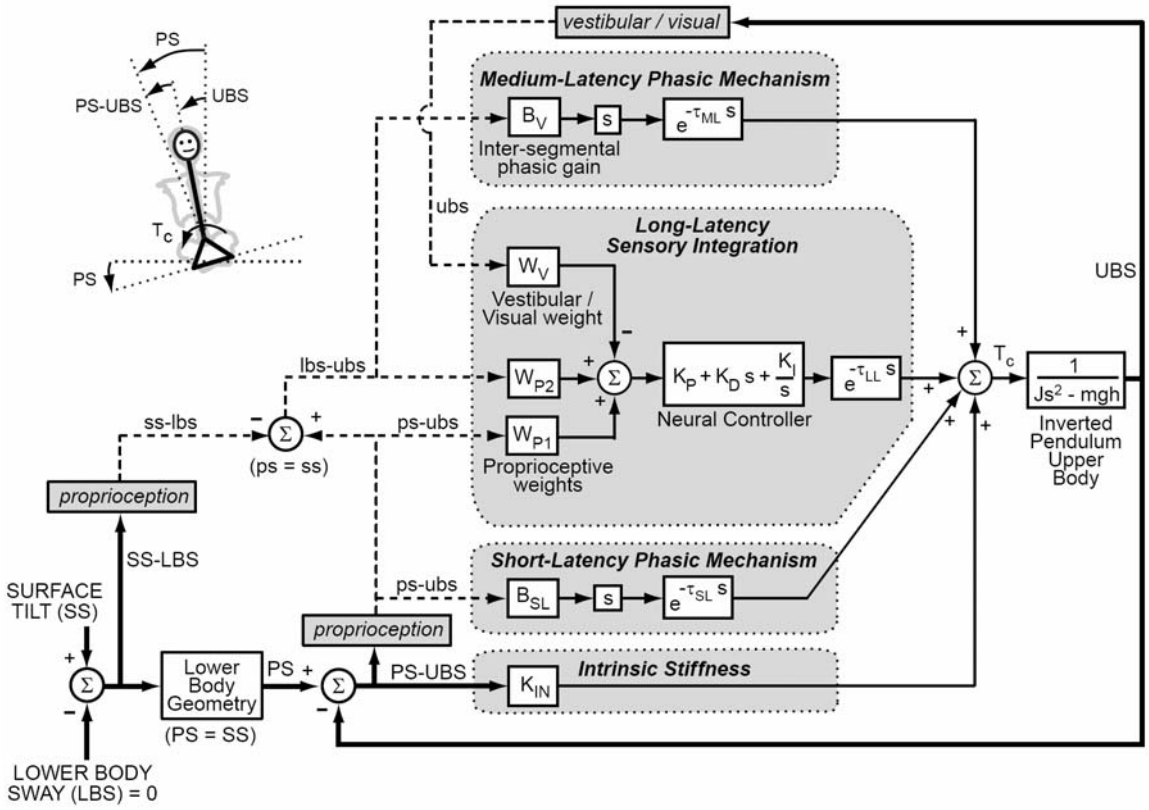


**FIG. 3.3.** *Model of upper body control with stationary visual field includes feedback from 4 mechanisms. The model input is surface tilt-in-space (SS) and output is upper body-in-space (UBS) tilt angle. Actual kinematic variables are represented as thick solid lines and capital letters while internal estimates of kinematic variables are represented as dashed lines and lower case letters. The visual/vestibular weight ($W_V$) replaced $W_{V1}$ and $W_{V2}$ in Fig. 2.5 because the visual surround was stationary in this study. Also, $B_V$ replaced $B_{V1}$ and $B_{V2}$ in Fig. 2.5 because inter-segmental contributions are represented in more detail.*

anthropometric methods (Erdmann 1997; Winter 2005). The mean values of these parameters in Cs were 3.2 kg·m$^2$, 40.2 kg, 0.22 m, respectively. Two of the three BVLs happened to be taller and heavier than most Cs. Therefore, mean values of *J*, *m*, and *h* in BVLs were larger than Cs and were equal to 5.8 kg·m$^2$, 44.0 kg, 0.30 m, respectively.

The input to the UB block in Fig. 3.3 is a corrective torque ($T_c$) generated from four mechanisms that are distinguished from one another based on the time delay of torque generation. Input to these four mechanisms are based upon either actual body

kinematics (capital letters and thick solid lines) or internal representations of kinematics (lower case letters and dashed lines) derived from proprioception, vestibular, or visual

sensory systems. Other types of feedback could have contributed to UB torque generation, such as UB torque feedback (Peterka 2003) or cutaneous information from pressure distributions on the feet (Maurer et al. 2006) or at the hips, but experimental data were sufficiently accounted for assuming feedback consisted only of segment kinematics.

The intrinsic stiffness mechanism tends to orient the UB perpendicular to the pelvis by generating instantaneous torque in proportion to the difference between the pelvis-in-space (*PS*) tilt angle and *UBS*. *PS* is a function of lower body sway (*LBS*), surface tilt (*SS*), and lower body geometry. However, because the lower body approximated a parallelogram, the model assumes *PS* = *SS*. The proportionality constant $K_{IN}$ represents the intrinsic stiffness of tendons, joints, spinal ligaments, and muscles in the trunk-pelvis musculoskeletal system and includes the effects of muscle cocontraction and intraabdominal pressure. The short-latency phasic mechanism generates a torque proportional to sensory signals encoding the tilt velocity of *UBS* relative to *PS* (*ps*-*ubs*) with a short-latency time delay ($\tau_{SL}$) and proportionality constant $B_{SL}$. This mechanism originates from proprioceptive cues and represents the contribution of phasic stretch reflex pathways. The model does not make fine distinctions between the other physiological and biomechanical contributions to intrinsic stiffness and short-latency phasic mechanisms, which include intrinsic damping in the trunk, tonic reflex mechanisms, and the effective time delay introduced by modeling non-rigid distributed spinal motion as a single link.

The medium-latency phasic mechanism generates a corrective torque proportional to sensory signals encoding the tilt velocity of the *LBS* relative to *UBS* (*lbs*-*ubs*). The proportionality constant is the inter-segmental phasic gain ($B_V$). Sensory input to this mechanism is based upon proprioceptive cues signaling the lower body proprioceptive sense of *LBS* relative to *SS* (*ss*-*lbs*) and the UB proprioceptive sense of *PS*-*UBS* (*ps*-*ubs*). The difference between *ps*-*ubs* and *ss*-*lbs* results in an inter-segmental proprioceptive signal *lbs*-*ubs*. Because *LBS* was constrained to zero, the lower body effectively becomes a vertical reference frame which the UB orients to through the inter-segmental proprioceptive signal *lbs*–*ubs*. This interpretation of the input to the medium-latency

mechanism is updated from Chapter 2 (Fig. 2.5) where it was previously assumed that vestibular and/or inter-segmental proprioceptive cues may be inputs.

The long-latency sensory integration mechanism generates angular position-related, angular velocity-related, and time integrated angular position-related torques via a "neural controller" in relation to a summation of sensory orientation signals with a long-latency time delay ($\tau_{LL}$). The sensory weights $W_{P1}$, $W_{P2}$, and $W_V$ represent the relative contributions of sensory systems that orient the UB toward the pelvis, the lower body, and vertical, respectively. $W_{P1}$ and $W_{P2}$ are proprioceptive weights and $W_V$ is a vestibular weight in the EC condition and a combination of vestibular and visual weights in the EO condition. Sensory weights were constrained to sum to unity ($W_{P1} + W_{P2} + W_V = 1$). Our previous model included similar weight factors representing vestibular and visual contributions, but included only one proprioceptive weight whose input was *ps-ubs*.

MODEL PARAMETERS. Model fits to individual BVLs data showed that overall stiffness ($K_P + K_{IN}$) in the system had a strong positive correlation coefficient (R = 0.93) with UB mass times UB center-of-mass height (*mh*). Similarly, parameters related to overall damping ($K_D + B_{SL} + B_V$) showed a strong positive correlation coefficient (R = 0.93) with *mh*. Because the BVLs sample size was only three, stiffness and damping correlations were not statistically significant although correlation values were similar to those in Cs. There was no apparent correlation between $K_I$ and *mh* in BVLs. It was previously shown in Cs that overall stiffness, overall damping, and $K_I$ had a strong positive correlation with *mh*, where R values equaled 0.98, 0.93, and 0.92, respectively, and were statistically significant (Goodworth and Peterka 2009). Because of these correlations, neural controller parameters as well as other parameters ($K_{IN}$, $B_{SL}$, and $B_V$) expected to vary with subject size were normalized by *mh* in Fig. 3.4.

Fig. 3.4A shows the parameters that could be held at fixed values across test conditions. Individual model parameters in BVLs related to intrinsic stiffness, short-latency reflex gain, and all time delays were generally within the 95% confidence interval on the mean parameter values in Cs. In all BVLs, normalized $K_{IN}$ and $B_{SL}$ were larger than mean normalized $K_{IN}$ and $B_{SL}$ in Cs. The two BVLs with $\tau_{ML}$ exceeding the 95% confidence interval on the mean $\tau_{ML}$ in Cs also had larger *mh* (15.7 and 16.4 kg·m)

compared to the mean Cs (9.1 kg·m); and there was a positive correlation coefficient (R = 0.90, although not statistically significant with 3 subjects) between $\tau_{ML}$ and *mh* in BVLs that was not present in Cs.

Fig. 3.4B shows the parameters that were necessary to vary across test condition in order to account for the FRF data. In all EC conditions and most EO conditions, BVLs had larger $W_{P1}$ values compared to the upper 95% confidence interval on the mean $W_{P1}$ in Cs. This result implies that BVLs oriented their UB more toward the pelvis tilt (and less toward vertical) than Cs, consistent with the generally larger experimental FRF gains in BVLs compared to Cs. In both Cs and BVLs, $W_{P1}$ decreased with increasing stimulus amplitude and differences were small between EO and EC conditions. In EC BVLs, $W_V$ =0 and $W_{P2} = 1 - W_{P1}$. Therefore, the decrease in $W_{P1}$ implies that $W_{P2}$ increased with increasing pelvis tilt amplitude indicating that BVLs shifted toward increased reliance on the inter-segmental proprioceptive signal that provided a vertical reference. In EO BVLs, $W_V$ represents the visual contribution and is functionally identical to $W_{P2}$, therefore $W_{P2} + W_V = 1 - W_{P1}$. A comparison of $W_{P2}$ on EC tests to $W_V + W_{P2}$ on EO tests shows that these weights are similar (mean EC $W_{P2} = 0.30$ across all BVLs and stimulus amplitudes; mean EO $W_V + W_{P2} = 0.37$), suggesting that visual orientation cues made only a small contribution to UB control.

In Cs, $W_V$ includes a representation of the vestibular contribution to UB control. The fact that $W_{P2} + W_V$ was larger in Cs than BVLs (mean $W_{P2} + W_V = 0.60$ in EC and 0.57 in EO in Cs) and similar in EC and EO conditions suggests that visual cues do not contribute significantly to UB control in Cs but that vestibular cues do contribute to UB control through the long-latency sensory integration mechanism.

Despite the small number of BVLs, repeated-measures ANOVA showed that $W_{P1}$ was significantly larger in BVLs compared to Cs. There was also a significant interaction between subject group and visual availability. This interaction effect related to the fact that EO compared to EC $W_{P1}$ values were reduced more in BVLs compared to Cs, although visual availability did not have a significant effect on $W_{P1}$ in either BVLs or Cs. There was a significant reduction in $W_{P1}$ with increasing stimulus amplitude in both BVLs and Cs, and there was a significant interaction effect between subject group and stimulus amplitude. This interaction effect related to the fact that increasing stimulus amplitude resulted in a greater reduction in $W_{P1}$ values in BVLs compared to Cs.

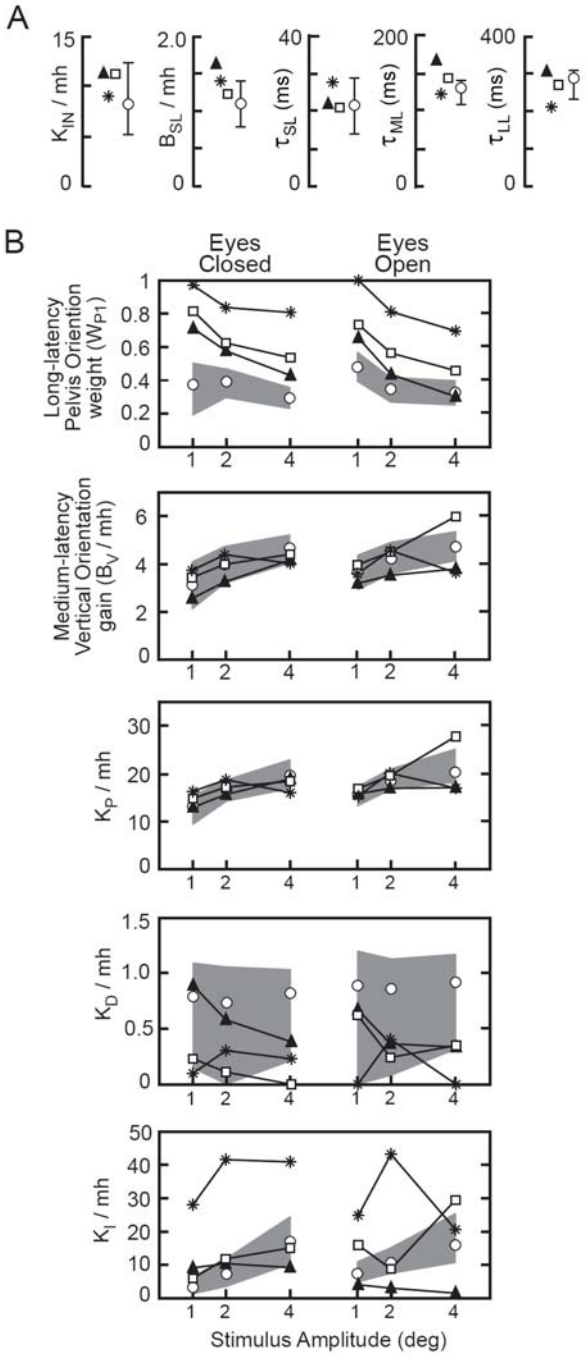


**FIG. 3.4.** *Model parameters for the three individual bilateral vestibular loss subjects (black triangle, asterisk, or white square) and mean of control subjects (open dot) with 95% confidence intervals (error bars or gray region). A: Parameters that had fixed values across all test conditions. B: Parameters that varied across test conditions. Units on $K_P$ are N·m/rad, units on $K_I$ are N·m/(rad·s), and units on $K_D$, $B_V$, and $B_{SL}$ are N·m·s/rad. Sensory weight $W_{P1}$ is unitless. All parameters except $W_{P1}$ and time delays were normalized by UB mass, m, times UB center-of-mass height, h. The mean m·h was 9.0 kg·m in control subjects and 13.2 kg·m in bilateral vestibular loss subjects. Weight parameters $W_{P2}$ and $W_V$ are not shown because they can be derived from $W_{P1}$. For BVLs in EC conditions, $W_V$ = 0 and $W_{P2}$ = 1 - $W_{P1}$. In EO conditions for BVLs and in all test conditions for Cs, $W_{P2} + W_V = 1 - W_{P1}$.*

The normalized $B_V$ increased with stimulus amplitude in both Cs and BVLs and was slightly larger in EO compared to EC conditions (8.5% in BVLs and 10% in Cs). In EC conditions, $B_V$ values in all BVLs were within the 95% confidence intervals on the mean $B_V$ in Cs. In EO conditions, there was more variability across BVLs, but $B_V$ values averaged across BVLs were within the 95% confidence intervals on the mean $B_V$ values in Cs. The slightly higher $B_V$ value in EO verses EC conditions indicates that there is a

visual contribution to the medium latency mechanism. For simplicity, this visual input is not represented in the Fig. 3.3 model, but was represented in Fig. 2.5.

In both Cs and BVLs, normalized $K_P$ increased with increasing stimulus amplitude and increased slightly with visual availability. $K_P$ averaged across BVLs was within the 95% confidence intervals on the mean $K_P$ in Cs. In both Cs and BVLs, normalized $K_D$ showed no consistent variation across stimulus amplitude or between EO/EC conditions and contributed little to overall damping of the UB control system. Specifically, 13% of the total damping (total damping = $K_D + B_{SL} + B_V$) was attributable to $K_D$ for Cs and 6% of the total damping was attributable to $K_D$ for BVLs averaged over all test conditions. Normalized $K_I$ exhibited large variability across BVLs, but the mean $K_I$ in BVLs increased with stimulus amplitude and was ~3.0 times larger than the mean $K_I$ in Cs in EC conditions and ~1.6 times larger in EO. For Cs, $K_I$ was similarly highly variable across individual fits (Fig. 2.6C) and the mean $K_I$ values increased with stimulus amplitude.

Parameter estimation results showed that the most consistent difference between BVLs and Cs was that BVLs had a larger pelvis-orienting weight, $W_{PI}$. Therefore, we explored the influence of $W_{PI}$ on FRFs to determine the extent to which differences in $W_{PI}$ values alone could explain the observed differences in the FRFs between subject groups. First, we generated the FRF predicted by the mean parameters in Cs shown in Fig. 3.4 for the EC 2° stimulus amplitude condition (thick dotted line in Fig. 3.5A). Then $W_{PI}$ was progressively increased while all other model parameters remained fixed (solid lines in 3.5A). The results showed that increases in $W_{PI}$ alone accounted for several of the differences in experimental FRFs between Cs and BVLs (compare 3.5A to Fig. 3.2). Specifically, increasing $W_{PI}$ resulted in FRF gain increases below ~1.1 Hz, gain decreases at ~1.6 Hz, slightly less phase lead below ~0.14 Hz, and more severe declines in phase values between ~0.6-1.2 Hz.

Increases in $W_{PI}$ could not fully account for the apparent resonant peak near 0.8 Hz in BVLs. This experimental feature was especially evident in EC conditions. Because parameter estimation results showed that the averaged normalized $K_I$ in BVLs was ~3.0 times larger than in Cs in EC conditions, the influence of $K_I$ alone on FRFs was investigated. Results showed that a peak in the FRF gain curve developed as $K_I$ was increased consistent with the results in BVLs (compare gains in Fig. 3.5B to Fig. 3.2).

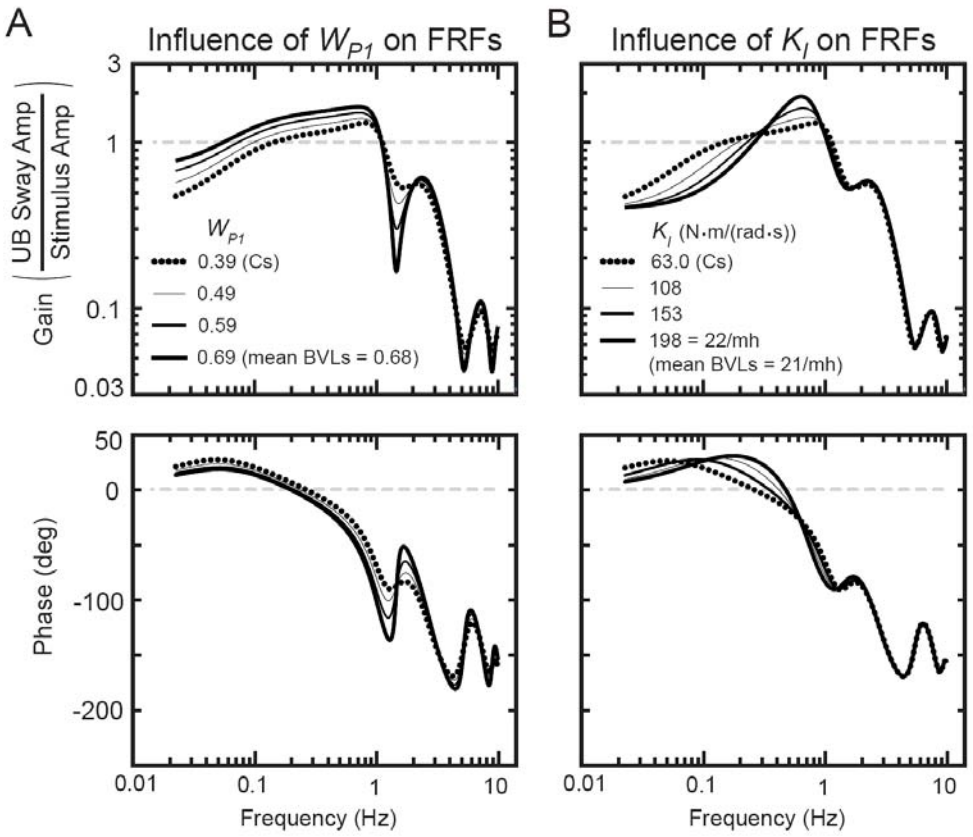


**FIG. 3.5.** *Influence of $W_{P1}$ and $K_I$ on FRFs shows that most of the FRF features that differ between control subjects (Cs) and bilateral vestibular loss subjects (BVLs) can be accounted for with A) larger $W_{P1}$ values in BVLs across all test conditions and B) larger $K_I$ values in BVLs across EC conditions. The thick dotted line is the FRF predicted for the EC 2° stimulus amplitude condition using the mean Cs model parameters: $K_{IN}$ =73.5 N·m/rad, $B_{SL}$ =9.87 N·m·s/rad, $\tau_{SL}$ =21.7 ms, $\tau_{ML}$ =131 ms, $\tau_{LL}$ =288 ms, $W_{P1}$ = 0.390, $B_V$ =35.7 N·m·s/rad, $K_P$ = 149 N·m/rad, $K_D$ = 6.60 N·m·s/rad, and $K_I$ = 63.7 N·m/(rad·s).*

Therefore, the differences in experimental FRFs between BVLs and Cs were accounted for mainly by BVLs having a larger pelvis-orienting sensory weight across all test conditions and a larger $K_I$ in EC conditions. The remaining small differences in experimental FRFs between subject groups were accounted for through the small differences in other model parameters between BVLs and Cs.

## DISCUSSION

The goals of this study were to determine the vestibular contribution to frontal plane spinal stability and to identify compensatory mechanisms used by BVLs. UB responses were evoked using continuous pelvis tilts while lateral sway of the lower body was prevented in both BVLs and Cs. BVLs had larger RMS UB sway compared to Cs and FRFs differed in gain and phase values across various frequency ranges. However, the overall frequency-dependent, amplitude-dependent, and visual-dependent changes in UB responses were similar between subject groups.

### *Proprioceptive input to medium-latency phasic mechanism*

Results from the current study indicated that the major source of system damping provided by the medium-latency phasic mechanism had an inter-segmental proprioceptive origin. Specifically, because the medium-latency inter-segmental gain ($B_V$) was very similar in EC conditions between Cs and BVLs, the sensory input to this mechanism could not have a vestibular origin in BVLs. While it is possible that a vestibular contribution to this mechanism exists in Cs, a simpler interpretation would be that the sensory input to the medium-latency phasic mechanism was of an inter-segmental proprioceptive origin in both Cs and BVLs. This result is consistent with evidence that inter-segmental signals also contribute to whole body stance control (Kiemel et al. 2008). Therefore, EC BVLs had no major loss of damping and did not need to compensate with the previously postulated increases in stretch reflex activation and intrinsic stiffness.

### *Compensation in BVLs*

RELIANCE UPON PROPRIOCEPTION. Previous studies investigating whole body sagittal plane sway in BVLs demonstrated that they compensate for absent vestibular function using heightened reliance upon proprioceptive information signaling body sway relative to support surface in EC conditions (Maurer et al. 2006; Peterka 2002). From a modeling perspective, EC BVLs exhibited a proprioceptive weight of one indicating that they relied entirely on proprioception that oriented the body toward the tilted surface and this proprioceptive weight did not vary across surface tilt amplitudes in EC conditions (Fig. 10 in Peterka 2002). In contrast, subjects with normal vestibular

function shifted toward increased reliance on vestibular and decreased reliance on proprioception with increasing surface tilt amplitude for both sagittal and frontal plane sway (Peterka 2002; Cenciarini and Peterka 2006).

By analogy to whole body stance control, we postulated in Chapter 2 that EC BVLs may have an UB-on-pelvis proprioceptive weight of one that did not vary across pelvis tilt amplitude and would cause the UB to orient toward the tilted pelvis. However, UB sway patterns from BVLs could not be accounted for without the additional inclusion of the inter-segmental proprioceptive input to the long-latency sensory integration mechanism. The relative contributions of these two proprioceptive inputs were represented in the Fig. 3.3 model as sensory weights $W_{P1}$ for pelvis-orienting proprioception and $W_{P2}$ for inter-segmental proprioception. In EC conditions, $W_{P1} + W_{P2} = 1$ because only proprioception information contributed to UB corrections in BVLs. Averaged across BVLs, $W_{P1}$ was 0.83 in the 1° pelvis tilt amplitude and monotonically decreased to 0.59 in the 4° pelvis tilt amplitude. $W_{P1}$ values larger than 0.5 indicate that BVLs had a greater reliance upon pelvis-orienting proprioceptive cues compared to reliance upon inter-segmental proprioceptive cues. BVLs also had a greater reliance upon pelvis-orienting proprioceptive cues compared Cs.

The systematic variation in $W_{P1}$ and $W_{P2}$ with pelvis tilt amplitude in EC conditions is similar to the sensory reweighting phenomenon whereby Cs shift away from reliance upon one sensory system and toward reliance upon a different sensory system (Maurer 2006; Oie et al. 2002; Peterka 2002). However, our model-based interpretation indicated that the variation in $W_{P1}$ and $W_{P2}$ values in BVLs in EC conditions was attributable to an *intra-proprioceptive system* reweighting. Specifically, BVLs shifted away from reliance upon proprioceptive information that oriented the UB toward the pelvis and shifted toward reliance upon proprioceptive information that oriented the UB toward the LB (and consequently more vertical in space) with increases in pelvis tilt amplitude.

RELIANCE UPON VISION. It has also been shown that BVLs can compensate with a heightened reliance upon visual information in freestanding conditions. During a visual sway-referenced test condition (i.e., visual surround rotation angle is equal to body sway rotation angle about the ankle joint at any point in time), Nashner et al. (1982)

observed that subjects with vestibular deficits swayed more than Cs. Increased sway in this test condition indicated that subjects with vestibular deficits had a heightened reliance upon visual information even when visual inputs were destabilizing and oriented their body away from upright. This compensation was also identified using external rotations of a visual surround and surface (Peterka 2002). Specifically, during surface rotations, EC BVLs had larger FRF gains compared to Cs, FRF gains were greatly reduced in EO compared to EC conditions in BVLs, and this reduction in EO FRF gains compared to EC was more prominent in BVLs compared to Cs.

In the current study, if BVLs had a heightened reliance upon visual information, then we expected to find reductions in FRF gains and lower values of the model parameter $W_{P1}$ in EO compared to EC conditions. Experimental results showed only minor reductions in FRF gains with EO for the 1° and 2° stimulus amplitudes and no reduction for the 4° stimulus amplitude. Furthermore, these minor reductions were similar for both BVLs and Cs. $W_{P1}$ was slightly lower in EO compared to EC in BVLs (0.63 in EO compared to 0.70 in EC) while in Cs there was no decrease in $W_{P1}$ with visual availability. Therefore, there was some evidence that BVLs used a heightened reliance upon visual information as a compensatory mechanism, but the overall visual contribution to UB control was small.

OTHER COMPENSATORY MECHANISMS. Another compensation mechanism that BVLs could have used was to heighten intrinsic stiffness and/or reflex gains. Increased background trunk muscle activity could increase intrinsic stiffness (Hogan 1990) and reflex gains (Moorhouse and Granata 2007), and it has been observed that BVLs exhibit larger background muscle activity in the trunk following a transient surface rotation (Carpenter et al. 2001). In the present study, however, we found only minimal evidence that intrinsic stiffness of the trunk was greater in BVLs compared to Cs. Specifically, although the intrinsic stiffness gains ($K_{IN}$) in all BVLs were greater than the mean $K_{IN}$ value in Cs, none were greater than the upper 95% confidence interval (Fig. 3.4A). Similarly, all three BVLs had a larger short-latency phasic gain ($B_{SL}$) than the mean $B_{SL}$ in Cs, but the gain in only one BVL subject exceeded the upper 95% confidence limit on the mean $B_{SL}$ in Cs.

BVLs exhibited an apparent resonance around 0.8 Hz where FRF gains were greater than gains in Cs. This resonance effect was especially prominent in EC conditions. It was found that increases in the neural controller integration factor $K_I$ in BVLs compared to Cs accounted for this resonance feature (Fig. 3.5B). Functionally, an increase in FRF gain could be considered to be anti-compensatory in that higher gains indicate that the UB shows greater sensitivity to pelvis tilts. However, larger $K_I$ values are also associated with lower gains at frequencies < ~0.2 Hz, and thus provide a beneficial compensatory effect at lower frequencies.

*Vestibular contribution to spinal stability*

If our conclusion is correct that a proprioceptive signal encoding inter-segmental motion contributes to UB control through the long-latency sensory integration mechanism, then it theoretically would be possible for this sensory source to completely compensate for a vestibular loss. That is, with the lower body constrained, body orientation information derived from a vestibular signal encoding UB tilt with respect to earth vertical is equivalent to orientation information derived from a proprioceptive signal encoding UB motion relative to the lower body. Thus, if both vestibular and inter-segmental proprioceptive cues normally contribute to UB control (both $W_V$ and $W_{P2} > 0$ in Cs), then responses to pelvis tilt stimuli in BVLs would be indistinguishable from those of Cs if the value of $W_{P2}$ in BVLs could be enhanced to the extent that $W_{P2}$ equaled the value $W_V + W_{P2}$ in Cs in a given test condition.

However, loss of vestibular function does in fact alter responses to pelvis tilt stimuli through changes primarily in the long-latency sensory integration mechanism. These changes provide evidence for a vestibular contribution to spinal stability in Cs and are in agreement with previous studies that inferred a vestibular contribution by evoking UB sway in seated subjects using galvanic vestibular stimulation (Day et al., 1997) and by observing that EC subjects can maintain stability while sitting on an unstable seat (Radebold et al. 2001; Reeves et al. 2006).

The fact that BVLs were unable to completely compensate for their vestibular loss by fully substituting the inter-segmental proprioceptive signal for the vestibular signal could be indicative of the properties of neural mechanisms that control the fusion of sensory cues. Previous investigations demonstrated that a weighted combination of

sensory cues can form an optimal, minimum variance perceptual estimate if the weights are determined by the signal-to-noise properties of the sensory sources such that the least noisy sensory source is weighted most heavily (Ernst and Banks 2002; van Beers et al. 1999). In the EC condition in our experiment, there were three sensory cues contributing to the long-latency sensory integration mechanism with their contributions represented by the weights $W_V$, $W_{P1}$, and $W_{P2}$. In EC Cs, $W_{P1}$ had a value of about 0.40 while the value $W_V + W_{P2}$ (which equals $1 - W_{P1}$) was therefore about 0.60. The larger weighting on the combined sensory signals that encode UB tilt with respect to vertical ($W_V + W_{P2}$) compared to the sensory signal that encodes UB tilt with respect to the pelvis ($W_{P1}$) suggests that these combined sensory signals had lower variance than the sensory signal for UB-on-pelvis tilt. Without vestibular function, the variance improvement afforded by combining vestibular and inter-segmental proprioceptive signals would be lost, $W_{P1}$ would be expected to increase, and the optimal sensory weights would be determined by the variances of the remaining two proprioceptive signals. The overall higher $W_{P1}$ values in BVLs of about 0.7 across all test conditions suggests that the inter-segmental proprioceptive signal had higher variance than the proprioceptive signal encoding UB-on-pelvis tilt.

*Generality of the model*

The model of UB control was identified while lower body sway was prevented. Because context dependency has been demonstrated in postural control (Cordo and Nashner 1982), it is likely that the UB system identified in the current study would change in some way to accommodate conditions where lower body sway is not prevented. Nevertheless, it is likely that many of the mechanisms identified in the current study would still contribute to frontal plane spinal stabilization. For example, the intrinsic stiffness mechanism represented the biomechanical properties of the trunk and pelvis system and would therefore be expected to contribute to spinal stability independent of constraints placed on the lower body. It is also likely that many of the sensory signals identified in the current study contribute to postural stability in more general conditions. Clearly the visual and vestibular signals could be beneficial in many contexts because these signals are used by subjects to estimate body orientation relative to earth vertical and to the visual field, respectively. It is also likely that the inter-segmental

proprioceptive signal, used to orient the UB toward the lower body, is used in postural control in general conditions. For example, in freestanding conditions, a mechanism that facilitates UB alignment with the lower body could contribute to the well known "ankle strategy" (Horak and Nashner 1986). A recent study by Kiemel et al. 2008 incorporated this inter-segmental signal in a two-segment model of the control of freestanding sagittal plane sway.

*Conclusion*

Results suggest that in both Cs and BVLs the major contributions to UB system damping came through medium-latency inter-segmental proprioceptive cues and major contributions to UB system stiffness came through intrinsic mechanical properties and long-latency sensory integration of inter-segmental proprioceptive cues and pelvis-orienting proprioceptive cues. Thus, loss of vestibular function did not severely impair spinal stability. However, BVLs oriented their UB more toward their pelvis than Cs because vestibular inputs do in fact contribute to spinal stability in Cs. Finally, enhanced utilization of visual orientation cues played only a minor role in the compensation for vestibular loss.

# CHAPTER IV.
# INFLUENCE OF FRONTAL PLANE STANCE WIDTH ON POSTURAL DYNAMICS AND COORDINATION IN HUMAN BALANCE CONTROL


## ABSTRACT

The influence of frontal plane stance width on postural dynamics and coordination in human bipedal stance was investigated. We tested the hypothesis that when subjects adopt a narrow stance width, they rely heavily on nonlinear control strategies and coordinated counter-phase upper and lower body motion to limit center-of-mass (CoM) deviations from upright; but as stance increases, the use of these strategies diminish. Freestanding frontal plane body sway was evoked through surface and visual surround rotations upon at various amplitudes. Subjects were either eyes open or closed and adopted various stance widths. Upper body, lower body, and CoM kinematics were characterized using frequency-response functions and impulse-response functions. CoM sway responses to visual rotations severely decreased with increasing stance width. For both surface and visual rotations, CoM results indicate the narrow stance postural system is nonlinear across stimulus amplitude in both EO and EC conditions while the wide stance postural system is more linear. The nonlinearity in narrow stance is likely due to an amplitude-dependent sensory reweighting mechanism. Upper and lower body sway was approximately in-phase at frequencies below ~ 1 Hz and out-of-phase at frequencies above 1 Hz for all test conditions. Therefore, results were inconsistent with the hypothesis that subjects made greater use of coordinated counter-phase upper and lower body motion in narrow compared to wide stance conditions.



Goodworth AD and Peterka RJ. Influence of frontal plane stance width on postural dynamics and coordination in human balance control. *J Neurophysiol*, in revision, 2010.

## INTRODUCTION

The maintenance of stable human bipedal stance requires that the vertical projection of the body's center-of-mass (CoM) remains within the base-of-support (BoS). In freestanding humans, the BoS is defined by the area under and between the feet and the CoM is determined by the orientation of individual body segments. To keep CoM motion within the BoS, humans can potentially use one or more of three basic strategies: 1) limit motion between individual body segments but regulate sway via nonlinear mechanisms that limit CoM sway by altering sensitivity to perturbations, 2) allow larger motion of body segments relative to one another, but in a coordinated manner so that the body's overall CoM motion remains small, and/or 3) increase the BoS by standing with feet farther apart thereby permitting the CoM greater range of motion before reaching the limits of the BoS. Very little is known about how these strategies interact. The goal of the current study is to understand how changes in the BoS in the frontal plane influence the way humans use the first two balance control strategies listed above.

In the first strategy, body segments move en bloc above the ankle joint with the upper body segment (UB) (body mass located above the pelvis) aligned to the lower body (LB), analogous to the "ankle strategy" described for sagittal plane sway (Horak and Nashner 1986). Subjects utilizing this strategy while responding to external perturbations could limit overall CoM motion by using a nonlinear control scheme that reduces the sensitivity of body sway responses to perturbations as the perturbation amplitude increases. Previous studies have shown nonlinear stimulus-response behavior whereby the stance control system reduced the influence of larger amplitude perturbations (Peterka 2002; Maurer et al. 2006; Oie et al. 2002; Cenciarini and Peterka 2006). This nonlinear stimulus-response behavior has been demonstrated for visual tilt (Peterka 2002), surface tilt (Peterka 2002; Maurer et al. 2006), and external force (Maurer et al. 2006) stimuli that evoke sagittal plane sway, and for surface tilt (Cenciarini and Peterka 2006), visual translation (Oie et al. 2002), and tactile stimuli (Oie et al. 2002) that evoke frontal plane sway in narrow stance conditions. However, the influence of stance width on this nonlinear behavior has not been investigated.

The second strategy is to use coordinated counter-phase motion of UB and LB segments to make rapid corrections in CoM position and to keep the overall CoM motion

small relative to BoS even though the motion of individual body segments may be large. This strategy, termed the "hip strategy," has long been recognized to contribute stance control in conditions where the BoS is very narrow (Horak and Nashner 1986), and when very rapid corrections are necessary (Kuo 1995). The hip strategy can also be considered one of the normal "eigen" modes of control (Alexandrov et al. 2005).

Although it is convenient to describe the hip strategy separate from the ankle strategy, in fact both are present simultaneously during unperturbed stance in the sagittal plane (Creath et al. 2005; Zhang et al. 2007). That is, at low frequencies, the UB and LB are nearly aligned and "in-phase" resembling the ankle strategy; however, at frequencies above about 1 Hz, the UB and LB move in opposite directions and exhibit an "out-of-phase" hip strategy. This simultaneous in-phase and out-of-phase body segment motion is also present when subjects respond to an external surface (Alexandrov et al. 2005; Creath et al. 2008) or visual (Kiemel et al. 2008) stimulus in the sagittal plane. Similar dynamics have been found during spontaneous sway in the frontal plane (Zhang et al. 2007), but the role of stance width in shaping counter-phase behavior is unknown.

It is clear from previous studies that nonlinear stimulus-response behavior and coordinated counter-phase motion of body segments are important strategies to keep the CoM within the BoS in some conditions. However, humans normally maintain a wider stance in the frontal plane than those adopted in the previous studies (Cenciarini and Peterka 2006; Oie et al. 2002) and often increase stance width during everyday activities that challenge balance such as standing on a moving train. A few studies have investigated the role of stance width in the frontal plane on balance control. Increasing stance width has been shown to be associated with reductions in frontal plane spontaneous body sway (Day et al. 1993; Kirby et al. 1987), reductions in responses to galvanic stimulation of the vestibular nerve (Day et al. 1997; Welgampola 2001), and reductions in center of pressure motion, trunk motion, and muscle activation levels during sudden surface translations (Henry et al. 2001). Although these reductions in balance related measures seem to be consistent across previous studies, the underlying cause of these reductions is unclear because the complex interaction between stance width in the frontal plane and neural control strategies for balance is still poorly understood.

Stance width in the frontal plane plays an important role by directly affecting the allowable range over which the center-of-mass can move (Horak and Macpherson 1996),

changing the mechanics of the LB, and modifying the proprioceptive sensory information available for balance control and the intrinsic mechanical properties of the LB by changing the relationship between LB sway and the stretching or shortening of muscles and tendons that span the hip joints (Scrivens et al. 2008; Day et al. 1993). Thus, it seems reasonable to predict that changing stance width would influence the dynamic characteristics of the frontal plane balance control system.

In addition, changes in stance width dramatically affect the relationship between LB sway and the pelvis orientation in space. For example, when a subject's stance width is narrower than the distance between their hip joints, the pelvis always tilts in the same direction as the LB sways. However, as a subject progressively increases stance width, pelvis orientation transitions from being in the same direction as LB sway, to being invariant to, and then being in the opposite direction of LB sway. Since the control of UB orientation is influenced by pelvis orientation (Goodworth and Peterka 2009), changes in stance width are expected to have an impact on UB segment dynamics and thus influence the coordination strategy used for balance control.

In the current study, we explore the influence of stance width on the dynamic response properties of frontal plane body sway by characterizing the linearity of responses to surface tilt stimuli of varying amplitude and by quantifying segment coordination. We test the hypothesis that when subjects adopt a small stance width, they will use a nonlinear control strategy and coordinated counter-phase motion of the UB and LB to control their CoM because stability requires minimal deviation of their CoM from upright and must therefore be tightly controlled. However, as the stance increases, CoM deviations from upright can be larger without jeopardizing stability. Therefore, we also test the hypothesis that as subjects adopt larger stance widths, nonlinear stimulus-response behavior and coordinated counter-phase motion will decrease. To test these hypotheses, we evoked body sway in the frontal plane through external rotations of the surface upon which subjects stood and a visual surround which subjects faced with various stimulus amplitudes. Subjects were either eyes open or closed and adopted various stance widths.

If nonlinear control behavior is used to limit CoM excursions when stance width is narrow, then we expect to see subjects become relatively less responsive to surface and visual tilt stimuli as the stimulus amplitude increases. In contrast, as stance width

increases, we expect that it would become less necessary for subjects to use a potentially more complex nonlinear control strategy to maintain balance because stimulus-evoked CoM excursions would never come close to the extended BoS afforded by wide stance. Therefore, subjects could adopt a simpler linear control strategy. Additionally, if increasing stance width reduces the need for coordinated counter-phase motion of the UB and LB, then we expect to see greater use of counter-phase motion in narrow stance to reduced CoM motion, compared to wide stance conditions.

## METHODS

### *Subjects*

Eight healthy subjects (4 male, 4 female) with no history of balance disorders participated in this experiment. All subjects gave their informed consent prior to being tested using a protocol approved by the Institutional Review Board at Oregon Health & Science University. The subjects had a mean age of 29 years ± 7 SD, mass of 69 kg ± 6.7, height of 173 cm ± 6.0 SD, L4/L5 above surface of 106 cm ± 3.9 SD, greater trochanter above surface of 89.3 cm ± 4.9 SD, and distance between hip joint centers of 17.3 cm ± 1.2 SD.

### *Experimental setup*

Body sway was evoked in the frontal plane in freestanding subjects through continuous external stimuli consisting of rotations of the support surface (SS) upon which subjects stood or rotations of the visual surround (VS) which subjects faced. SS and VS rotations were controlled by servomotors and the rotation axes were horizontal and perpendicular to the subject's frontal plane at ankle height halfway between the subject's heels. The VS had a half-cylinder shape (70-cm radius) lined with a complex checkerboard pattern of white, black, and three gray levels and was illuminated by fluorescent lights attached to the right and left edges of the surround (Peterka 2002). For each test, subjects maintained a stance width of either 5, 12, 21.5, or 31 cm between the medial malleoli, defined as the intermalleolar distance (IMD). Because ankle geometry and foot width varied for each subject, IMDs corresponded to different BoS (distance between outside edges of the feet) for each subject. Specifically, IMDs of 5, 12, 21.5, and

31 cm corresponded to mean BoS widths across subjects of 24.0, 31.0, 40.5, and 50.0 cm ± 0.66 SD. For the remainder of this paper, we refer to these stance widths as narrow, parallel, medium, and wide. In the parallel stance, subjects' mid-heel to mid-heel distance was approximately equal to the distance between hip joint centers. A previous study showed that the preferred stance width is about 17 cm between heel centers (McIlroy and Maki 1997), corresponding to an IMD of approximately 11 cm.

*Data collection*

In all experiments, stimulus delivery and data sampling occurred at 200 Hz. Sampled data included: SS and VS angular position and lateral displacements of the upper trunk and pelvis. The trunk and pelvis displacements were measured with rods connected to earth-fixed potentiometers (Midori America, part number CP-2URX-04) that rested on small lightweight metal hooks. The hooks were positioned on the midline of the trunk between the C6 and T3 vertebrae and on the center of buttock at approximately the hip joint level, respectively. The rods could slide freely on the hooks. From known positions of the potentiometers, lengths of the sway rods (distance from the potentiometers to hooks in the upright position), and height of the hooks relative to the assumed rotational axes of the upper and lower body segments, appropriate trigonometric conversions were used to calculate frontal plane linear displacements of the upper trunk and pelvis from rotational motion of each rod recorded by the potentiometer. Upper trunk and pelvis displacements were used to calculate angular displacements of the upper body (UB) and lower body (LB) with respect to earth-vertical (Fig. 4.2A). The UB sway angle was defined as the rotation angle about vertical with respect to an axis located midway between the hip joint centers (Goodworth and Peterka 2009; Seidel et al. 1995) and LB sway angle was defined as the rotation angle about vertical with respect to an axis located midway between the ankle joints.

In addition, whole body CoM displacements in the frontal plane were estimated using a biomechanical model that included two legs, one pelvis, and a detailed representation of the UB geometry that accounted for arm location (Erdmann 1997). Body segment dimensions were estimated via anthropomorphic measures (Erdmann 1997; Winter 2005). Body segment orientations were calculated at each time step and were determined by the measured SS angles and the LB and UB displacements. Whole

body CoM displacements were converted to angular displacements so that the CoM sway angle was defined as the rotation angle about vertical of the whole body CoM with respect to the axis located midway between the ankle joints. UB, LB, and CoM sway angles were considered to be the response variables while SS and VS rotation angles were considered to be the stimulus variables.

*External stimuli*

SS and VS rotational stimuli were presented continuously according to a pseudorandom waveform based on a pseudorandom ternary sequence (PRTS) of numbers (Davies 1970; Peterka 2002). Each number was assigned an angular velocity value of either +a, 0, or –a that was maintained constant for a specified state duration of $\Delta t$ s. The angular velocity waveform was mathematically integrated to derive the angular position waveform. The angular position waveform was scaled to a specific peak-to-peak value for each test condition and was used to drive either the SS or VS rotation.

SS stimuli were created from a 2186-length PRTS with 0.02 s state duration and cycle length of 43.72 s, giving a power spectrum of stimulus velocity with approximately equal amplitude spectral components ranging from 0.023 Hz to about 16.7 Hz. Seven PRTS cycles were presented in the lowest amplitude test and six cycles were presented in the higher amplitude tests because responses to higher amplitude tests were large enough that low variance estimates of mean responses could be made with less averaging across individual stimulus cycles. VS rotation stimuli were created from a 242-length PRTS with 0.09 s state duration and cycle length of 21.78 s, giving a velocity power spectrum bandwidth of 0.046 Hz to 3.7 Hz. Twelve PRTS cycles were presented in each visual tilt test. A stimulus based on a PRTS was used because there are advantages to using periodic wide-bandwidth stimuli compared to random white-noise type stimuli for obtaining lower variance estimates of stimulus-response functions (Pintelon and Schoukens 2001).

*Protocol*

Subjects performed a total of 41 tests in three or four test sessions. Each test session lasted 2½ hours and was performed on a different day. The tests included 8 spontaneous sway tests where no stimulus was given, IMDs were 5, 12, 21.5, or 31 cm,

and with eyes open (EO) or eyes closed (EC), 24 SS tests with peak-to-peak SS amplitudes of 1, 2, or 4º, IMDs of 5, 12, 21.5, or 31 cm, and with EO or EC, and 9 VS tests with peak-to-peak VS amplitudes of 1, 2, or 4º, and IMDs of 5, 12, or 31 cm with EO. These 41 tests were randomized to offset potential biases due to fatigue and learning. Each test lasted approximately 5½ minutes and subjects were given the opportunity to rest after every test.

Subjects were instructed to maintain straight knees throughout the test and to respond naturally. Subjects wore headphones and listened to their choice of novels or short stories to mask environment and equipment sounds and to maintain alertness.

*Analysis*

Experimental data were analyzed by calculating frequency-response functions, coherence functions, and impulse-response functions. Frequency-response functions enable the detection of frequency-dependent changes across test conditions, such as in-phase to out-of-phase transitions between the UB and LB as well as the identification of changes in response sensitivity. Impulse-response functions enable the detection of time dependent changes across test conditions, such as onset delays of sensory integration mechanisms. These analyses provided a linear analysis of the system dynamics under the given test condition and have been previously described in detail (Goodworth and Peterka 2009) and are briefly described below.

FREQUENCY-RESPONSE FUNCTIONS (FRFs). FRFs were defined as the ratio of the discrete Fourier transform of the response signal to the discrete Fourier transform of the stimulus signal (Pintelon and Schoukens 2001). FRFs were calculated for each stimulus cycle (except the first cycle in order to avoid transient behavior) and were then smoothed by first averaging FRFs over the stimulus cycles, and then averaging FRFs across adjacent frequency points. An increasing number of adjacent points were averaged with increasing frequency to reduce the variance of estimates at higher frequencies while maintaining adequate frequency resolution (Otnes and Enochson 1972). The final FRF estimates were approximately equally spaced on a logarithmic scale ranging from 0.023 to 5.9 Hz for SS tests and 0.046 to 2.6 Hz for VS tests (the upper frequency range was limited by the signal-to-noise ratio of the experimental data).

Each FRF was expressed as a set of gain and phase values that vary with frequency. Each gain value indicates the ratio of the response amplitude to the stimulus amplitude at its particular frequency and each phase value indicates the relative timing of the response compared to the stimulus (expressed in degrees and in most analyses was "unwrapped" using the "phase" function in the Matlab Signal Processing Toolbox (The MathWorks, Natick, MA)). The stimulus signal was the SS angle and response signals were UB, LB, or CoM sway angles. Use of these angular response signals allows FRF measures to indicate the extent to which the UB, LB, and CoM aligned to the SS or VS stimuli at any particular stimulus frequency. That is, a gain of one and phase of zero at a particular frequency indicates perfect alignment to the stimuli with no lead or lag in timing.

COHERENCE FUNCTIONS. Coherence functions measure the extent to which power in the sway response was linearly related with the power in the stimulus. Coherence function values vary from 0 to 1, with values of 1 indicating a perfect linear relationship between stimulus and response with no noise in the system or measurements. Coherence functions were defined as the squared magnitude of the stimulus-to-response cross-power spectrum divided by the product of the stimulus power spectrum and response power spectrum (Bendat and Piersol 2000). The cross-power and power spectra were calculated from the discrete Fourier transform of each stimulus cycle and were smoothed by averaging across individual stimulus cycles and by averaging adjacent frequency points. The coherence functions had the same frequency spacing as the FRFs.

IMPULSE RESPONSE FUNCTIONS (IRFs). IRFs were calculated for SS stimuli using an appropriately scaled cross correlation between the ideal SS PRTS velocity waveform and the UB, LB, and CoM response waveforms (Goodworth and Peterka 2009; Davies 1970). The cross-correlation provides an IRF estimate because the PRTS velocity waveform is an approximate white-noise stimulus (Davies 1970). The IRFs displayed in figures were convolved with a unit impulse of stimulus velocity and are shown with units of angular velocity. IRFs were not calculated for VS stimuli because the lower bandwidth of the visual surround actuator did not permit accurate estimates of IRFs.

The IRF of a linear system is the time domain equivalent of the frequency domain FRF (Davies 1970; Westwick and Kearney 2003). Although IRF and FRF representations of the system dynamics are equivalent for linear time-invariant systems, system properties are often easier to appreciate in one representation compared to another. For example, a time delay is easier to recognize in an IRF than an FRF where its effects are distributed.

PEAK-TO-PEAK & ROOT-MEAN-SQUARE MEASURES. Peak-to-peak (PP) and root-mean-square (RMS) measures of the LB, UB, and CoM were calculated for each subject and test condition. First, LB, UB, and CoM time series were averaged over the stimulus cycles (excluding the first cycle). Then, the RMS was calculated as the root-mean-square of the averaged and zero-meaned LB, UB, and CoM time series and the PP was calculated as the maximum minus the minimum values of the averaged LB, UB, and CoM time series.

STATISTICS. To test if stimulus amplitude, visual availability (EO compared to EC), and stance width (IMD) had statistically significant effects on RMS sway of the LB, UB, and CoM, we used repeated-measures ANOVAs with three experimental factors: stimulus amplitude, visual availability, and stance width. Stimulus amplitude and stance width were continuous variables in the statistical model. Null hypothesis rejection was set to $p < 0.05$ for all tests. In addition, mean LB, UB, and CoM FRFs include 95% confidence intervals that were determined using the percentile bootstrap method with 1,000 bootstrap samples (Zoubir and Boashash 1998).

## RESULTS

### *Sway responses to SS stimuli*

CoM SWAY. SS stimuli and the CoM sway response for the three stimulus amplitudes, four stance widths, EO and EC, are shown in Fig. 4.1A. CoM sway waveforms (averaged over all subjects) generally followed the tilting SS stimulus

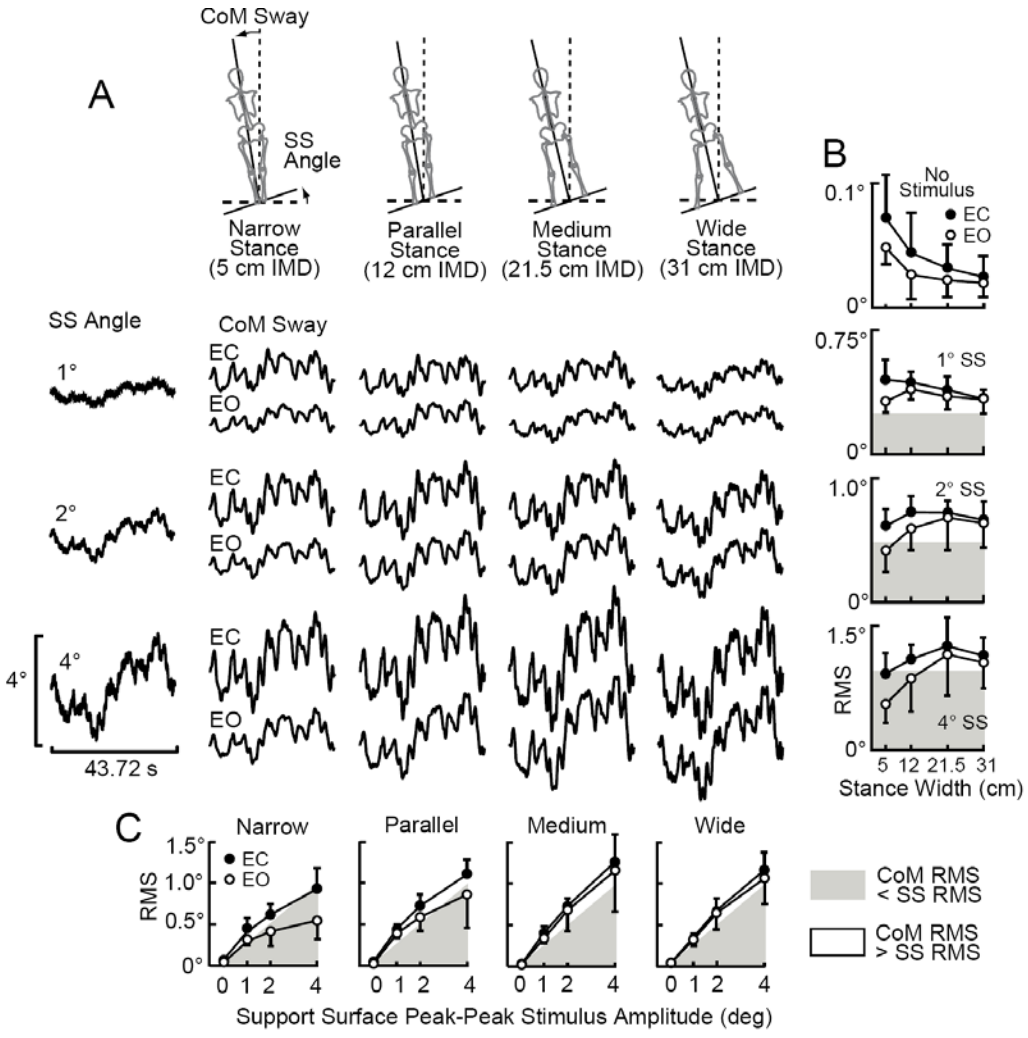


**FIG. 4.1.** *Center-of-mass (CoM) responses to support surface (SS) stimuli. A: Average cycle of CoM sway obtained by averaging across subjects and across all individual stimulus cycles showed dependency on stance width (intermalleolar distance, IMD), stimulus amplitude, and visual availability (eyes open, EO, or closed, EC). B: Root-mean-square (RMS) CoM sway as a function stance width for each stimulus amplitude (mean ± 1 SD). C: CoM RMS sway as a function of SS stimulus amplitude for each stance width (mean ± 1 SD).*

meaning that subjects tended to align to the SS. However, the extent of this alignment toward the SS depended upon visual availability, stimulus amplitude, and stance width.

Increasing stance width generally reduced RMS sway at low stimulus amplitudes but increased RMS sway at higher stimulus amplitudes (Fig. 4.1B). Specifically, for RMS sways across combined EO and EC conditions, increasing stance width resulted in a statistically significant decrease in RMS sway during spontaneous sway and the 1°

stimulus amplitude, and a significant increase in RMS sway during the 2° and 4° stimulus amplitudes (Fig. 4.1B). Visual availability (EO compared to EC) resulted in significant reductions in RMS sway during spontaneous sway and all stimulus amplitudes. There was a significant interaction between visual availability and stance width at 1° and 2° stimulus amplitudes. These interactions related to the fact that visual availability reduced sway to a greater extent in the narrow and parallel stances compared to the medium and wide stances. Similar interaction trends were evident for spontaneous sway (Fig. 4.1B, top) and 4° stimulus amplitude (Fig. 4.1B, bottom) but these interactions were not statistically significant.

Increasing stimulus amplitude resulted in a significant increase in RMS sway at all stance widths (Fig. 4.1C). This increase in RMS sway with SS amplitude was approximately linear in medium and wide stances whereas in narrow and parallel stances RMS sway showed some tendency toward saturation. Across all stimulus amplitudes, visual availability resulted in significant reductions in RMS sway in narrow and parallel stances, but not in medium or wide stances (Fig. 4.1C). A significant interaction between visual availability and SS amplitude was present in narrow stance (Fig. 4.1C, left). This interaction relates to the fact that increasing stimulus amplitude increased RMS sway to a lesser extent in EO compared to EC. A similar interaction trend was evident for the parallel stance condition, but this interaction was not statistically significant.

LB & UB SWAY. UB and LB sway averaged across all subjects during the 4° SS test for narrow and wide stance are shown in Fig. 4.2B. UB and LB RMS sway as a function of SS stimulus amplitude, stance width, and visual availability are shown is Fig. 4.2C and D. Variability in UB and LB RMS sway tended to be higher across subjects compared to CoM sway (compare error bars in Fig. 4.1 and Fig. 4.2). LB and CoM RMS sway exhibited very similar patterns as a function of SS amplitude, stance width, and EO/EC (compare Fig. 4.1B and Fig. 4.2C left column and compare Fig. 4.1C and Fig. 4.2D top row). For RMS sways across combined EO and EC conditions, increasing stance width resulted in a statistically significant decrease in LB RMS sway during spontaneous sway, no significant effect in the 1° stimulus amplitude, and a significant increase in RMS sway during the 2° and 4° stimulus amplitude (Fig. 4.2C left column). Visual availability resulted in significant reductions in LB RMS sway during the 1°

stimulus amplitude and there was a significant interaction between visual availability and stance width during the 1° stimulus amplitude (Fig. 4.2C left column).

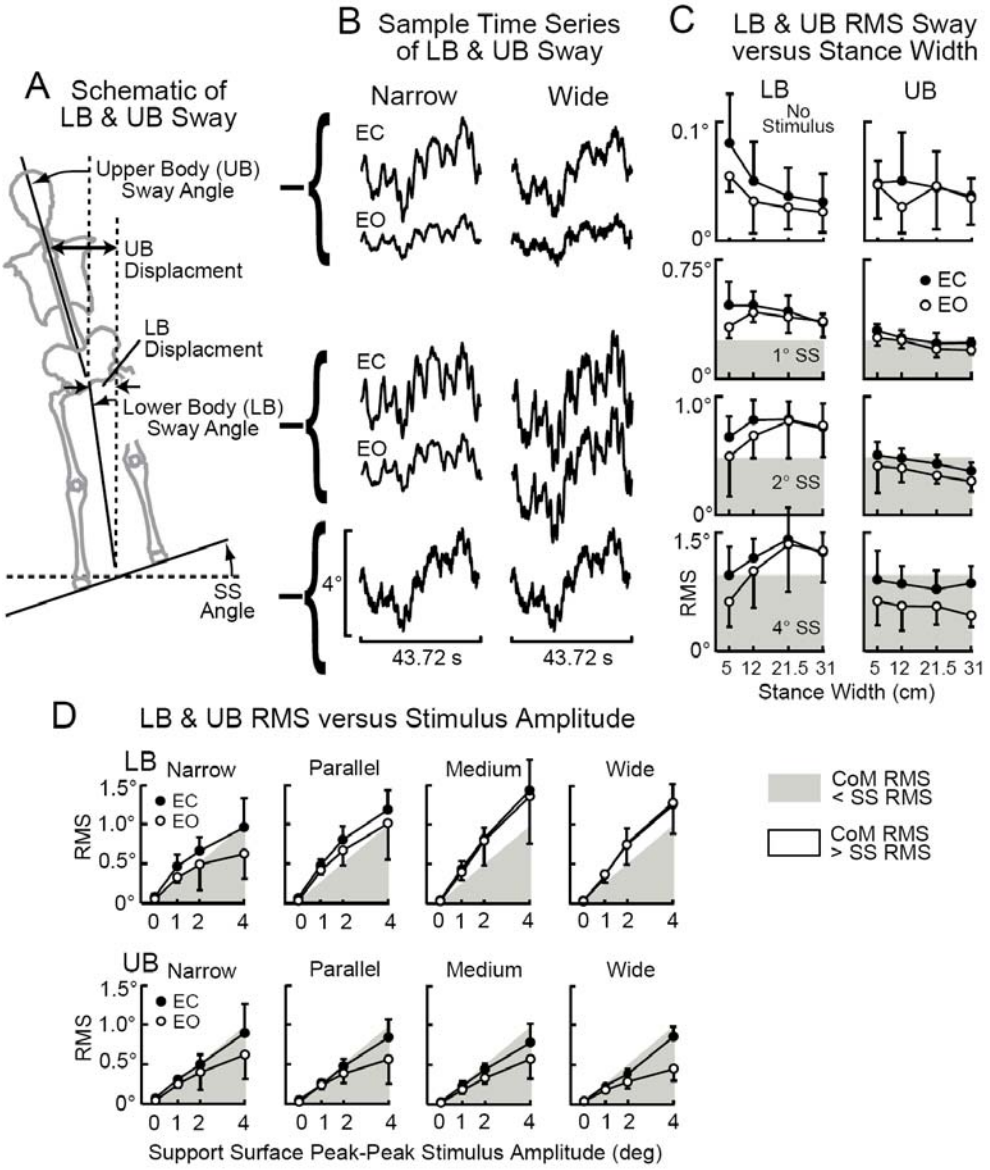


**FIG. 4.2.** *Lower body (LB) & Upper body (UB) responses to support surface (SS) stimuli. A: Definition of LB and UB sway. B: Average cycle of LB and UB sway responses obtained by averaging across subjects and across all individual stimulus cycles for the 4° SS tests. C: LB and UB root-mean-square (RMS) sway as a function of stance width for each stimulus amplitude (mean ± 1 SD). D: LB and UB RMS sway as a function of stimulus amplitude for each stance width (mean ± 1 SD).*

Increasing stimulus amplitude resulted in a significant increase in LB RMS sway in all stance widths (Fig. 4.2D top row). For RMS sways across stimulus amplitudes, visual availability significantly reduced LB RMS sway in narrow and parallel stances, but not in medium or wide stance widths (Fig. 4.2D top row).

Patterns of UB RMS sway were different from LB and CoM. For RMS sways across combined EO and EC conditions, increasing stance width significantly reduced UB RMS sway during the 1° and 2° stimulus amplitudes (Fig. 4.2C right column). Visual availability resulted in significant reductions in UB RMS sway during 1°, 2°, and 4° stimulus amplitudes (Fig. 4.2C right column). There was no significant interaction effect between vision and stance width on UB RMS sway during any SS test condition.

Increasing stimulus amplitude resulted in a significant increase in UB RMS sway in all stance widths (Fig. 4.2D bottom). Visual availability significantly reduced UB RMS sway in all stance widths (Fig. 4.2D bottom). There was a significant interaction between stimulus amplitude and visual availability in UB RMS sway in parallel and wide stance conditions (Fig. 4.2D bottom). Interaction trends were also evident in narrow and medium, but were not statistically significant. Taken together, these results imply that subjects used visual information to reduce their UB sway in all stance widths. This result is in contrast to LB sway where subjects only used visual information to reduce their LB sway in narrow and parallel stances.

CoM DISPLACEMENTS RELATIVE TO BASE-OF-SUPPORT. To determine the extent to which subjects' CoM approached the limits of their BoS, PP CoM displacements were divided by BoS for each test condition (represented as white bars in Fig. 4.3). PP CoM displacements did not exceed 26% of the BoS on any test condition. Larger stimulus amplitudes were associated with larger PP CoM displacements, similar to RMS sway. Increasing stance width (and therefore also the BoS) resulted in lower PP CoM displacements relative to BoS. EO PP CoM displacements were lower than EC, especially in narrow stance.

We quantified the role of body segment coordination in shaping CoM displacements. First, a hypothetical CoM displacement that would have occurred if the UB was perfectly aligned was calculated (represented as black bars in Fig. 4.3). Then, this hypothetical CoM displacement was compared to the experimental CoM

displacement. Experimental CoM displacement would have been less than the hypothetical if either 1) the actual UB PP sway angle was less in magnitude than the LB PP sway angle or 2) if the actual UB motion was out-of-phase with the LB so that peak UB sway did not occur at the same point in time as peak LB sway. In all test conditions, experimental CoM displacements were only slightly lower than those predicted if the UB was perfectly aligned. Specifically, in the narrow stance, experimental CoM displacements were 91% in EC 1°, 97% in EC 4°, 90% in EO 1°, and 89% in EO 4° SS tests of the CoM displacements that would have occurred if the UB and LB were aligned. In wide stance, experimental CoM displacements were 91% in EC 1°, 89% in EC 4°, 86% in EO 1°, and 80% in EO 4° SS tests of the CoM displacement that would have occurred if the UB and LB were aligned.

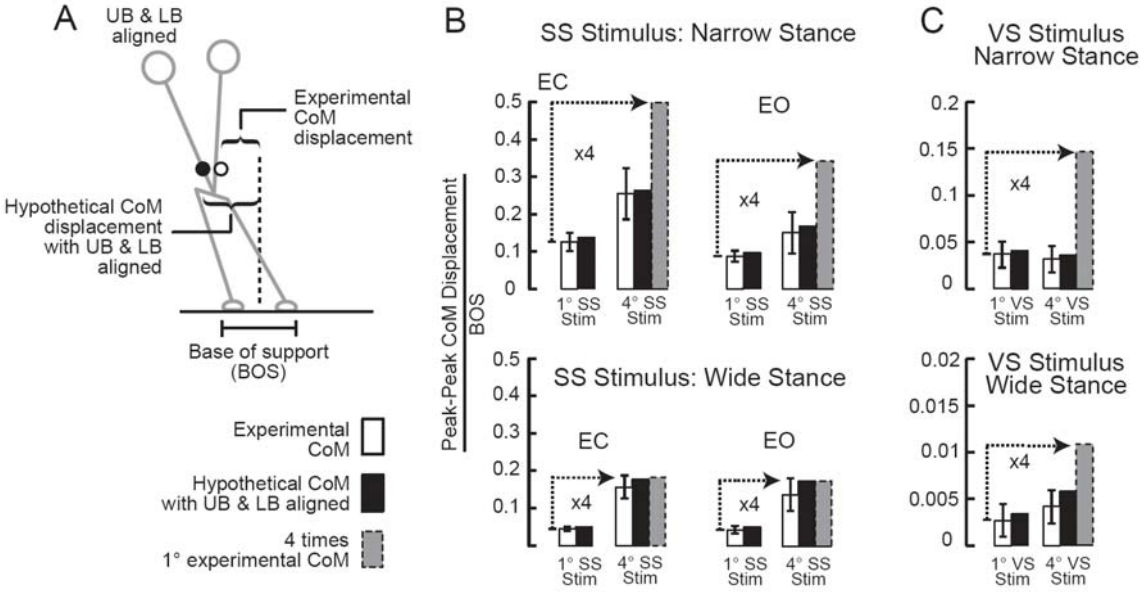


**FIG. 4.3.** *Peak-to-peak (PP) center-of-mass (CoM) displacements divided by base-of-support (BoS). A: Schematic of BoS, experimental CoM displacement, and hypothetical CoM displacement with UB and LB perfectly aligned. B: PP CoM displacements, where experimental CoM is represented as white bars and hypothetical CoM with UB and LB alignment represented as black bars. The grey bars represent a predicted linear increase in CoM displacement from 1° to 4°. C: Evoked PP CoM displacements by VS stimuli. Across-subject mean with ± 1 SD shown for the experimental CoM displacements.*

In addition to coordination of body segments, peak CoM displacements could have been reduced if the responsiveness of the postural system diminished with increasing stimulus amplitude such that the sway responses did not scale linearly with SS amplitude. To quantify the role of a stimulus-response nonlinearity in limiting the PP CoM displacements with respect to BoS, we compared the experimentally measured PP CoM displacement on the 4° SS test to the linear prediction that CoM displacement would be 4 times larger on the 4° SS test compared to the 1° SS test (represented as grey bars in Fig. 4.3B). There were no conditions where experimental PP CoM displacements increased linearly from 1° to 4°. In narrow stance, experimental CoM displacements during 4° SS stimuli were much smaller than the linear prediction (white bars / grey bars = 51% in EC and 43% in EO). However, in wide stance, experimental PP CoM displacements during 4° SS were much closer to the linear prediction (87% in EC and 80% in EO) than in narrow stance.

*Sway responses to VS stimuli*

VS stimuli and the CoM sway response for the three stimulus amplitudes and three stance widths are shown in Fig. 4.4A. CoM sway evoked by VS stimuli was low compared to CoM sway evoked by SS stimuli (compare to Fig. 4.1). There was a statistically significant decrease in RMS sway with increasing stance width across all three VS stimulus amplitudes (Fig. 4.4B), implying that subjects used visual information to orient their CoM most in narrow stance and least in wide stance. Stimulus-evoked CoM RMS sway was significantly greater than spontaneous sway in narrow and parallel stances, but not in the wide stance (Fig. 4.4C). Increasing VS stimulus amplitude did not have a significant effect on CoM sway in any stance width (Fig. 4.4C).

The general trend of LB and UB RMS sway during VS tests (data not shown) was similar to CoM, i.e. increased sway with decreased stance width. UB and LB RMS sway were similar to each other in narrow and parallel stances, but UB RMS sway was larger than LB sway in wide stance at all stimulus amplitudes. This result is consistent with UB sway patterns observed during SS tests where visual information influenced UB sway more than LB sway in the wide stance condition (Fig. 4.2C right column).

The relationship between subjects' PP CoM displacements and their BoS during VS tests is summarized in Fig. 4.3C. VS stimuli evoked PP CoM displacements that were

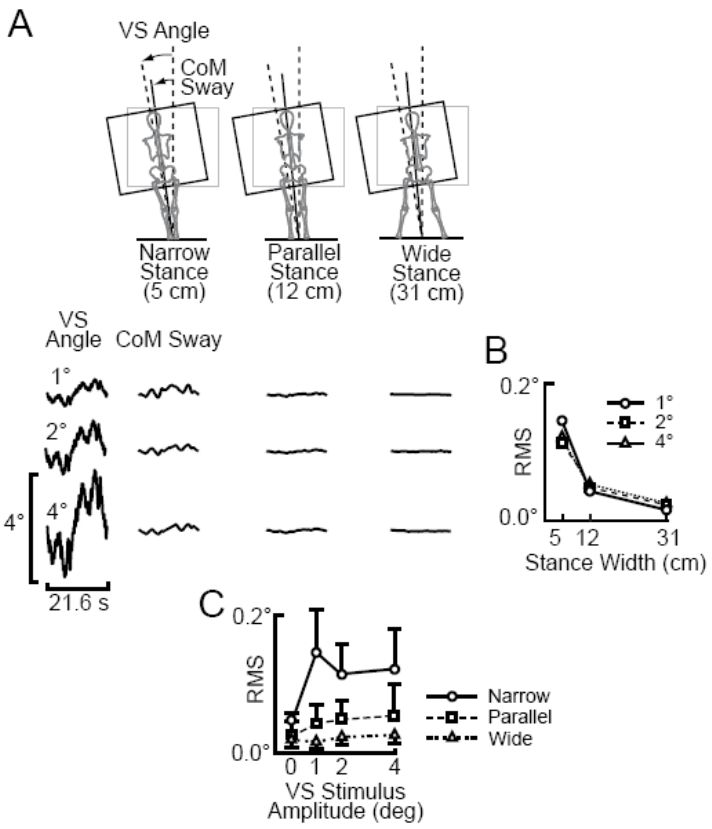


**Fig. 4.4.** *Center-of-mass (CoM) responses to visual surround (VS) stimuli. A: CoM sway averaged across subjects and stimulus cycles. B: Root-mean-square (RMS) CoM sway drastically decreased as stance width increased (mean ± 1 SD). C: CoM RMS sway as a function of VS stimulus amplitude (mean ± 1 SD).*

much smaller than displacements evoked during SS stimuli and were on average less than 5% of the BoS in narrow stance and less than 0.5% of the BoS in wide stance. In narrow stance, experimental PP CoM displacements were close to the displacements that would have occurred if the UB and LB were aligned (90% in 1° and 91% in 4° VS tests). In wide stance, experimental PP CoM displacements were 79% and 74% of the displacements that would have occurred if the UB and LB were aligned in the 1° and 4° VS tests, respectively. Experimental PP CoM displacements did not come close to the linear prediction that CoM displacements would be 4 times larger on the 4° VS test compared to the 1° VS test. Experimental PP CoM displacements were 22% and 39% of the displacements that would have occurred with a linear increase from 1° to 4° in the narrow and wide stance, respectively.

These PP results imply that a coordination strategy where the UB was not perfectly aligned with the LB was used to only a minor extend in narrow stance; but in wide stance, this coordination strategy was used more. In contrast, nonlinear PP displacements across stimulus amplitude were evident in both narrow and wide stance.

This nonlinearity did not seem necessary for balance control because CoM displacements could have increased linearly with the VS stimuli from 1° to 4° without exceeded 15% of the BoS – see grey bars in Fig. 4.3C).

*Frequency-response analysis of sway responses to SS stimuli*

CoM ANALYSIS. The variation across frequency of FRF gains was similar for all stance widths, stimulus amplitudes, and EO/EC conditions (Fig. 4.5). Gains in the 0.02- to 0.6-Hz range increased with increasing frequency to reach a peak value around 0.3 to 0.6 Hz. Gains decreased rapidly above 1 Hz, showed a minor peak or plateau around 4 Hz, and then decreased again for frequencies above 4 Hz. In frequency regions where gains were greater than one, subjects' CoM sway amplitude exceeded that of the SS stimulus.

Subjects exhibited amplitude-dependent changes in FRF gains in narrow and parallel stances, but amplitude-dependent changes were very minor in medium and wide stances. In narrow and parallel stances, increases in stimulus amplitude resulted in gain reductions at frequencies below about 1-1.5 Hz. Similarly, visual availability resulted in gain reductions below about 1-1.5 Hz for narrow and parallel stances, but had little effect on gains in medium and wide stances.

All phase curves showed some phase lead relative to the SS stimulus at frequencies below about 0.1 Hz. Phases generally decreased (more phase lag) with increasing frequency and exhibited a small peak or plateau around 3 Hz (Fig. 4.5). At each stance width, neither stimulus amplitude nor visual availability had a noticeable impact on phase curves. However, increasing stance width resulted in slightly reduced phase leads at frequencies < 0.1 Hz, slightly less phase lag at frequencies between 0.1 and 3 Hz (and consequently an apparent reduction in the peak at 3 Hz). Above 3 Hz, phases did not change as a function of stance width.

All SS stimuli resulted in coherences between 0.6 and 0.98 at frequencies < 1 Hz and coherences decreased sharply at frequencies greater than 1 Hz (Fig. 4.5). Increasing stimulus amplitude and increasing stance width generally resulted in higher coherences across all measured frequencies.

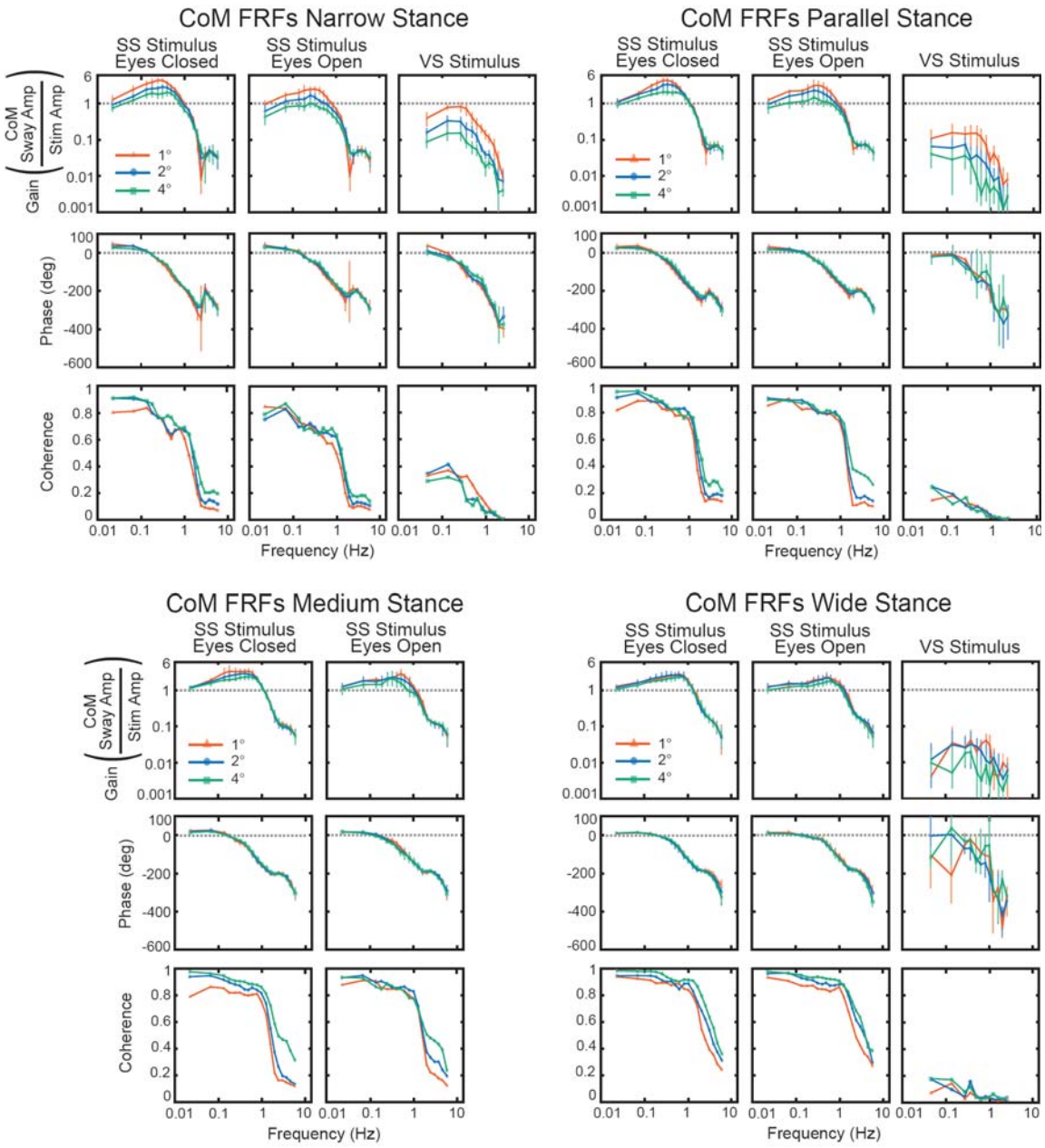


**FIG. 4.5.** *Center-of-mass (CoM) frequency-response functions (FRFs) and coherence functions for support surface (SS) and visual surround (VS) stimuli averaged across all subjects showed that stimulus amplitude and/or visual availability influenced FRFs more in narrow compared to wide stance conditions. Error bars on FRFs show 95% confidence intervals on mean gain and phase at each frequency.*

LB & UB ANALYSIS. For all EC tests, UB segment dynamics were similar across subjects. However, in five EO tests (2° and 4° narrow, 2° and 4° parallel, 2° medium), one subject exhibited a clearly different UB control strategy compared to the remaining 7 subjects (see Fig. 4.11 for more detail). Therefore, to make comparisons across test conditions, this particular subject's data were not included in figures describing UB and LB sway responses to SS stimuli (Fig. 4.6, 6, 7, and 9).

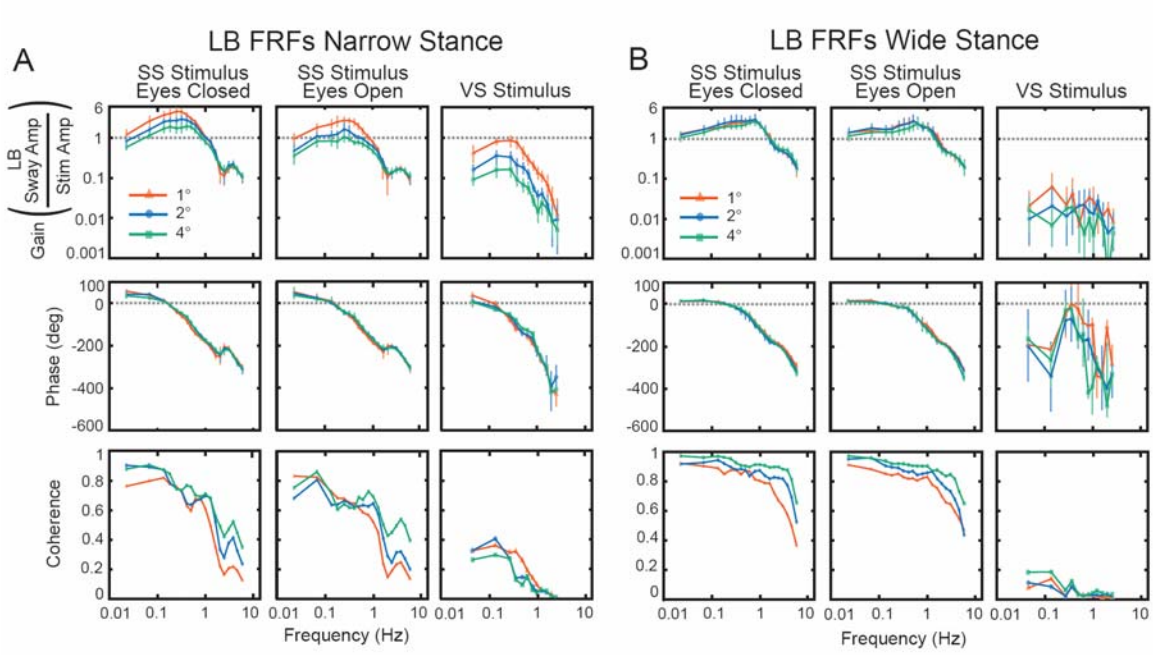


**FIG. 4.6.** *Lower body (LB) frequency-response functions (FRFs) and coherence functions for support surface (SS) and visual surround (VS) stimuli for narrow and wide stance show that patterns of LB FRFs were very similar to center-of-mass FRFs (compare to Fig. 4.5). Error bars on FRFs show 95% confidence intervals on mean gain and phase at each frequency.*

LB gains and phases were similar to CoM for all tests. Figure 4.6 shows LB gain and phase curves for the narrow and wide stance (compare to Fig. 4.5). In the narrow stance condition, there were LB gain reductions at frequencies below about 1 Hz with increasing stimulus amplitude and in EO compared to EC conditions (Fig. 4.6A). In the wide stance condition, LB gains were nearly invariant across stimulus amplitude and were only slightly reduced for EO compared to EC in the 0.2–1 Hz range (Fig. 4.6B). LB phase curves were essentially invariant across stimulus amplitude and between EO/EC conditions. LB coherences were similar to CoM coherences in that LB coherences were

generally high (above 0.7) at low frequencies and decreased with increasing frequency (Fig. 4.6). At frequencies above 1 Hz, LB coherences were higher than CoM coherences.

UB gains differed in several ways from LB and CoM gains. Most UB gain curves exhibited notches around 0.8-1 Hz where gains were much lower than surrounding frequencies (Fig. 4.7). Low gains indicate that the UB was upright in space and therefore relatively unaffected by the SS stimulus. Increasing stance width generally resulted in lower and more constant gains at frequencies below 0.8 Hz and larger gains between 2 and 6 Hz. Increases in stimulus amplitude were associated with gain reductions in all stances below 0.8-1 Hz, but these gain reductions were most systematic in the narrow and parallel stances. EO UB gains were more variable than EC and EO UB gains were lower than EC gains at frequencies below about 4 Hz for the narrow stance and below 0.8-1 Hz for all remaining stance widths.

EC UB phases were similar across all stance widths and stimulus amplitudes. Specifically, EC UB phases were nearly in-phase with the SS stimulus at the lowest frequencies (<0.1 Hz) and declined (more lag) with increasing frequency until reaching value of about -180º at 0.8 to 1 Hz, which corresponds with the frequency where most gain curves showed a notch. The EC phase curves wrap to ~+180º at about 1 Hz and then continue to show a monotonic decrease that reached ~-140º at 5.9 Hz.

There were many similarities, but also some differences between EC and EO UB phases. Across all stance widths and stimulus amplitudes both EC and EO phases were close to zero at frequencies below 0.1 Hz, and showed a monotonic decrease with increasing frequency at frequencies above 2 Hz. On some, generally lower amplitude test conditions (1° and 2° narrow stance and the 1° parallel, medium, and wide stances), EO and EC phase curves were very similar across all stimulus frequencies. However, on the other, generally higher amplitude trials, EO phases showed amplitude-dependent effects in the 0.3 to 2 Hz frequency range.

UB coherences were high at low frequencies, decreased with increasing frequency to a minimum around 0.5 at 1.3 Hz, then increased with increasing frequencies up to a peak around 3-4 Hz, and then decreased at frequencies above 3-4 Hz (Fig. 4.7). The peaks and valleys in UB coherence curves coincide with peaks and valleys in UB gain curves, consistent with reduced signal-to-noise ratios in the experimental data at frequencies where gains were low.

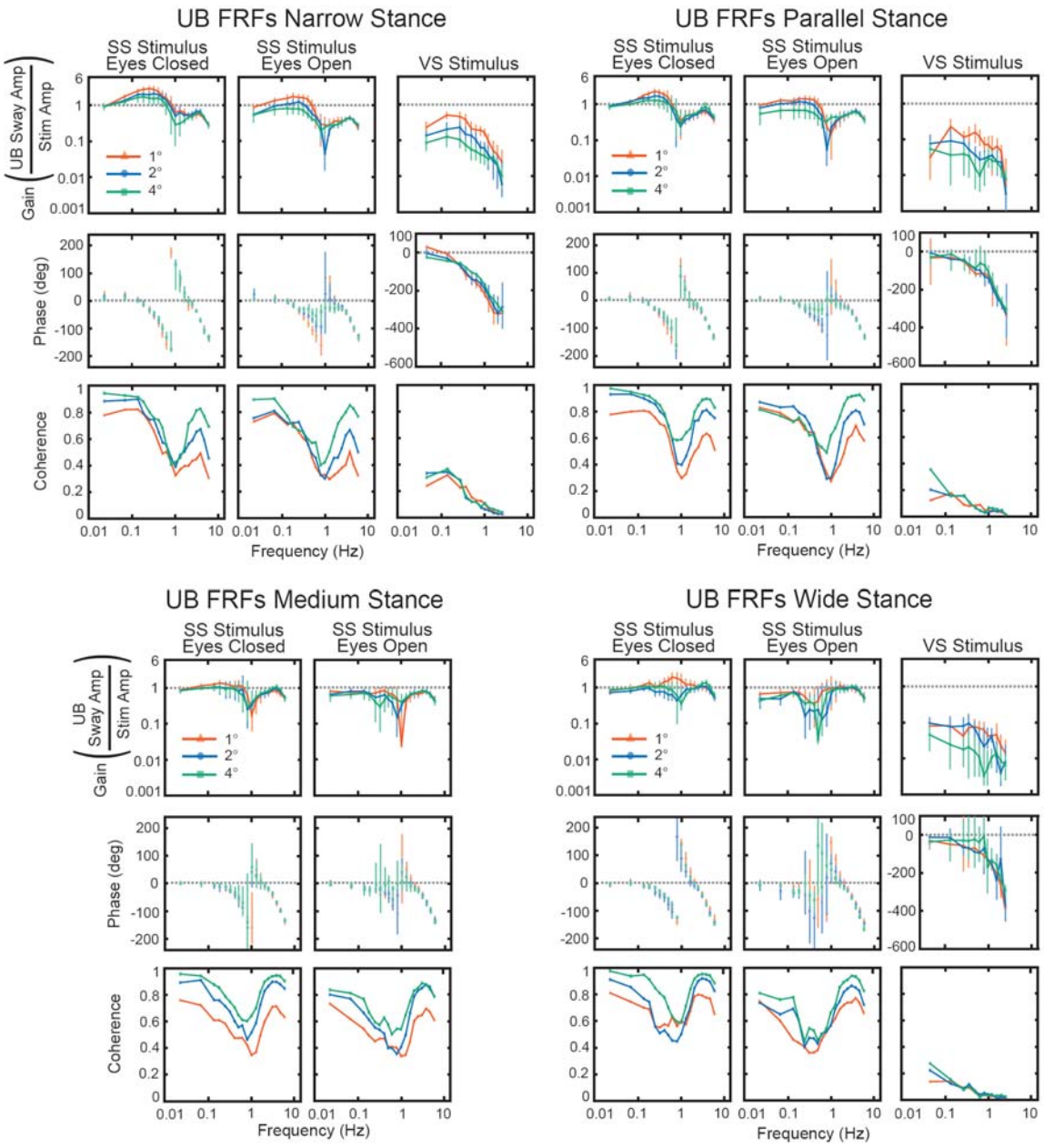


**FIG. 4.7.** *Upper body (UB) frequency-response functions (FRFs) and coherence functions for support surface (SS) and visual surround (VS) stimuli. Phases were not "unwrapped" like LB and CoM phases in Figs. 3.5 and 3.6 because several UB FRFs did not vary smoothly across all stimulus frequencies such that unwrapping algorithms did not perform consistently thus giving a false impression that phases differed greatly between some trials. Error bars on FRFs show 95% confidence intervals on mean gain and phase at each frequency.*

RELATIVE LB & UB MOTION. UB gains relative to LB gains (i.e. the ratio of UB gain / LB gain) and UB phase relative to LB (i.e., the difference of UB-LB phase) are shown in Fig. 4.8A. At the lowest stimulus frequency (0.023 Hz), UB gains were between 0.33 and 1.5 times LB gains. Above 0.023 Hz, in all stance widths, UB gains decreased relative to LB gains until about 1 Hz where a sharp transition occurred and UB gains increased relative to LB gains. At frequencies above 3 Hz, UB gains were 2.1-3.2 times larger than LB gains.

Increasing stimulus amplitude resulted in larger UB gains relative to LB gains at low stimulus frequencies (< ~0.5 Hz) in EC/EO narrow and EC parallel conditions. Visual availability had the most consistent effect on medium and wide stance conditions where EO UB gains relative to LB gains were 0.81 and 0.55 times EC averaged across frequencies below 0.4 Hz in medium and wide, respectively.

On all EC tests, UB phase relative to LB showed that UB sway lagged the LB at frequencies less than ~0.1 Hz, was approximately in-phase with the LB at ~ 0.18 Hz, and transitioned to being out-of-phase (~ -180º) with the LB at frequencies above 2 Hz. Transitions from in-phase to out-of-phase behavior were similar across stance widths and were not influenced by stimulus amplitude on EC tests.

The relative phase on EO SS tests were similar to EC at low frequencies (<0.3 Hz) and at higher frequencies (>2 Hz), but in the frequency range between 0.3 to 2 Hz transitions from in-phase to out-of-phase showed some dependence on stimulus amplitude and stance width. The most obvious difference between EO and EC phases occurred on the 4° SS tests where the phase of UB relative to LB increased systematically with increasing frequency from 0.3 to 1 Hz prior to becoming out-of-phase (±180º) at higher frequencies.

Frequencies where the phase transitions occurred coincided with frequencies where UB gains relative to LB gains were lowest. UB gains relative to LB gains were highest when the UB moved 180º out-of-phase with the LB.

*Frequency-response analysis of sway responses to VS stimuli*

CoM ANALYSIS. For VS stimuli, gains were very dependent on stance width (Fig. 4.5). In narrow stance, gain curves had one peak around 0.2 Hz and showed reductions with increasing stimulus amplitude across all measured frequencies (0.046 to

2.6 Hz). In parallel stance, gain curves were lower and more variable compared to narrow stance, but otherwise exhibited similar features. In wide stance, gain curves were very low (10 times smaller than narrow stance) and variable due to poor signal-to-noise.

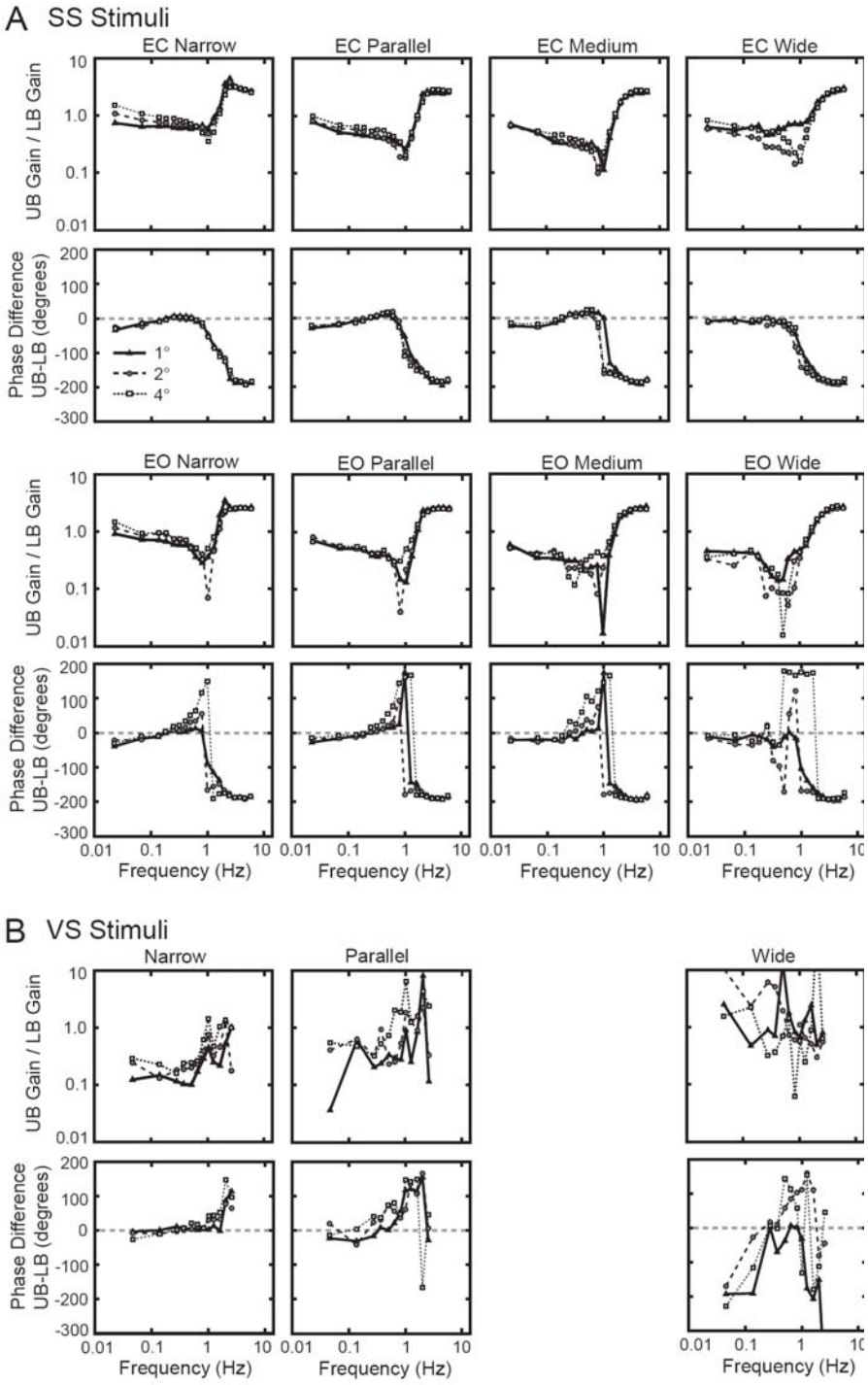


**FIG. 4.8.** *Ratios of upper body (UB) gain to lower body (LB) gain and phase difference between UB and LB versus stimulus frequency for A) SS stimuli and B) VS stimuli.*

Phases were approximately 0º at 0.046 Hz and generally decreased with increasing frequency. There was little or no change in phases across stimulus amplitudes in the narrow and parallel stances. However, wide stance phases were approximately -110º at 0.046 Hz for the 1° and 4° stimulus amplitude, indicating that subjects' CoM was not in-phase with the visual stimuli at the lowest stimulus frequency.

Coherences were below 0.5 for all VS tests and decreased with increasing frequency. Increasing stance width generally decreased coherences.

LB & UB ANALYSIS. For VS stimuli, LB gains were similar to CoM gains. Gain reductions occurred across all measured frequencies with increasing stimulus amplitude and gains were much lower in the wide stance compared to the narrow stance (compare Fig. 4.6 to Fig. 4.5).

LB phases in the narrow (Fig. 4.6) and parallel (not shown) stances were similar to CoM phases. However, in the wide stance condition at all stimulus amplitudes, LB phases were ~ -180º at 0.046 Hz indicating that, in the wide stance condition, the LB was out-of-phase with the VS at the lowest stimulus frequency.

LB coherences were below 0.5 for all VS tests and decreased with increasing frequency. Increases in stance width were associated with lower LB coherences.

UB gains showed similarities with LB and CoM gains such that gains decreased with increasing stimulus amplitude across the measured frequencies and gains decreased with increasing stance width. In narrow stance, UB gains were about 1.5-2 times smaller than LB gains at frequencies below 1 Hz (Fig. 4.8B). However, in the wide stance condition, UB gains were about 4-5 times larger than LB gains at frequencies below 1 Hz. This pattern of UB and LB gains indicate that subjects oriented their UB to visual stimuli more than their LB in the wide stance and less than the LB in narrow stance.

Across all stimulus amplitudes and stance widths, UB phases were approximately 0º at 0.046 Hz and generally decreased with increasing frequency (Fig. 4.7). In narrow stance, the UB was relatively in-phase with the LB at the lowest frequencies (<~0.5 Hz) but tended to lead the lower body between 0.5 and 1.5 Hz (Fig. 4.8B) and this phase lead increased with frequency similar to several of the EO SS test conditions (Fig. 4.8A). In parallel stance, UB phase relative to LB was similar to narrow but was more variable. In the wide stance, the UB was out-of-phase with the LB at the lowest VS stimulus

frequency (0.046 Hz) (Fig. 4.8B), but at higher frequencies interpretation was difficult because of the low responses and consequently high variability in body segment kinematics.

UB coherences were below 0.5 for all VS tests and decreased with increasing frequency. Increases in stance width were associated with lower UB coherences.

*Time-domain analysis*

Time-domain analysis of the dynamic responses to SS perturbations was accomplished by computing impulse-response functions (IRFs). Although continuous rotations were used to estimate IRFs, an IRF can be intuitively thought of as the time course of a subject's rotational sway velocity evoked by a sudden SS tilt of 1° (i.e. a velocity impulse). Negative IRF values indicate sway velocity in a direction opposite to the SS tilt and positive IRF values indicate sway velocity in the same direction as the SS.

CoM IRFs. Fig. 4.9A shows the computed SS IRF velocity impulse, which includes the dynamics of the SS actuator and servo-control, and Fig. 4.9B shows the CoM IRFs. In all SS tests, CoM IRFs exhibited a very brief small negative peak at ~0.05 s, followed by a sharp positive rise up to a first local maximum of 0.9 to 5.1°/s at ~0.2 s, followed by a brief dip or plateau before another positive rise up to a second local maximum (usually corresponding to the overall IRF maximum) of 1.6 to 6.4°/s at ~0.3-0.55 s. IRFs then decreased to a minimum value of -0.3 to -2.3°/s at ~0.8-1.6 s, and finally decayed to approximately zero within 4 s.

The detailed time course of IRFs depended on stance width, stimulus amplitude, and visual availability. CoM IRFs showed stance-width dependency after 0.05 s. Increasing stance width resulted in larger first local maximum values, but did not affect the time required to reach the first local maximum at ~0.2 s. In contrast, the time required to reach the second local maximum decreased as stance width increased (~0.3 s for wide stance compared to ~0.55 s for narrow stance). Also, increases in stance width were associated with IRFs that decreased in value faster following the IRF peak and reached a minimum in less time (~0.8 s for wide stance compared to ~1.6-1.8 s for narrow stance).

Stimulus amplitude-dependent changes were most pronounced in narrow and parallel stances. In narrow and parallel stances, increases in stimulus amplitude were

associated with a slight decrease in CoM IRF magnitude beginning at ~ 0.1 s (not clearly evident on the scale of Fig. 4.9B plots), followed by a larger decrease in CoM IRF magnitude beginning at ~0.2 – 0.25 s.

The availability of vision affected CoM IRFs after a time delay of about 0.15 s in all stance widths where EO IRFs had lower magnitudes than EC (Fig. 4.9C). Differences between EO and EC CoM IRFs were greatest in narrow stance and least in wide stance conditions.

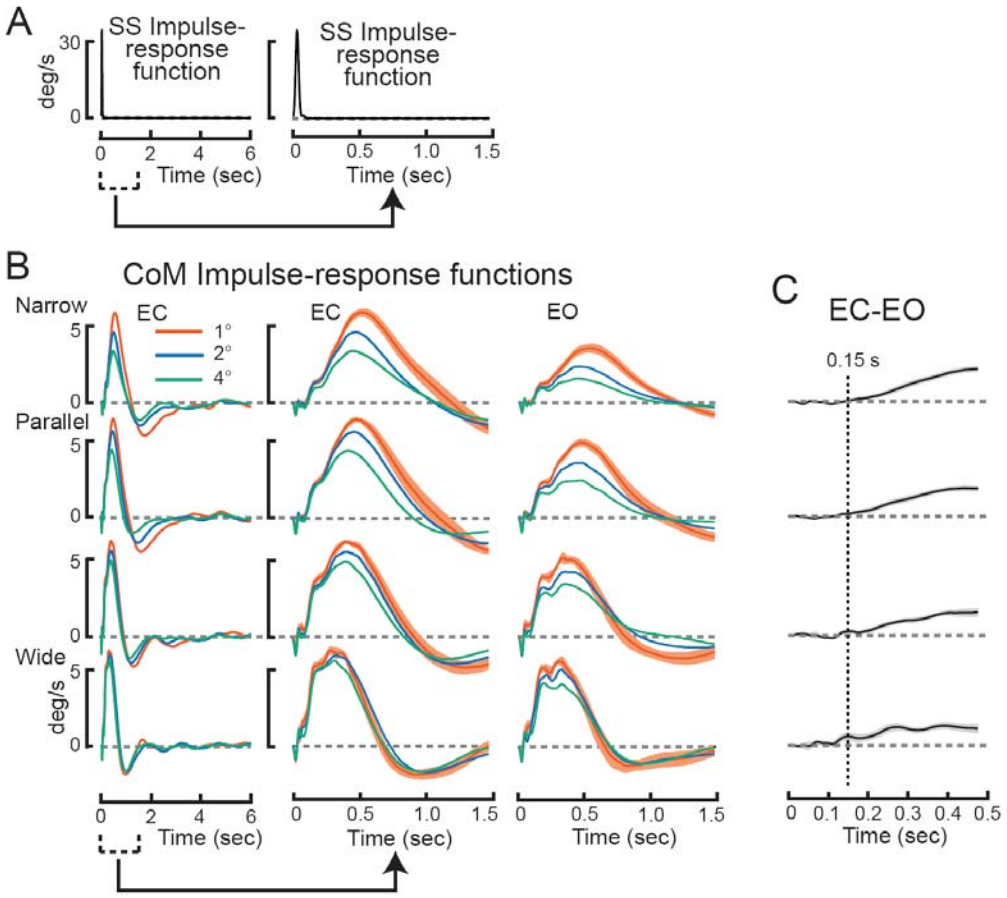


**FIG. 4.9.** *Center-of-mass (CoM) impulse-response functions (IRFs) from support surface (SS) stimuli. A: SS tilt stimulus IRFs calculated between the ideal PRTS velocity and the actual support surface velocity. B: Eyes closed (EC) and eyes open (EO) CoM IRFs derived from the three different SS stimulus amplitudes. Across-subject mean with ± 1 SE shown for the 1° stimulus. C: EC minus EO CoM IRFs averaged across subjects and stimulus amplitudes (mean ± 1 SE) and displayed between 0-0.5 s to show time delay before onset of visual contribution, approximately 0.15 s (vertical dashed line).*

LB & UB IRFs. The overall shape of LB IRFs (Fig. 4.10A) were similar to CoM IRFs (Fig. 4.9B), however, LB IRF curves exhibited more pronounced features compared to CoM. Specifically compared to CoM, LB IRFs exhibited larger and longer initial negative peaks at ~0.05 s, larger first local maximums of 1.6 to 8.5°/s at ~0.2 s, larger second maximums of 1.8 to 7.3°/s at ~0.3-0.55 s, and larger minimums of -0.31 to -2.7°/s at ~0.8-1.6 s. Changes in stance width, stimulus amplitude, and visual availability had very similar effects on both LB and CoM IRFs.

The time course of UB IRFs differed from LB and CoM (Fig. 4.10B). UB IRFs began with a large initial positive peak of 4.2 to 11°/s at ~0.05 s, followed by a negative peak of -1.3 to -7.7°/s at ~0.2 s, followed by a positive rise up to a local maximum of 0.6 to 5.5°/s at ~0.4-0.7 s, and eventual decay to zero by 3 s. At times < 0.25 s, the initial positive and negative peaks in UB IRFs generally coincided in time with, but were opposite in sign to, the initial negative and positive peaks in LB IRFs. This result means that for the first ~0.25 s following a sudden SS rotation, UB and LB sway velocities were opposite in direction in all SS tests.

Increasing stance width affected UB IRFs in several ways. Wider stances resulted in larger initial positive peaks at ~0.05 s and then larger negative peaks at ~0.2 s. Increases in stance width were also associated with IRFs that reached local maximums with less delay (~0.4 s in wide compared to ~0.7 s in narrow) and local minimums with less delay (~1 s in wide compared to ~2 s in narrow). Increases in stimulus amplitude and visual availability were associated with lower UB IRF magnitudes evident in all stance widths. This result is different from LB and CoM IRFs where stimulus amplitude- and visual-dependent changes were more evident in narrow and parallel stance widths compared to medium and wide.

*Counter-phase UB sway in one subject*

In five EO tests (2° and 4° narrow stance, 2° and 4° parallel stance, and 2° medium stance), one subject exhibited a clearly different control strategy compared to all other tests and compared to the remaining 7 subjects. Fig. 4.11 compares the UB sway of this subject to the mean results from the remaining 7 subjects during the 4° EO SS test, narrow stance condition. Figure 4.10A shows that UB sway tended to be counter-phase

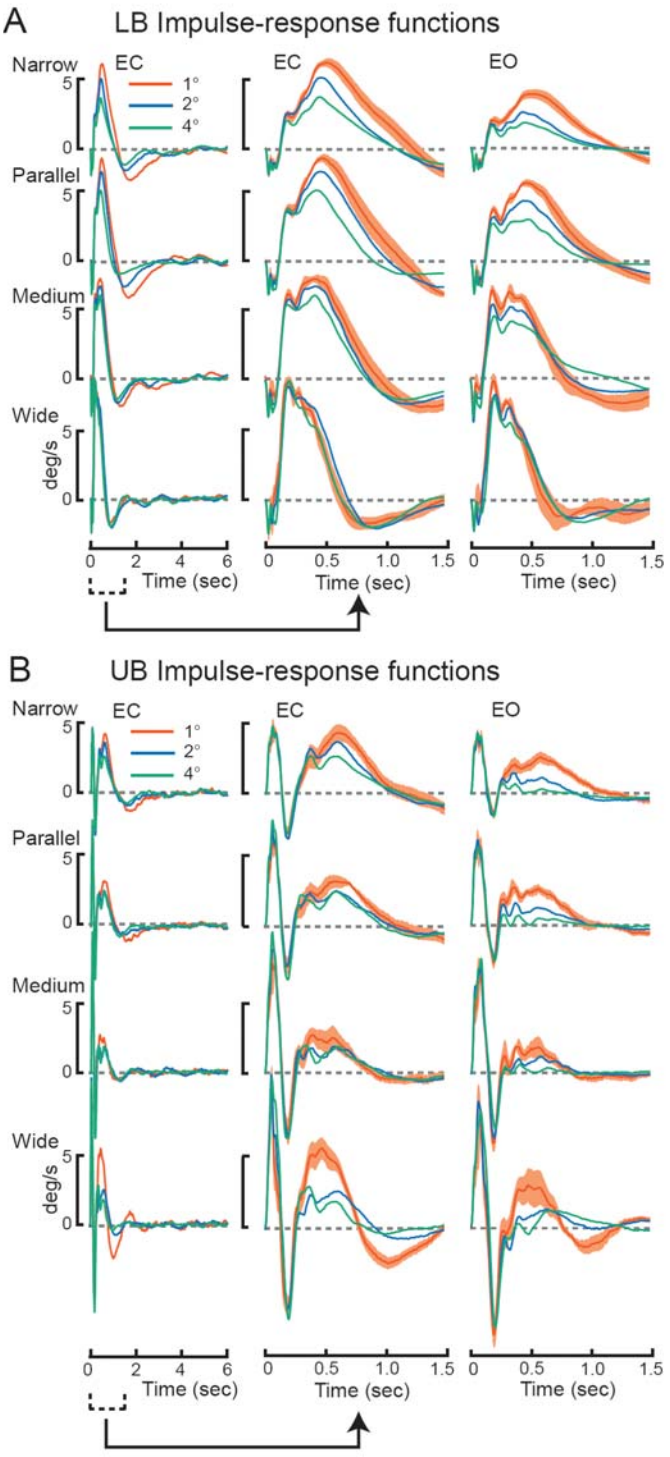


**FIG. 4.10.** *Impulse-response functions (IRFs) for A) lower body (LB) and B) upper body (UB) eyes closed (EC) and eyes open (EO) conditions. Across-subject mean with ± 1 SE shown for the 1° stimulus.*

with the SS in this particular subject whereas UB sway tended to align toward the SS stimulus in the remaining 7 subjects. The counter-phase UB sway in this particular subject had larger gains compared to the remaining 7 subjects at the lowest stimulus

frequency (0.023 Hz) and between 0.4-0.6 Hz, but at all other frequencies, gains were similar across all subjects (Fig. 4.11B). UB phases in this particular subject differed most from the remaining 7 subjects at low frequencies where phases were out-of-phase with the SS at the lowest stimulus frequency and monotonically decreased with increasing stimulus frequency to ~-80º at 5.9 Hz (Fig. 4.11B). UB IRFs were similar between the counter-phase subject and the remaining 7 subjects before 0.25 s (Fig. 4.11C). However, between 0.25-1.5 s, the counter-phase subject's UB IRF was more negative than the remaining 7 subjects', consistent with the UB moving in the opposite direction as the SS.

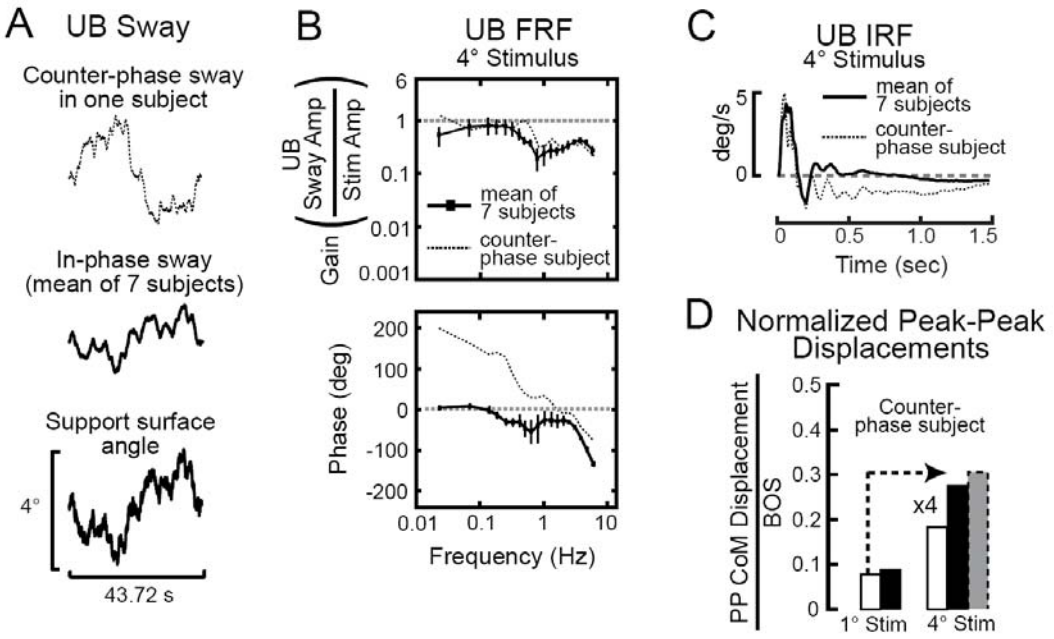


**FIG. 4.11.** *Example data from the single subject that used a counter-phase control strategy in several eyes open (EO) test conditions. Results of EO narrow UB analysis in the individual subject compared to mean results in the remaining 7 subjects are shown for A) sway waveforms, B) frequency-response functions, and C) impulse-response functions. D: Peak-to-peak (PP) CoM displacements divided by base-of-support for the 1° and 4° stimulus. Experimental CoM represented as white bars and hypothetical CoM with UB and LB alignment represented as black bars. The grey bar represents a predicted linear increase in CoM displacement from 1° to 4°.*

The sway behavior in Fig. 4.11 exemplified a coordinated use of a hip-strategy at low frequencies. This coordination strategy was quantified through measures of PP CoM displacements divided by BoS for the EO 1° and 4° tests (Fig. 4.11D). During the 1° test,

experimental PP CoM displacements (white bar) were 88% of the displacements that would have occurred if the UB and LB remained aligned (black bar). This result was similar across all subjects (compare Fig. 4.10D to Fig. 4.3B). However, as SS amplitudes increased to 4°, this particular subject exhibited counter-phase UB sway so that experimental PP CoM displacements were 66% of the displacements that would have occurred with aligned UB and LB segments. Even with this counter-phase strategy, there was still some contribution due to nonlinear scaling of postural responses as SS amplitudes increased from 1° to 4° because experimental PP CoM displacement was only 59% of the displacement that would have occurred assuming a linear increase in sway from 1° to 4° (grey bar).

## DISCUSSION

Frontal plane sway was evoked in freestanding subjects using continuous rotations of the SS. The stimulus was delivered at various amplitudes and subjects stood at one of several possible stance widths ranging from narrow to wide with either eyes open or closed. Kinematic responses of the UB, LB, and CoM were summarized with RMS and PP measures of body sway and the dynamic characteristics of body sway were described in detail through FRFs and IRFs. We determined the stance-width dependence of response sensitivity to identify the contribution of nonlinear control behavior in limiting CoM excursions and tested the extent to which UB and LB coordination influenced CoM excursions.

### *Coordination strategy*

One potential strategy to limit CoM excursions from upright is to use coordinated counter-phase motion of UB and LB segments to keep the overall CoM motion small relative to the BoS even though the motion of individual body segments may be large. We tested the hypothesis that coordinated counter-phase motion of the UB and LB is used in narrow stance conditions to limit CoM displacements relative to the small BoS. Additionally, we hypothesized that this coordinated counter-phase strategy is used less at wider stance widths because CoM displacements can be larger without jeopardizing

stability. If these hypotheses are true, then we expected to see greater use of coordinated counter-phase LB and UB motion in narrow compared to wide stance conditions.

Coordinated counter-phase UB and LB motion and perfect alignment of the UB and LB represent two extremes on a continuum of possible coordination strategies. Perfect alignment means that UB and LB have identical gains and phases (in-phase with each other) while coordinated counter-phase sway means that UB and LB have opposite phases. Neither perfect alignment nor coordinated counter-phase sway occurred across all stimulus frequencies. Instead, strategies emerged in a frequency-dependent manner.

At low stimulus frequencies (<0.5-1 Hz) and in narrow stance conditions, subjects' UB and LB motion was approximately in-phase (Fig. 4.8) and had similar gain values. At low stimulus frequencies (<0.5-1 Hz) and in wide stance conditions, subjects' UB and LB were also approximately in-phase, but UB gains were smaller than LB gains (Fig. 4.6 and 6) indicating less body segment alignment compared to narrow stance. Thus, at low frequencies, the hypothesis that coordinated counter-phase UB and LB motion is high in narrow stance and decreases with increasing stance width was not supported. At high stimulus frequencies (>1-2 Hz), UB and LB sway was approximately out-of-phase (Fig. 4.8) across all stance widths. Thus, the hypothesis that coordinated counter-phase motion is higher in narrow stance was also not supported.

There were two exceptions to the preceding conclusion. First, during wide stance VS tests, the UB was about 8 times more responsive to the VS stimuli compared to the LB. We speculate that this larger UB response, that was in-phase with the VS at low frequencies, could have produced interaction torques on the LB that were large enough to evoke LB sway in the opposite direction of the UB. However, the high variability in this test condition made interpretation difficult. Second, in several EO test conditions (generally conditions with small BoS and higher stimulus amplitudes), one subject exhibited UB sway that was out-of-phase with the LB across all stimulus frequencies (Fig. 4.11). Thus in select conditions this subject employed coordinated movements that were beneficial in the sense of reducing CoM sway. We do not have an explanation for this behavior and can only point out that visual availability must have had an important influence on the control strategy used by this subject because the UB phase relative to LB in this subject was similar to all other subjects during EC tests. Previous studies have shown that numerous factors can influence the use of a hip versus an ankle strategy

(Horak and Macpherson 1996), including availability of sensory information (Horak et al. 1990). It also seems plausible that other subjects might have used a counter-phase coordination strategy at low stimulus frequencies if sway was evoked with larger stimulus amplitudes than those used in the current study.

*Nonlinear stimulus-response strategy*

A second potential strategy to limit CoM excursions from upright is to employ a nonlinear control scheme that reduces the sensitivity to perturbations of increasing amplitude. Overall results indicate that a nonlinear control strategy played an important role in limiting CoM excursions in narrow stance conditions. The role of this strategy decreased with increasing stance width such that its contribution was very small in the wide stance condition. For example, in narrow stance responses to SS stimuli, as stimulus amplitudes increased, and in EO compared to EC, there were CoM FRF gain reductions at frequencies below 1-1.5 Hz with minimal phase changes (Fig. 4.5). Furthermore, CoM gain reductions were accompanied by UB and LB gain reductions typically below 1 Hz while UB and LB phases were approximately in-phase at corresponding frequencies (Fig. 4.6, 6, and 7). In responses to VS stimuli, there were similar UB and LB phase behavior and UB and LB stimulus amplitude-dependent nonlinearity across stimulus amplitude in narrow stance conditions. Thus, the nonlinearity present in narrow stance during SS stimuli (EO and EC) and VS stimuli was not attributable to a change in coordination.

On the other hand, during SS stimuli, in both EO and EC wide stance conditions, CoM RMS sway and PP displacements increased nearly in direct proportion to the SS amplitude, but this nearly linear increase was not present in narrow stance (Fig. 4.1 and 3B). Furthermore, CoM FRF gains showed only minor reductions with increasing SS stimulus amplitude both in EO and EC wide stance conditions, but there were clear reductions in gains in narrow stance (Fig. 4.5). Similarly, there were only minor reductions in IRF peak amplitudes associated with increases in SS stimulus amplitude in wide stance IRFs compared to the much larger reductions in narrow stance (Fig. 4.9). Thus, in wide stance conditions, subjects appeared to adopt a "simpler" linear control strategy compared to the nonlinear control present in narrow stance conditions during SS stimuli. CoM FRFs in VS stimuli showed only minor evidence nonlinear control across stimulus amplitude.

*Evidence for sensory reweighting*

Because changes in stance width alter LB mechanics, it was not possible to determine what factors (i.e., mechanics and/or neural control) contributed to the changes in postural dynamics as a function of stance width. However, for a given stance width, LB mechanics are essentially fixed. Therefore, the observed amplitude-dependent changes in FRFs at a given stance width must be due to changes in the underlying control system. There is previous evidence that the nonlinear stimulus-response behavior, particularly prominent at narrower stance widths, is attributable to a sensory reweighting phenomenon.

There are two previous studies of frontal plane stance control where sensory reweighting was identified as a dominant contributor to the experimentally observed system nonlinearity (Cenciarini and Peterka 2006; Oie et al. 2002). The study of Oie et al. (2002) identified an amplitude-dependent nonlinearity in visually-evoked sway when subjects maintained a very narrow stance (tandem-Romberg). They determined that their data were more accurately explained by a control system model that attributed the nonlinear behavior to an amplitude-dependent re-weighting of sensory orientation cues rather than to a change in control properties (i.e., changes in the stiffness and damping of neural controller). The similarities between visually-evoked sway behavior in the previous study and the sway during VS tests (Fig. 4.5) in the current study suggest that a similar sensory reweighting mechanism occurred in narrow stance conditions.

The study by Cenciarini and Peterka (2006) used varying amplitude pseudorandom SS rotations to evoke frontal plane sway in subjects standing with feet close together (~10 cm IMD). In addition to the SS stimulus, this previous study simultaneously presented a pulsed galvanic stimulation of the vestibular system that was mathematically uncorrelated with the SS stimulus. With increasing SS stimulus amplitude, subjects became more responsive to the galvanic stimulation and relatively less responsive to the SS stimulus exhibiting gain reductions with minimal change in phase at frequencies below 1-2 Hz. The increased responsiveness to galvanic vestibular stimulation and the gain reductions and with increasing SS amplitude were attributed to a sensory reweighting mechanism whereby subjects shifted away from reliance upon proprioceptive cues that orient the body to the SS and toward reliance upon vestibular

cues that orient the body more upright. The similarities between the narrow stance FRF SS stimuli results at frequencies below 1-2 Hz in the current and previous study (Cenciarini and Peterka 2006) provides evidence that sensory reweighting contributed to a relatively lower responsiveness to SS stimuli as the SS amplitude increased. By extension to wider stance width conditions, where FRF gains showed less dependency on stimulus amplitude, the diminished amplitude-dependent behavior is consistent with a diminished role of sensory reweighting in compensating for perturbations of different amplitudes.

IRF results are also consistent with the interpretation that sensory reweighting contributed to the amplitude-dependent nonlinearly in narrower stance conditions. Because IRFs represent the time course of a subject's response to a sudden SS tilt, IRFs can be used to detect sensorimotor time delays in the balance control system. Sensorimotor time delays include the time required to process sensory information, transmit signals through axons, synapses, and neuromuscular junctions, and activate muscle contractions. If the relative reductions in CoM responsiveness to SS stimuli with increases in SS amplitude were due to a neurally-mediated sensory reweighting mechanism, then we expect to see changes in IRFs across SS amplitude after a time delay consistent with delays associated with sensory integration for balance control, considered to be at least 100 ms (Peterka 2002; Van der Kooij et al. 1999). In contrast, IRF changes at shorter delays would be indicative of changes in muscle stiffness (possibly due to co-contraction) or short-latency reflex activation.

In narrower stance conditions with both EO and EC, CoM IRFs showed minimal differences across SS amplitudes in the first ~150 ms (Fig. 4.9B). After ~150 ms, IRF peak amplitudes decreased with increasing stimulus amplitude. Thus, after a time delay consistent with delays associated with sensory integration, subjects became less responsive to the SS stimulus as SS amplitude increased. The difference between the time courses of EO versus EC CoM IRFs is also consistent with visual availability contributing to changes in stimulus-response dynamics through a sensory reweighting mechanism. Specifically, visual availability altered the time course of the EO IRF relative to the EC IRF only after a delay of ~150 ms (Fig. 4.9C).

*Biomechanical contributions to UB IRFs*

The time course of UB IRFs (Fig. 4.10B) gives insight into the mechanisms contributing to the control of UB orientation on the pelvis. The initial sharp rise in the UB IRFs occurred with no time delay indicating a mechanical origin to this early feature of these IRFs. The biphasic time course over the first ~0.2 s increased in magnitude with increasing stance width but was relatively unaffected by visual availability and stimulus amplitude. Short latency reflexes, such as a stretch reflex, could have contributed to later portions of the initial biphasic time course (Skotte et al. 2005; Cresswell et al. 1994), but the invariance of the early portion of the UB IRF to stimulus amplitude indicates that any reflex contribution scaled proportionally with the stimulus amplitude. For example, in narrow stance, a sudden SS tilt of 1˚ would produce a sudden pelvis tilt that is less than 1˚. But as stance width increases, a sudden SS tilt of 1˚ would produce larger pelvis tilts and the tilt would exceed 1˚ for medium and wide stance widths. Therefore, intrinsic stiffness and reflexive mechanisms that tend to orient the UB perpendicular to the tilted pelvis would produce torque in proportion to the angle between the pelvis and UB and this torque would increase as stance width increases. This larger torque at wider stances would produce a larger magnitude early time course of UB IRFs and the initial UB IRF defection would be in the same direction of the tilted pelvis and SS. In addition, this sharp rise in UB velocity would influence the LB through an interactive torque that would act to move the LB in a direction opposite to the UB. This interaction torque likely contributed to the early negative peak in the LB IRFs (Fig. 4.10A).

*UB & LB phase behavior*

UB and LB phase results are in agreement with previous studies that have shown in-phase sway of the UB and LB below 1 Hz and out-of-phase sway above 1 Hz during spontaneous sway in the sagittal and frontal plane (Creath et al. 2005; Zhang et a. 2007) and during frontal plane balance responses to visual stimuli (Kiemel et al. 2008). The underlying cause of in-phase and out-of-phase sway in the UB and LB is still unknown. However, there is evidence that the out-of-phase behavior arises from the mechanical properties of the balance control system "plant", which includes the musculoskeletal multi-segmented body (Kiemel et al. 2008). We found that the overall feature of in-phase UB and LB sway at low frequencies and out-of-phase at high frequencies was present in

all conditions of visual availability, stimulus amplitude, and stance width. The fact that neither visual availability nor stimulus amplitude affected the out-of-phase behavior at high frequencies is consistent with the notion that out-of-phase behavior arises from the "plant" because visual availability and stimulus amplitude primarily influence the sensory systems and not the mechanical properties of the balance control system. However, it is surprising that out-of-phase behavior was not influenced by stance width because changes in stance width do affect the mechanical properties of the balance control system.

The transition from in-phase to out-of-phase behavior (0.5 – 1 Hz) was influenced by sensory information and stimulus amplitude. In EO SS tests and VS tests the UB-LB phase showed an increasing phase lead beginning at about 0.2 Hz that was not present on EC SS tests. A previous study also found the UB leading LB at frequencies above ~0.2 Hz using a sum-of-sines visual stimulus to evoke sagittal plane sway (Kiemel et al. 2008). The similarity between sagittal plane segmental motion evoked in the previous study (Kiemel et al. 2008) and frontal plane segmental motion evoked in the current study suggests that common balance control strategies are used in all directions of sway when the BoS is small.

*Limits of interpretation in this study*

Because the CoM is determined by the orientation of individual body segments, understanding how individual body segments are controlled is necessary for a thorough understanding of balance control. Accurate conclusions about how individual body segments were controlled in this experiment cannot be made without accurately accounting for the physical laws of multi-segment motion where motion of one body segment generates interaction torques on adjacent body segments (Zajac and Gordon 1989). The interaction torques that arise during multi-segment motion mean that sensory information used to orient one body segment will necessarily influence the orientation of other body segments. Therefore, LB and UB sway responses in this study cannot be viewed as independent of each other. Interpretation of segmental behavior would benefit from a mathematical model that can represent sensory systems and capture behavior of multi-link dynamics.

# CHAPTER V.
# MODELING FRONTAL PLANE MULTI-LINK CONTROL


## ABSTRACT

Previously obtained experimental results showed balance responses to continuous surface rotations were dependent on frontal plane stance width. In narrow stance, lower body (LB) and upper body (UB) frontal plane sway dynamics were nonlinear across stimulus amplitude in both eyes closed (EC) and eyes open (EO) conditions. As stance width increased, LB sway dynamics were more linear across stimulus amplitude. In the current study, a model was developed to account for experimental results. The proposed multi-link model controlled LB and UB segments with intrinsic mechanisms that generated torque with no time delay and active mechanisms that generated torque based on time-delayed feedback of segment motion derived from sensory systems. In narrow stance, LB control was primarily based on active mechanisms. Changes in the LB active mechanism across stimulus amplitude suggested sensory reweighting contributed to nonlinear LB dynamics whereby subjects shifted away from reliance on proprioceptive cues that oriented the LB toward the surface and shifted toward reliance on vestibular/visual cues that oriented the LB upright as stimulus amplitude increased in both EO and EC conditions. In contrast, the model indicated that the UB nonlinearity was due to less active stiffness (lower contributions from all sensory systems to UB control) as stimulus amplitude increased and in EO compared to EC. As stance width increased, overall UB stiffness and damping decreased while LB intrinsic stiffness increased making the LB system more stable. This increase in LB stability was also accompanied by active LB control that was more linear across stimulus amplitude.

## INTRODUCTION

Control mechanisms underlying frontal plane human balance control were recently explored in our laboratory (Goodworth and Peterka 2010). Subjects adopted several frontal plane stance widths while external perturbations were used to evoke lower body (LB) and upper body (UB) sway responses. General observations were made about balance system dynamics and coordination strategies. However, many features of the experimental data could not be easily interpreted because more than one explanation could potentially account for many of the results. Thus, the identification of frontal plane balance control mechanisms was limited. In the current study, a multi-link parametric model was developed to distinguish between conflicting interpretations of previously obtained experimental data.

One salient feature of the experimental data was that the narrow stance system (ankles separated by a few centimeters) was nonlinear across stimulus amplitude. Specifically, subjects were relatively less responsive to the external stimulus as the stimulus amplitude increased (Goodworth and Peterka 2010). This finding was similar to other frontal plane studies where subjects adopted a narrow stance (Oie et al. 2002 and Cenciarini and Peterka 2006). In Oie et al. 2002 and in Cenciarini and Peterka 2006, stimulus amplitude-dependent changes in the balance system were attributed to a sensory reweighting mechanism whereby subjects shifted away from reliance upon sensory systems that oriented the body toward the stimulus and shifted toward reliance upon sensory systems that oriented the body more vertical in space. This interpretation was based on center-of-mass (CoM) results. However, because CoM measures are determined by the orientation of individual body segments, a more complete understanding of sensory reweighting could be found if control mechanisms underlying multi-link control were known. A multi-link model with separate LB and UB control could determine if sensory reweighting is used in LB and/or UB control and to determine if mechanisms other than sensory reweighting contributed to the reduced responsiveness to external stimuli observed in our experimental findings.

Another important experimental finding was that the balance control system appeared to become more linear as stance width increased (Goodworth and Peterka 2010). This conclusion was based on the observation that LB and CoM responses to

external stimuli scaled linearly with stimulus amplitude in both EO and EC conditions when subjects adopted a wide stance width, but not in narrow stance conditions. The underlying cause of this apparent shift toward LB system linearity with increasing stance width is not known. It is possible that changes in LB system linearity with stance width could be linked to changes in LB biomechanics with stance width. It has been proposed that the contribution of LB intrinsic mechanical properties to the LB system increases with stance width (Scrivens et al. 2008). There are two reasons for this idea. First, as stance width increases, muscles and tendons that span hips joints are stretched to a greater length in wide compared to narrow stance widths resulting in a higher spring constant (due to nonlinear spring properties) and more force resisting the rotation of one LB segment relative to another in wide compared to narrow stance conditions (Scrivens et al. 2008; Day et al. 1993). Second, a given CoM rotation of the LB results in greater rotation about hip joints, and consequently more resistive force from mechanical properties of muscles/tendons spanning hip joints, in wide compared to narrow stance widths. An increased contribution from intrinsic mechanical properties of the LB with stance width would make the system appear more linear if torque generated about LB joints from intrinsic mechanisms scaled linearly with stimulus amplitude.

Alternatively, LB intrinsic stiffness and damping may have little to do the observed shift toward linear dynamics with increasing stance width. Instead, the contribution of intrinsic stiffness may be negligible compared to the contribution from neural activation of LB muscles. Then, in wide stance conditions, the neural control mechanism could simply adopt a "simple" linear control strategy where the active generation of LB torque scales linearly with stimulus amplitude. Thus, it may be that a "complex" nonlinear control strategy is not required when subjects adopt a large base of support because the CoM can have a large range of motion. A model representing both intrinsic LB stiffness and damping that act with no time delay and representing neurally activated control mechanisms that act with time delay could quantify the influence of LB biomechanics on sway behavior and system linearity.

Most existing multi-link control models have been developed to describe sway in the sagittal plane (Alexandrov et al. 2005; Barin 1989; Kuo 1995; Park 2002; Park et al. 2004; Koozekanani et al. 1980; van der Kooij et al. 1999). In these models, body segments are connected as an open-chain with the bottom segment connected to the floor.

Several important mechanisms of control have been identified and included in these sagittal plane models. For example, there is evidence that sensory feedback from segments across the entire body contribute to torque generation at each joint (Alexandrov et al. 2005; Barin 1989, Kuo 1995; Park 2002; Park et al. 2004) and the gain between segment kinematics and torque generation changes with stimulus amplitude and biomechanical constraints (Kuo 1995; Park 2002; Park et al. 2004). For sway in the frontal plane, however, a different model is required. In the frontal plane, the LB forms a closed-chain and consequently the equations governing LB motion vary with changes in stance width. Furthermore, there is evidence that pelvis orientation, which is a function of stance width, surface tilt, and LB sway, is an important kinematic variable influencing UB control (Goodworth and Peterka 2009). It would therefore be beneficial to consider pelvis orientation in models of frontal plane posture control. To our knowledge, there have been no published models of frontal plane sway that include these features.

Therefore, in the present study, a multi-link frontal plane model is proposed that accounts for changes in LB equations of motion with stance width and includes pelvis orientations. The model includes torque generation about both LB and UB joints so that LB and UB control mechanisms can be identified. Control includes on intrinsic mechanisms (intrinsic mechanical stiffness and damping in muscles, tendons, joints, and ligaments) that generate torque with no time delay and based on active mechanisms (neural activation of muscles) that generate torque based on time-delayed feedback of segment motion derived from sensory systems. By representing both intrinsic and active mechanisms, the model is able to determine the influence of intrinsic stiffness and damping on the apparent shift toward linear system dynamics with increasing stance width. The model of frontal plane balance control is used to distinguish between competing interpretations of experimental results and therefore contributes to our understanding of frontal plane balance control.

## METHODS

*Experimental data*

Experimental data used in the model were obtained from the seven subjects described in Chapter 4 of this dissertation who exhibited similar control strategies across all test conditions. Body segment dimensions in the model were set to the average dimensions of the seven subjects. These dimensions were mass of 68 kg, height of 172 cm, L4/L5 joint above surface of 106 cm, greater trochanter above surface of 89.5 cm, hip joint center above surface of 91.2 cm, and distance across hip joint centers of 17.5 cm. The L4/L5 joint level was estimated as the iliac crest height (Skotte 2001). The UB segment mass and moment of inertia was calculated with respect to the L4/L5 joint. The distance between hip joint centers was estimated using a regression equation relating hip-joint distance to inter-ASIS distance; and hip joint center height above the surface was estimated using a regression equation relating ASIS height to inter-ASIS distance (Seidel et al. 1995). Body segment mass and moment of inertia were estimated via anthropomorphic measures (Erdmann 1997; Winter 2005). Data used as model inputs were the experimentally measured surface rotation angles and data used as model outputs were LB and UB sway averaged across the seven subjects as displayed in frequency-response functions (FRFs) in Figs. 4.6 and 4.7 and impulse-response functions (IRFs) in Fig. 4.10.

*Physical description of model*

Fig. 5.1A shows a schematic of the frontal plane multi-link model. In the model, *LBS* (LB in space) is the hip mid-point tilt angle with respect to earth vertical about an axis midway between heels at ankle height. *SS* and *PS* are the surface and pelvis tilt angles with respect to earth horizontal, respectively. A linear approximation to the trigonometric relationship of *PS* to *LBS* and *SS* was found by first calculating LB joint angles using equations from Day et al. (1993). Second, because all LB joint angles are determined once any single angle is specified, we varied one ankle angle relative to *SS* between ± 2° in 0.1° increments to calculate a range of ankle and hip angles compatible with the range in experimental data. Third, from the set of joint angles and segment lengths, the coordinates of hip-joint centers and the hip mid-point were calculated for

each ankle angle. Forth, hip-joint center coordinates were used to calculate *PS*. Fifth, hip mid-point coordinates were used to calculate *LBS* relative to the axis midway between ankles. Sixth, this procedure was repeated for *SS* angles between ± 2° in 0.1° increments. Finally, the "pelvis ratio", $P_R$, was found that minimized the mean-square-error between *PS* values obtained from the procedure described above and *PS* values obtained by the following equation,

$$PS = P_R \cdot SS + (1 - P_R) \cdot LBS \tag{5.1}$$

The minimum $R^2$ value between the direct calculation of *PS* and the equation (5.1) approximation across all stance widths was 0.9999974. When heel to heel distance is equal to the distance between hip joint centers (~12 cm IMD), $P_R$ =1 and *PS* = *SS* (Fig. 5.1C). At stance widths less than ~12 cm IMD, $P_R$ is less than one and positive *SS* and *LBS* values both result in positive values of *PS*. However, at stance widths greater than ~12 cm IMD, $P_R$ is greater than one and positive *SS* gives positive *PS* while positive *LBS* gives negative *PS* values.

*UBS* (UB in space) is the UB center-of-mass tilt angle with respect to earth vertical. To simply the model, the pelvis-UB joint was assumed to be located at the mid-point between hip joint centers. This simplification meant that the pelvis-UB joint location at any point in time is influenced only by *LBS*. A more anatomically accurate model would include the distance between hip joint centers and L4/L5 joint, which would result in a pelvis-UB joint that is influenced by *PS*, which is a function of both *SS* and *LBS*. This pelvis-UB joint simplification was previously shown to affect the early time course (<50 ms) of UB IRFs (Fig. 2.10) via additional interaction torques between *SS* and *UBS*.

In the model, UB torque ($T_{UB}$) is the summation of all torques generated from UB muscle activation and intrinsic mechanical properties of the UB musculoskeletal system applied about a joint between the pelvis and UB. LB torque ($T_{LB}$) is the summation of all torques generated from LB muscle activation and intrinsic mechanical properties of the LB musculoskeletal system applied about the LB joints. $T_{LB}$ is assumed to be generated equally about all four LB joints (two ankle joints and two hip joints). The implications of this LB torque distribution

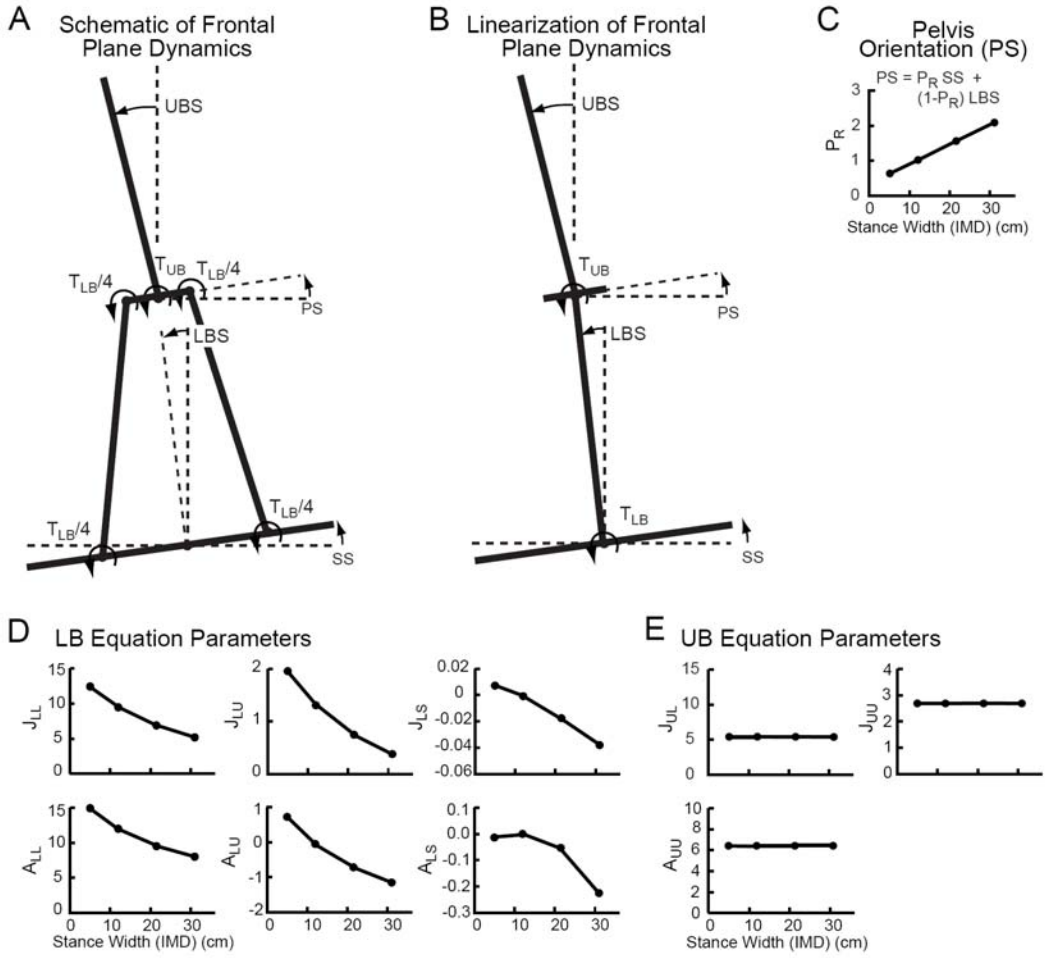


**FIG. 5.1.** *Physical model of frontal plane dynamics where parameters values correspond to the equations of motion (Eqns. 5.2 and 5.3).*

assumption are described in the discussion. Interaction torques applied about the LB and UB joints are represented as separate inputs to the LB and UB segments (Fig. 5.2B). Equations of motion in the frontal plane were calculated by developing free body diagrams (D'Alembert's principle) of the surface, two legs, a pelvis, and an UB in an earth-fixed Cartesian coordinate system (Koozekanani et al. 1980). Free body diagram equations were solved simultaneously using the Symbolic Math Toolbox in Matlab (The MathWorks, Inc, Natick, MA) so that LB and UB torque was related to segment motion (position, velocity, and acceleration) and segment dimensions (mass, length, center-of-mass location, moments of inertia, and stance width). Although the LB consists of two leg segments and one pelvis segment, the LB has only one degree of freedom in the

frontal plane (assuming straight knees) because the two legs and pelvis form a closed loop system (Day et al. 1993).

The LB and UB equations of motion were linearized about the vertical orientation. The schematic in Fig. 5.1B shows the linearized system represented as a 2-link inverted-pendulum. But unlike an actual 2-link inverted-pendulum, the parameters in the equations of motion depend on the LB configuration (stance width) of the actual system and the surface angle. This system is described by the following set of equations,

$$\begin{aligned} T_{LB} = {} & J_{LL} \cdot \ddot{LBS} + J_{LU} \cdot \ddot{UBS} + J_{LS} \cdot \ddot{SS} \\ & - A_{LL} \cdot g \cdot LBS - A_{LU} \cdot g \cdot UBS - A_{LS} \cdot g \cdot SS \end{aligned} \tag{5.2}$$

$$T_{UB} = J_{UL} \cdot \ddot{LBS} + J_{UU} \cdot \ddot{UBS} - A_{UU} \cdot g \cdot UBS \tag{5.3}$$

In the LB equation of motion (5.2), $J_{LL}$, $J_{LU}$, and $J_{LS}$ are constants related to the acceleration of *LBS*, *UBS*, and *SS*, respectively; and $A_{LL}$, $A_{LU}$, and $A_{LS}$ are constants related to *LBS*, *UBS*, and *SS*, respectively. In the UB equation of motion (5.3), $J_{UL}$, $J_{UU}$, and $A_{UU}$ are constants related to *LBS* acceleration, *UBS* acceleration, and *UBS*, respectively. All parameters in the LB equation vary as a function of stance width (Fig. 5.1D). $J_{LL}$ and $A_{LL}$ are larger than $J_{LU}$ and $A_{LU}$ across all stance widths while parameters related to the surface ($J_{LS}$ and $A_{LS}$) are the smallest of all. In UB equation 4.3, $J_{UL}$ is about twice $J_{UU}$ and there is negligible variation in parameter values across stance width (Fig. 5.1E).

*Control of body segments*

A proposed control scheme of the multi-link model is shown Fig. 5.2. *SS* is the model input and *UBS* and *LBS* are the model outputs (Fig. 5.2A). In the block diagrams, physical segment kinematic variables are represented as capital letters with thick solid lines, internal estimates of segment kinematics or torques are represented as lower case letters with dashed lines, and torques are thin solid lines. The LB and UB control are not independent of each other because of interaction torques and because inputs to LB and UB control mechanisms are assumed to be influenced by both body segment motion and by the surface rotation. A detailed representation of LB and UB control mechanisms is provided in Figs. 5.2B and C. To facilitate readability of these block diagrams, feedback

lines were omitted; however LB and UB mechanisms are based on feedback control, as described below.

The LB control system generates torque ($T_{LB}$) to stabilize the LB segments based on intrinsic and active mechanisms. The intrinsic LB mechanism generates torque with no time delay in proportion to *SS-LB* (stiffness parameter $K_{L4}$) and in proportion to the derivative of *SS-LB* (damping parameter $B_{L4}$). This intrinsic mechanism represents the intrinsic stiffness and damping from muscles tendons, joints, and ligaments in the LB musculoskeletal system that tend to orient the LB perpendicular to the surface. The active LB mechanism generates torque based on a time-delayed ($\tau_{LB}$) summation of feedback signals derived from sensory systems multiplied by gain factors. Specifically, torque is generated in proportion to *-lbs*, *lbs-ubs*, and *ss-lbs* (stiffness parameters $K_{L1}$, $K_{L2}$, and $K_{L3}$, respectively) and in proportion to the derivative of *-lbs*, *lbs-ubs*, and *ss-lbs* (damping parameters $B_{L1}$, $B_{L2}$, and $B_{L3}$, respectively). An additional component of torque is generated in proportion to a low-pass filtered ($G_t$ / ($\tau_t$ s +1)) sensory signal that encodes LB torque $t_{LB}$. The sensory signal *ss-lbs* could be derived from the LB proprioceptive system. The inter-segmental sensory signal *ubs-lbs* could also have a proprioceptive origin. The sensory signal *-lbs* could be derived from vestibular and/or visual (in EO conditions) sensory systems in combination with the inter-segmental proprioceptive inputs. The low-pass filtered $t_{LB}$ signal represents LB torque feedback and could be derived from golgi-tendon organs (Peterka 2003). The LB time delay ($\tau_{LB}$) can be thought of an "effective" time delay that does not attempt to represent the possibility that different components of active control might have different time delays.

The UB control system generates torque ($T_{UB}$) to stabilize the UB segment based on intrinsic and active mechanisms. The intrinsic UB mechanism generates torque with no time delay in proportion to (stiffness parameter $K_{U4}$) *PS-UB* and in proportion to the derivative (damping parameter $B_{U4}$) of *PS-UB* and tends to orient the UB perpendicular to the pelvis. The active UB mechanism generates torque based on a time-delayed ($\tau_{UB}$) summation of feedback signals derived from sensory systems multiplied by gain factors. Specifically, torque is generated in proportion to *-ubs*, *lbs-ubs*, and *ps-ubs* (stiffness parameters $K_{U1}$, $K_{U2}$, and $K_{U3}$, respectively), and in proportion to the derivative of *-ubs*, *lbs-ubs*, and *ps-ubs* (damping parameters $B_{U1}$, $B_{U2}$, and $B_{U3}$, respectively). The sensory signal *ps-lbs* could be derived from the UB proprioceptive system encoding the angle

between the UB and pelvis. The sensory signal *-ubs* could be derived from either the vestibular and/or visual (in EO conditions) systems. Similar to $\tau_{LB}$, the UB time delay ($\tau_{UB}$) can be thought of an "effective" time delay.

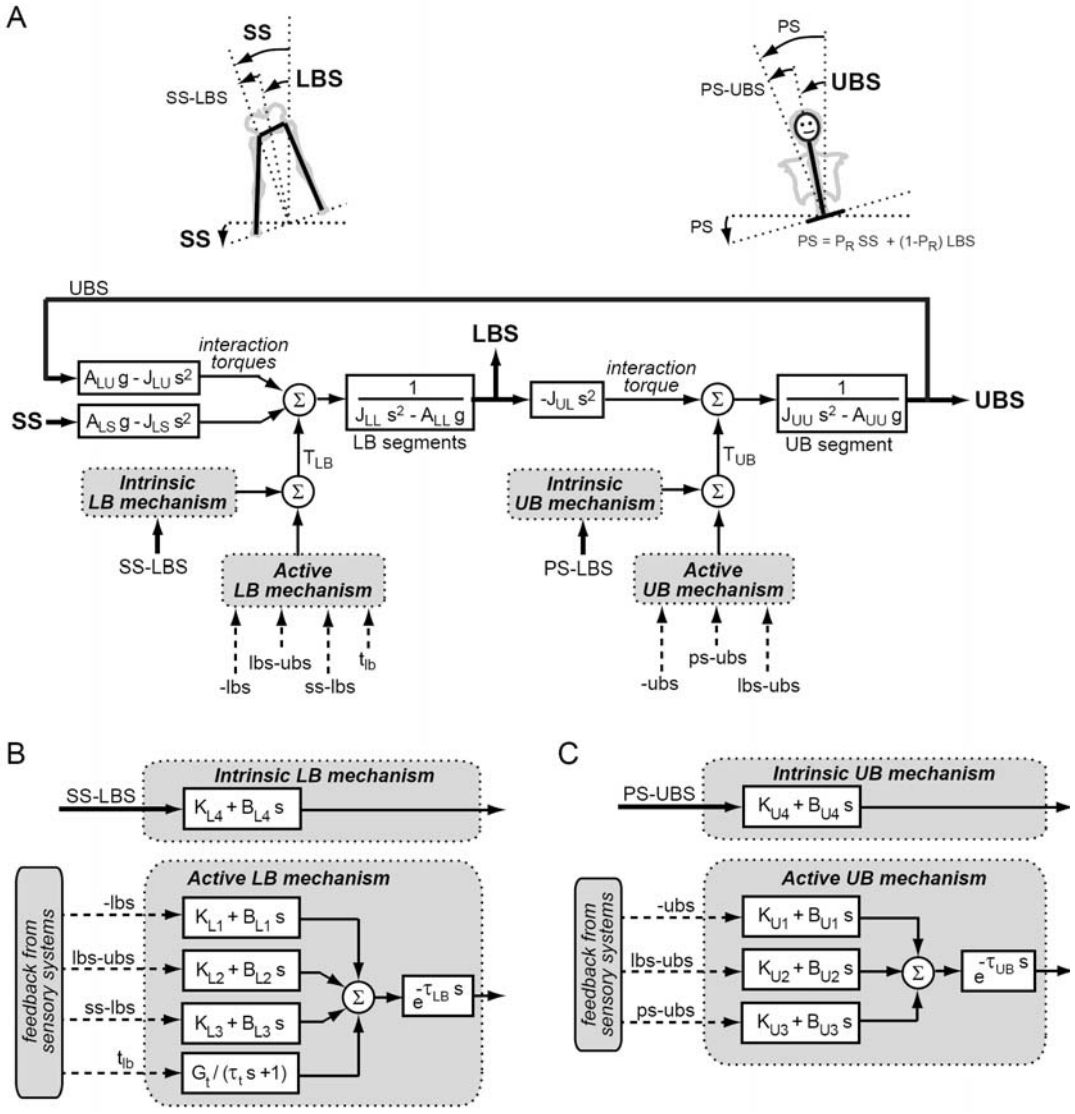


**FIG. 5.2.** *Block diagram of proposed lower body (LB) and upper body (UB) control system showing A) the interaction torques and torques from intrinsic and active mechanisms that move LB and UB segments, and B) the input signals and gains in the intrinsic and active mechanisms of the LB control system and C) UB control system. The LB and UB control systems are closed-loop although feedback lines are omitted to enhance readability of the block diagram.*

*Determination of model parameters*

In Fig. 5.2A, the values for model parameters inside the interactive torque blocks ($A_{LU}$, $J_{LU}$, $A_{LS}$, $J_{LS}$, and $J_{UL}$), the UB segment block ($J_{UU}$ and $A_{UU}$), and the LB segment block ($J_{LL}$ and $A_{LL}$) are displayed in Fig. 5.1D and E for different stance widths. In Fig. 5.2B and C, the feedback and time delay parameters were determined using a constrained nonlinear optimization routine 'fmincon' (Matlab Optimization Toolbox, The MathWorks, Natick, MA) to minimize a cost function equal to the total mean-squared-error of the normalized difference between model FRFs and experimental FRFs (Peterka 2002) at frequencies between 0.023 and 7.7 Hz. IRFs were calculated from simulated LB and UB sway using Simulink (The MathWorks, Natick, MA). Simulated LB and UB sway was evoked from surface rotations identical to the rotations measured from the surface during the experiments and the simulated LB and UB responses were analyzed to calculate simulated IRFs in a manner identical to the method used to calculate experimental IRFs.

In order to minimize the possibility of the optimization results corresponding to a local rather than a global minimum of the cost function, 100 to 500 fits were performed with different initial parameter values for each model fit. Also, the total number of free parameters was reduced by adding constraints on the fitting routine. Reducing the number of free parameters provided more reliable parameters estimates (Pintelon and Schoukens 2001) and enabled a more parsimonious explanation for the changes in FRFs across test condition compared to determining parameters without any constraints. Adding model constraints consisted of fixing parameter values across certain test conditions as described below.

Across all test conditions, UB intrinsic stiffness ($K_{U4}$) was fixed and determined from results in a previous study that investigated UB on pelvis control (see Table 2.1). In our previous study, the time course of IRFs at latencies prior to a fixed time delay did not show changes across stimulus amplitude and between EO/EC conditions, consistent with a fixed contribution of intrinsic stiffness and short-latency reflexes. The similarity of UB relative to pelvis movements in the previous and current study suggested that the intrinsic stiffness of the UB could also be considered invariant across test conditions in the current study.

Time delays ($\tau_{LB}$ and $\tau_{UB}$) were also fixed across all test conditions and were determined from model fits to EC narrow stance FRFs. Time delays were obtained from EC narrow stance conditions because these tests had low variability across subjects and provided consistent estimates with the least amount of sensitivity to different initial parameter values. A single value for $\tau_{LB}$ and a single value for $\tau_{UB}$ were obtained by fixing time delays across stimulus amplitude for the EC narrow stance conditions.

For each stance width, LB intrinsic stiffness ($K_{L4}$) and damping ($B_{L4}$), UB intrinsic damping ($B_{U4}$), torque feedback time constant ($\tau_t$), and torque feedback gain ($G_t$) were fixed across stimulus amplitude. Similar to Goodworth and Peterka 2009, the early time course of UB and LB IRFs were invariant across stimulus amplitude, consistent with fixed contributions from intrinsic stiffness and damping parameters across stimulus amplitude. However, these parameters were not fixed across stance width because changes in stance width are expected to influence intrinsic LB mechanisms (Day et al. 1993; Scrivens et al. 2008) and perhaps also torque feedback. Intrinsic UB damping was also allowed to vary across stance width because the early time course of experimental UB IRFs was inconsistent with a fixed $B_{U4}$ across stance width.

Finally, between EC and EO tests, $K_{L4}$, $K_{U4}$, $B_{L4}$, $B_{U4}$, and $\tau_t$ were fixed. These parameters were obtained from EC test conditions because EC tests had lower variability that provided for more consistent parameter estimates compared to EO conditions, especially at larger stance widths where UB FRFs were particularly variable in EO conditions (see Fig. 4.7 in Chapter 4).

## RESULTS

### *Narrow stance control system*

Experimental results showed that, in the narrow stance condition, the system was nonlinear across stimulus amplitude in both EC and EO conditions. Specifically, increases in stimulus amplitude resulted in gain reductions in both LB and UB FRFs at frequencies below about 3 Hz (Fig. 5.3B and 5.4B) and IRFs exhibited stimulus amplitude dependent changes after a fixed time delay (Fig. 5.3C and 5.4C). Modeling was used to identify a LB and UB control system that could account for experimental results and to determine if the observed system nonlinearity was due to sensory

reweighting. Because each active mechanism gain represented the contribution to system stiffness or damping from a particular signal derived from sensory systems, sensory reweighting is identified in the model as a monotonic increase in at least one active mechanism with a monotonic decrease in at least one other gain as stimulus amplitude increased.

EC PARAMETER VALUES. In the EC LB narrow stance control system, the largest contribution to system stiffness was the $K_{L3}$ gain which tended to orient the LB toward to surface tilt (Fig. 5.3A, top plot). The largest contributions to system damping was the $B_{L1}$ and $B_{L2}$ gains which tended to move the LB upright in space and opposite to the UB, respectively (Fig. 5.3A, 2$^{nd}$ plot down). The intrinsic stiffness $K_{L4}$ and damping $B_{L4}$ of the LB were zero indicating that the intrinsic mechanism did not contribute to narrow stance control. The torque feedback was heavily low pass filtered ($\tau_t$ = 10.5 s, ~0.015 Hz cutoff frequency). Consistent with this finding, a sensitivity analysis on $G_t$ showed that torque feedback primarily contributed to gain reductions and phase leads below 0.15 Hz. The LB effective time delay $\tau_{LB}$ was 109 ms. The values of parameters fixed across stimulus amplitude are presented in Table 5.1.

Changes in LB parameters across stimulus amplitude were more prominent in stiffness-related parameters compared to damping-related parameters, indicating that LB control system nonlinearity was mostly due to changes in stiffness and not damping. As stimulus amplitude increased, $K_{L1}$ monotonically increased while $K_{L2}$ and $K_{L3}$ decreased. This result is consistent with sensory reweighting whereby the LB control system shifts toward higher gains (with $K_{L1}$) that orient the LB upright in space and shifts toward lower gains (with $K_{L3}$) that orient the LB toward the surface. Variation in $K_{L2}$ indicates there was a shift toward lower use of the inter-segmental proprioceptive signal *lbs-ubs* as stimulus amplitude increased.

The UB control system was similar to the LB system in that the largest contribution to system stiffness came from the $K_{U3}$ gain which tended to orient the UB toward pelvis tilt (Fig. 5.3A, 3$^{rd}$ plot down), whereas the largest contributions to system damping came from $B_{U1}$ and $B_{U2}$ which tended to move the UB upright and opposite of the LB, respectively (Fig. 5.3A, 3$^{rd}$ bottom plot). The UB intrinsic stiffness $K_{U4}$ and damping $B_{U4}$ contributed less than 20% to the overall stiffness and damping (Table 5.1),

but this contribution was larger than the contribution from intrinsic mechanisms in the LB control system (which was zero).

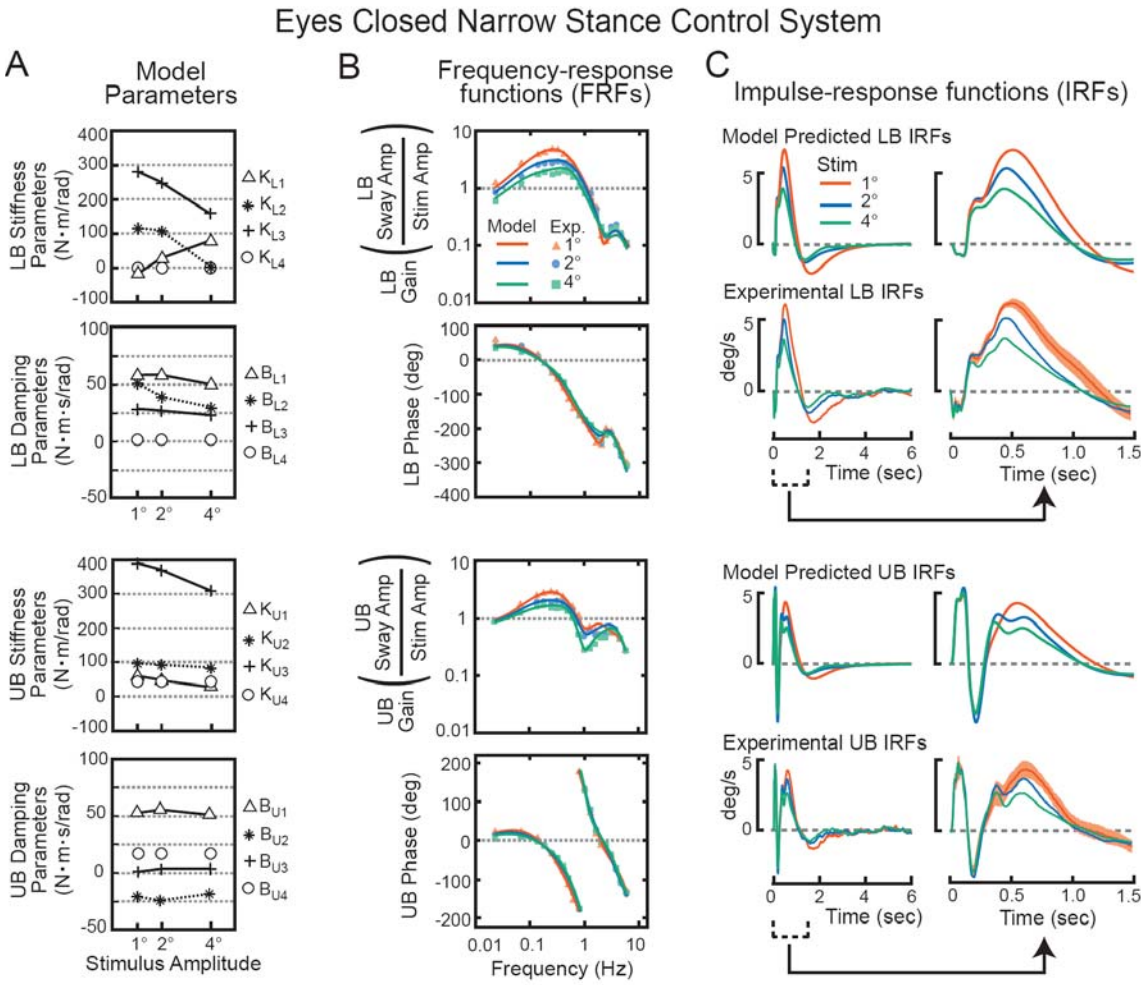


**FIG. 5.3.** *The eyes closed narrow stance lower body (LB) and upper body (UB) control systems A) exhibited gain changes across stance width primarily in stiffness related parameters (values of $G_t$, $\tau_t$, $\tau_{LB}$, and $\tau_{UB}$ are shown in Table 5.1) and accounted for B) experimental frequency-response functions and C) impulse-response functions.*

Changes in UB parameters across stimulus amplitude were more prominent in stiffness-related parameters compared to damping-related parameters, similar to the LB control system. However, unlike the LB system, changes in stiffness parameters $K_{U1}$, $K_{U2}$, and $K_{U3}$ were inconsistent with sensory reweighting because all these parameters monotonically decreased (and none increased) with increasing stimulus amplitude. This result indicates that the UB control system had lower gains to all sensory inputs, resulting

in less overall stiffness, as stimulus amplitude increased. The UB effective time delay $\tau_{UB}$ was 53 ms, approximately half the value of $\tau_{LB}$.

**TABLE 5.1.** *Parameters fixed across stimulus amplitude*

| | ***Narrow*** | ***Parallel*** | ***Medium*** | ***Wide*** |
|---|---|---|---|---|
| $\boldsymbol{K_{L4}}$ (Nm/rad) | 0 | 5.10 | 77.1 | 274 |
| $\boldsymbol{K_{U4}}$ (Nm/rad) | 50.1 | 50.1 | 50.1 | 50.1 |
| $\boldsymbol{B_{L4}}$ (Nm s/rad) | 0 | 0 | 0 | 0 |
| $\boldsymbol{B_{U4}}$ (Nm s/rad) | 15.7 | 14.7 | 11.4 | 9.93 |
| $\boldsymbol{G_t}$, EC | 2.26 | 1.52 | 0.32 | 0 |
| $\boldsymbol{G_t}$, EO | 1.53 | 0.685 | 0.154 | 0 |
| $\boldsymbol{\tau_t}$ (s) | 10.5 | 7.50 | 4.54 | n/a |
| $\boldsymbol{\tau_{LB}}$ (ms) | 109 | 109 | 109 | 109 |
| $\boldsymbol{\tau_{UB}}$ (ms) | 53 | 53 | 53 | 53 |

EC MODEL FRFs AND IRFs. Fig. 5.3B shows the model predicted FRFs for the EC narrow stance balance system. The detailed features of experimental LB and UB FRFs were accounted for in the model. These features included peaks in LB gains at about 0.3 Hz and 4 Hz, LB and UB phase leads below 0.15 Hz, LB phase increase (less phase lag) at about 2.5 Hz, UB gain notch at about 1 Hz, and LB and UB gain reductions with increasing stimulus amplitude below 3 Hz.

Experimental IRFs were also accounted for by the model (Fig. 5.3C). Specifically, LB IRFs showed a brief initial negative peak at ~0.05 s, then a first local maximum at ~0.2 s, then a second maximum at ~0.5 s, then a minimum at ~1.5 s, and then eventual decay to zero by 4 s. Amplitude-dependent changes were most noticeable after ~0.2 s consistent with experimental IRFs. UB IRFs showed a large initial positive peak at ~0.05 s, then a negative peak at ~0.2 s, then a positive rise up to a local maximum at ~0.7 s, and then eventual decay to zero by 3 s. Similar to LB IRFs, amplitude-dependent changes were most noticeable after about ~0.2 s.

Because active mechanisms were associated with a time delay, the early time course of narrow stance IRFs can be explained by the UB intrinsic mechanism (LB intrinsic mechanisms were zero). IRFs represented the velocity time course of responses to a sudden surface tilt of 1°. In response to a sudden surface tilt, the pelvis tilts in the same direction. This pelvis tilt results in an immediate UB sway toward alignment with

the pelvis tilt because the UB intrinsic mechanism generates torque in proportion to *PS-UBS* and the velocity of *PS-UBS* with no time delay. Thus, the initial UB IRF trajectory is positive and in the same direction as pelvis and surface tilt. This positive UB motion produces initial negative LB motion through interaction torques.

EO NARROW STANCE SYSTEM. Parameter values and parameter changes in the EO narrow stance system (Fig. 5.4A) were similar to the EC. $K_{L3}$ and $K_{U3}$ tended to be high compared to other stiffness parameters and $B_{L1}$, $B_{U1}$, and $B_{U2}$ tended to be larger than other damping parameters. In the LB system, $K_{L2}$ and $K_{L3}$ values decreased while

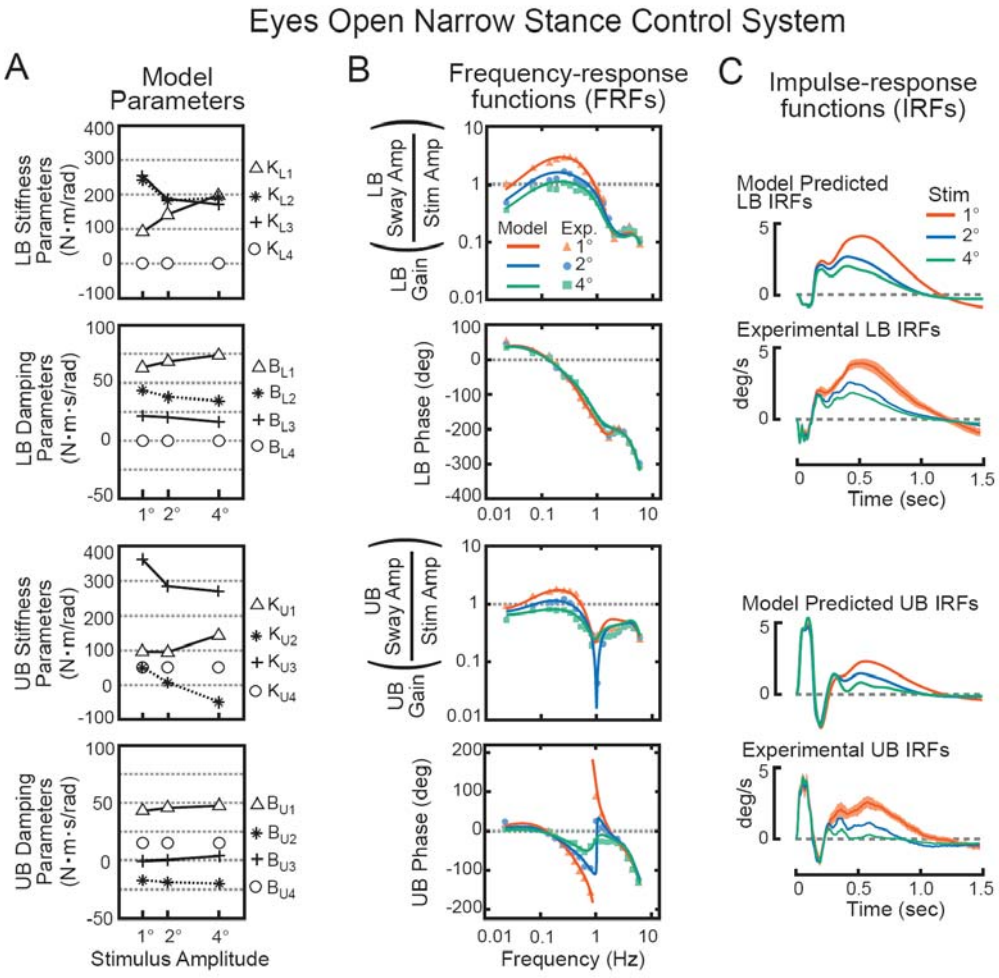


**FIG. 5.4.** *The eyes open (EO) narrow stance lower body (LB) and upper body (UB) control system A) exhibited similar gains to the eyes closed (EC) narrow stance system with the except of a larger $K_{L1}$, $K_{U1}$, and $B_{L1}$ in EO compared to EC (values of $G_t$, $\tau_t$, $\tau_{LB}$, and $\tau_{UB}$ are shown in Table 5.1) and accounted for B) experimental frequency-response functions and C) experimental impulse-response functions.*

$K_{L1}$ values increased as stimulus amplitude increased. These variations in parameters contributed to the LB FRF gain reductions with increasing stimulus amplitude (Fig. 5.4B), and were consistent with a sensory reweighting mechanism contributing to LB control.

However, there were several features of the EO system that differed from EC. $K_{L3}$ was lower in EO compared to EC while $K_{L1}$, $K_{L2}$, $B_{L1}$, and $K_{U1}$ were larger. Most parameters values that were larger in the EO system tended to orient body segments more vertical ($K_{L1}$, $B_{L1}$, and $K_{U1}$). This is consistent with the overall lower FRF gains in EO and compared to EC (compare Fig. 5.4B to 5.3B) and the smaller magnitude EO IRFs compared to EC IRFs after ~0.2 s (compare Fig. 5.4C to 5.3C), and indicates an important contribution of vision to the narrow stance control system.

*Changes with stance width*

With increases in stance width, LB experimental FRFs showed progressively less dependency upon stimulus amplitude in both EC and EO conditions (Fig. 5.5). This result indicated that increases in stance width result in the LB control system approaching that of a linear system. The model was used to characterize control mechanisms that change with stance width and to determine if the apparent shift toward LB system linearity was due to 1) a shift toward linear control at wider stance widths in the active mechanism (as indicated by an invariance in active gains with changes in stimulus amplitude) and/or 2) an increased contribution from the LB intrinsic mechanism with increases in stance width (as indicated by a relative increase in $K_{L4}$ and $B_{L4}$ compared to active stiffness and width.damping).

Fig. 5.5 displays the EC parallel, medium, and wide stance control systems. The parallel stance system was overall similar to narrow stance (Fig. 5.3A). For example, the largest contributions to LB and UB stiffness came from the $K_{L3}$ and $K_{U3}$ parameters, respectively, and $K_{L3}$ decreased while $K_{L1}$ increased with increasing stimulus amplitude. The main difference between the parallel and narrow stance system was that UB parameters $B_{U1}$ and $B_{U2}$ varied more across stimulus amplitude in parallel compared to narrow stance

At medium and wide stance widths, the largest contribution to LB and UB stiffness still came from the $K_{L3}$ and $K_{U3}$ parameters, respectively, but these were only

slightly larger than the $K_{L2}$ and $K_{U2}$ parameters, respectively. This result indicates that the signals *ss-lbs* and *ps-ubs* of assumed proprioceptive origin contributed relatively less to LB and UB stiffness, respectively as stance width increased. On the other hand, the

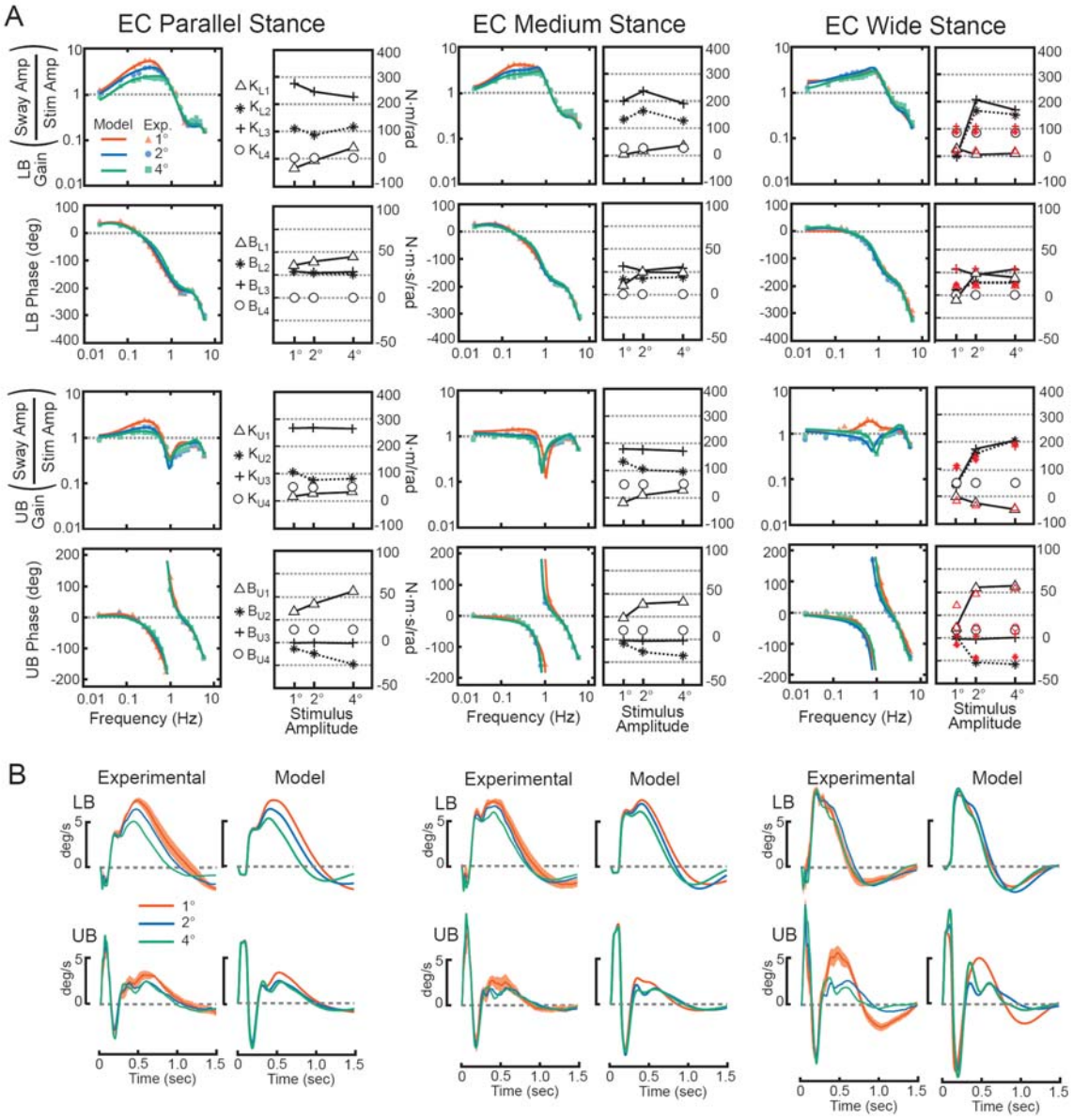


**FIG. 5.5.** *Influence of stance width on eyes closed lower body (LB) and upper body (UB) control system. Modeling accounted for most features of the A) frequency-response functions (FRFs) and B) impulse-response functions (IRFs). Values of $G_t$, $\tau_t$, $\tau_{LB}$, and $\tau_{UB}$ are shown in Table 5.1. In wide stance, red symbols represent model parameters from a fitting routine that constrained the LB system to be linear across stimulus amplitude. Model-predicted FRFs and IRFs from the linear LB system fit in wide stance were nearly indistinguishable from those shown in the figure.*

contribution of intrinsic stiffness, $K_{L4}$ and $K_{U4}$, relative to other stiffness contributions increased with stance width (Fig. 5.6A). LB intrinsic damping $B_{L4}$ was zero across all tests. Although UB intrinsic damping $B_{U4}$ monotonically decreased with increasing stance width (Table 5.1), $B_{U4}$ varied little in the relative contribution to UB damping because damping from active UB mechanisms also tended to decrease with increasing stance width. Finally, $G_t$ decreased with increasing stance width indicating that torque feedback from the LB contributed less to LB torque generation as stance width increased (Fig. 5.6B).

Across stimulus amplitude, UB parameters $B_{U1}$ and $B_{U2}$ showed similar variation in medium and wide stance widths across stimulus amplitude compared to parallel. However, across stimulus amplitude, LB parameters showed less systematic variation in medium and wide stance widths compared to narrow and parallel. For example, only $K_{L1}$ and $B_{L1}$ increased monotonically with stimulus amplitude in medium stance and this change was minimal compared to the monotonic changes in parameters in narrow and parallel stance widths. In wide stance conditions, several parameters exhibited a jump in value between 1° and 2° stimulus amplitude. Given the invariance in LB FRFs across

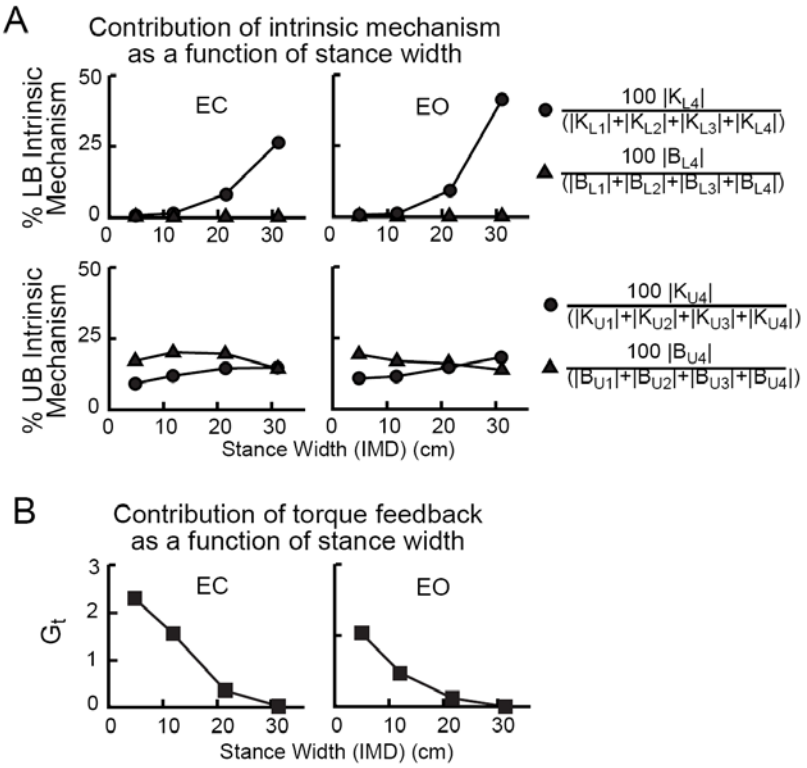


**FIG. 5.6.** *The contribution of A) intrinsic stiffness of the lower body (LB) and upper body (UB) increase as stance width increases and B) torque feedback decreases as stance width increases. At each stance width, gains were averaged across stimulus amplitude.*

stimulus amplitude, the jump in LB parameters between 1° and 2° seemed like an unlikely representation of the LB system. Therefore, we explored the effect of fixing active LB gains across stimulus amplitude. LB and UB gains resulting from the fit with fixed LB gains are red symbols in Fig. 5.5A wide stance. Results from this fit showed LB gains were generally in-between those estimated from fits without fixing gains across stimulus amplitude. UB parameters were only minimally influenced by fixing LB gains across stimulus amplitude and showed similar variation across stimulus amplitude. Furthermore, model FRFs and IRFs with fixed LB gains were nearly identical to those displayed in Fig. 5.5.

Most detailed features of experimental FRFs (Fig. 5.5A) were accounted for by the model. For example, in parallel stance, LB model FRFs exhibited stimulus amplitude dependent gains at frequencies below 3 Hz, while LB model FRFs were fairly constant across stimulus amplitude in wide stance conditions. The model accounted for UB FRF notches at 1 Hz and the UB FRF resonance at 1 Hz in the 1° wide stance width. The only feature of experimental FRFs not fully accounted for in the model was the lowest stimulus frequency point (0.023 Hz) in the UB gains in medium and wide stance widths.

Model IRFs (Fig. 5.5B) were also very similar to experimental IRFs. The overall time course of IRFs and stimulus-amplitude dependent changes were accounted for in the model across all stance widths. The only experimental IRF feature not fully accounted for in the model was the initial negative spike in LB IRFs in medium and wide stance widths.

Increases in stance width had similar effects on the EO system compared to EC. For example, active stiffness parameters $K_{L3}$ and $K_{U3}$ contributed less to overall stiffness while intrinsic stiffness parameters $K_{L4}$ and $K_{U4}$ contributed more to overall stiffness as stance width increased (Fig. 5.6A and 5.7A). $G_t$ also decreased with increasing stance width in EO conditions (Fig. 5.6B). Similar to EC conditions, there was less EO variation in LB gains across stimulus amplitude as stance width increased. In the EO wide stance condition, there a jump in parameter values between the 2° and 4° stimulus amplitude. Because of the high variability in EO UB FRFs (see Fig. 4.7 for confidence intervals) and small differences in LB FRFs across stimulus amplitude, we have less confidence that the jump in LB parameters between 2° and 4° was an accurate representation of the LB system. Similar to EC conditions, it was found that the EO LB system could be modeled as linear across stimulus amplitude without loosing noticeable accuracy of model-

predicted FRFs and IRFs. Parameter values of the linear LB system are shown as red symbols in Fig. 5.7 wide stance.

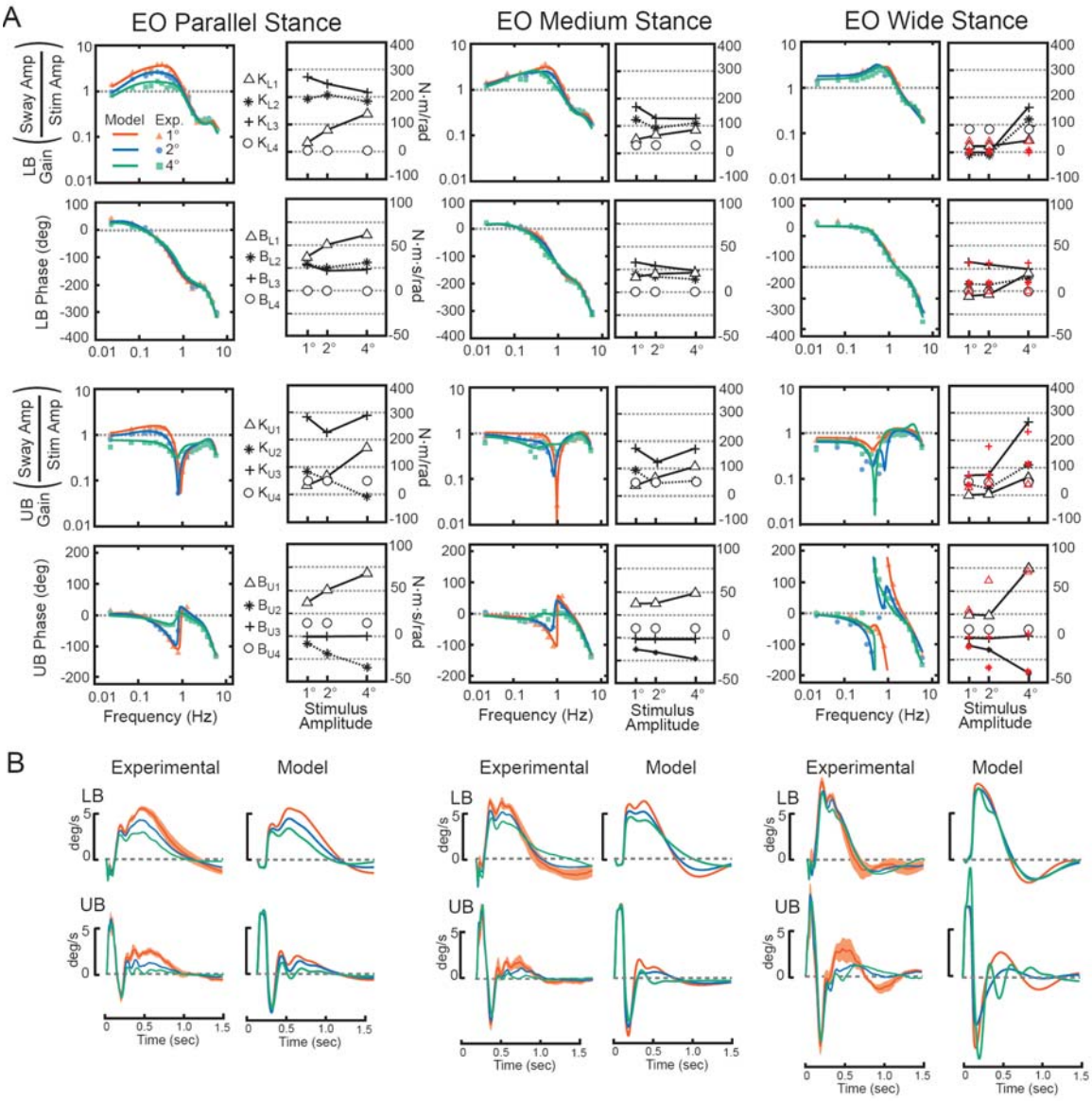


**FIG. 5.7.** *Influence of stance width on eyes open lower body (LB) and upper body (UB) control system. Modeling accounted for most features of the A) frequency-response functions (FRFs) and B) impulse-response functions (IRFs). Values of $G_t$, $\tau_t$, $\tau_{LB}$, and $\tau_{UB}$ are shown in Table 5.1. In wide stance, red symbols represent model parameters from a fitting routine that constrained the LB system to be linear across stimulus amplitude. Model-predicted FRFs and IRFs from the linear LB system fit in wide stance were nearly indistinguishable from those shown in the figure.*

One consistent difference between the EO and EC system is that active stiffness parameters $K_{L1}$ and $K_{U1}$ were larger in EO conditions compared to EC. Fig. 5.8 shows the larger contributions of $K_{L1}$ and $K_{U1}$ to system stiffness in EO compared to EC conditions, where parameters were averaged across stimulus amplitude for each stance width. Because $K_{L1}$ and $K_{U1}$ gains tend to orient body segments toward earth-vertical, the increase in $K_{L1}$ and $K_{U1}$ is consistent with a visual contribution in EO conditions. There was minimal difference in the contribution of $B_{L1}$ and $B_{U1}$ to system damping in EO compared to EC conditions.

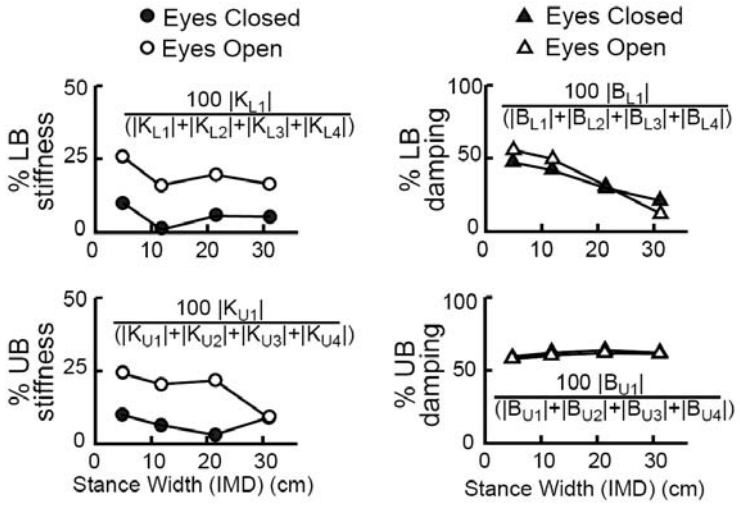


**FIG. 5.8.** *The contribution of vertical-orienting gains ($K_{L1}$, $B_{L1}$, $K_{U1}$, and $B_{U1}$) across test conditions in the lower body (LB) and upper body (UB) control systems. At each stance width, gains were averaged across stimulus amplitude.*

## DISCUSSION

### *Model approximations and limitations*

LINEARIZATION OF EQUATIONS OF MOTION. The equations of motion (Eq. 5.2 and 5.3) were linearized about vertical. This linearization greatly simplified the equations because the inertial and gravitational coefficients in the full solution (i.e., without linearization of the equations) are not simple constants at a given stance width as shown in Fig. 5.1D and E, but rather vary as a function of *LBS*, *UBS*, and *SS*. Furthermore, the full solution contained additional terms related to the segmental velocity squared. To determine the accuracy of the linearized set of equations, LB and UB torque predicted from the linearized equations was compared to torque predicted from full solution for each test condition. For the linearized set of equations, *SS*, *LBS*, and *UBS* positions and accelerations were set equal to the mean experimental time series used in

the current study, which was 43.72 s in length (see Fig. 4.2 for sample data). Similarly, for the full set of equations, *SS*, *LBS*, and *UBS* position, velocity, and accelerations were set equal to the mean experimental time series. $R^2$ values were calculated over the 43.72 s. It was found that the minimum $R^2$ value across all test conditions was 0.99997. Therefore, the linearized equations provided an accurate description of body dynamics over the range of LB and UB sway that occurred in the current study.

LB TORQUE ASSUMPTION. It was assumed that LB torque was generated equally across all LB joints. However, identical LB segmental motion can occur with an appropriately scaled torque generated about only one LB joint or about any combination of joints. With this type of system, it is likely that the proportion of torque generation about one joint compared to another is dictated by optimization principles so that some cost function is minimized (Todorov 2004), such as metabolic energy (Hoyt and Taylor 1981). However, it was beyond the scope of the current study to investigate the optimal distribution of LB torque. Instead, the current study focused on identifying contributions to $T_{LB}$, the summation of all intrinsic and active mechanisms that generate LB torque applied about all LB joints (Fig. 5.1B). Therefore, the assumption that LB torque was generated equally across all LB joints was chosen for simplicity and was arbitrary. Had a different assumption been made about which LB joint or joints torque was applied, determination of all UB parameters, the LB time delay ($\tau_{LB}$), and torque feedback parameters ($\tau_t$ and $G_t$) would have been unaffected; while the remaining LB gains would scale to accommodate the assumption. The following three paragraphs will focus on these remaining LB gains and do not pertain to LB parameters $\tau_{LB}$, $\tau_t$, and $G_t$ or any UB parameters.

Consider how LB model gains scale to accommodate different torque assumptions in the parallel stance condition. In parallel stance, the LB configuration approximates a parallelogram and a given torque applied at any particular LB joint results in identical segmental motion as if the torque were applied at any one of the other three LB joints. Consequently, LB gains determined with our assumption that LB torque is applied equally about all four LB joints will be exactly one-half the gains determined with the assumption that LB torque is generated about only two LB joints. The above example is particularly simple due to the parallelogram configuration because torque at any LB joint

contributes equally to LB motion. At stance widths other than parallel, torque applied about the ankle results in different motion than that which would have occurred if the same torque were generated about the hip. Specifically, in narrow stance ankle torque is more effective than hip torque, and vice versa with wide stance width. The gain parameter scaling is therefore dependent on stance width, but remains predetermined for any particular assumption about which LB joint or joints torque is applied.

Some limitations exist on the interpretation of variations in LB gains both within a particular stance width and across stance widths. At a particular stance width, it is not possible to determine if changes in LB torque resulted from increased/decreased muscle activation or if changes in LB torque resulted from a change in the joint or joints about which LB torque was applied. For example, the EC narrow stance system $K_{L3}$ decreases with increasing stimulus amplitude (Fig. 5.3A). This decrease in $K_{L3}$ could represent a change in the balance system where either 1) the proprioceptive gain on the *ss-lbs* signal is reduced so that the LB is less responsive to surface tilt stimuli as the stimulus amplitude increases, or 2) the gain on *ss-lbs* is fixed across stimulus amplitude, but the application of LB torque is shifted toward hips and away from the ankles resulting in relatively less LB motion as stimulus amplitude increases. Either way, any change in LB gains across stimulus amplitude or between EO/EC conditions indicates a neurally mediated change in the active LB control mechanism that altered the dynamic characteristics of the LB.

Across stance widths, differences in LB model gains cannot be used to infer changes in LB control. Instead, a change in LB control across stance width is only indicated by changes in relative parameter values within one particular stance width compared to another. For example, it was found that the intrinsic LB stiffness increases relative to total LB stiffness as stance width increases (Fig. 5.6). This result indicates there was a change in LB control across stance width whereby the proportion of stiffness provided by the intrinsic LB mechanism compared to active mechanisms increased with stance width.

*Mechanisms of narrow stance control*

LB SYSTEM IN NARROW STANCE. Model results from the proposed LB control system consisted only of an active mechanism with inputs from proprioception,

vestibular, and visual (in EO). Of these sensory systems, surface-orienting proprioception made the largest contribution to LB system stiffness, while inter-segmental proprioception and the combination of inter-segmental proprioception and vestibular/visual made the largest contribution to LB system damping. Nonlinear LB dynamics across stimulus amplitude were accounted for in the model through sensory reweighting whereby inter-segmental and surface-orienting proprioceptive contributions to system stiffness decreased with increasing stimulus amplitude while the vertical-orienting sensory contributions increased with increasing stimulus amplitude in both EO and EC conditions. Vertical-orienting sensory contributions were assumed to come from a combined vestibular and inter-segmental proprioceptive origin in EC and a combined vestibular, visual, and inter-segmental proprioceptive origin in EO. Specifically, an estimate of *lbs* is assumed to arise from the transformation of visual and/or vestibular information, encoding head-in-space orientation, through inter-segmental proprioceptive signals, encoding the orientation of one body segment to another (Mergner and Rosemeier 1998).

The proposed LB control system has many similarities to an existing model of whole body CoM control in narrow stance (Cenciarini and Peterka 2006). In Cenciarini and Peterka, eyes closed subjects where attached to a single-link backboard that rotated about the axis midway between the feet at ankle height. The body was modeled as a single-link inverted pendulum and CoM sway was the variable under control. Similar to the current study, control was based on proprioceptive inputs that oriented the body toward the surface, vestibular inputs that oriented the body toward vertical, and a low-pass filtered torque feedback all with one effective system time delay. Also, in both studies, changes in parameters were consistent with a sensory reweighting mechanism whereby subjects shifted away from reliance on proprioception information and toward reliance on vestibular information as stimulus amplitude increased in EC conditions. The similarities between studies are not surprising because whole body CoM position is largely influenced by LB sway. However, differences between models are also expected because the equations of motion differ greatly between the single link whole body model in the previous study and the multi-link model in the current study. In particular, an inter-segmental proprioceptive signal was found to be an important sensory input in current

study; but this signal has no meaning in the previous whole body study where single-link dynamics were enforced.

UB SYSTEM IN NARROW STANCE. The proposed UB system was controlled with an active mechanism that included proprioception, vestibular, and visual (in EO conditions) inputs and an intrinsic mechanism that included the mechanical properties of the UB/pelvis musculoskeletal system. While the overall structure of UB and LB control were similar, there was only sensory one input (*lbs*-*ubs*) shared in common. It is possible that additional inputs could be shared between active LB and UB mechanisms (such as *ss*-*lbs* and *lbs* to the UB system and *ps*-*ubs* and *ubs* to the LB system), but the ability of the model to account for experimental results did not warrant the inclusion of additional input signals.

In the UB system, pelvis-orienting proprioception made the largest contribution to UB system stiffness while inter-segmental proprioception and vestibular/visual made the largest contributions to UB system damping. The EC nonlinear UB dynamics across stimulus amplitude were accounted for in the model with a decrease in the overall UB stiffness (primarily through a decrease in $K_{UI}$) as stimulus amplitude increased and thus did not support the hypothesis that sensory reweighting contributed to EC UB control in narrow stance. The EO nonlinear UB dynamics across stimulus amplitude were accounted for with both an overall decline in UB stiffness and also with sensory reweighting whereby contributions to UB stiffness from proprioception decreased while vestibular/visual increased as stimulus amplitude increased (Fig. 5.4). Differences between EO and EC narrow stance conditions underscore the important role of vision in the narrow stance system where UB orientation is more vertical in space with visual availability.

Several comparisons can be made between the model of UB control in the current study and a previously developed model of spinal stability (Chapter 2). In the previous study, UB control was characterized in conditions where LB sway was prevented with a frame and roller system (Fig. 2.1). A model was developed that included intrinsic stiffness, a short-latency phasic mechanism, a medium-latency phasic mechanism, and a long-latency mechanism. The intrinsic stiffness and short-latency phasic mechanisms together were approximately equal to the UB intrinsic mechanism in the current study

because the short-latency time delay was only ~25 ms. Also, inputs to the long-latency mechanism (-*lbs*, *lbs*-*ubs*, and *ps*-*ubs*) in the spinal stability model were identical to inputs for the active mechanism in the current study.

In both studies, the pelvis-orienting damping from active mechanisms ($B_{U3}$ in the current study) was low; but in the previous spinal stability study inter-segmental proprioception was found to make the largest contribution to UB damping whereas in the current study both vestibular/visual and inter-segmental proprioception made important contributions to UB damping. This difference could simply indicate that UB control differed in the two studies due to the different constraints on the LB (Cordo and Nashner 1982). Alternatively, because it was not possible to distinguish between vestibular and inter-segmental proprioception in normal subjects in the spinal stability study, it is possible that vestibular cues made a greater contribution to UB damping than was previously assumed.

Another difference between studies was the shorter UB effective time delay in the current study compared to time delays associated with both medium-latency (~135 ms) and long-latency (~281 ms) mechanisms in the spinal stability study. Because $\tau_{UB}$ in the current study is consistent with time delays associated with sagittal plane UB torque generated in another freestanding study (Alexandrov et al. 2005), it is likely that active control of the UB is more rapid in freestanding conditions compared to conditions where LB sway is prevented. But it is also possible that contributions from intrinsic mechanisms and reflexive responses not specifically represented in the model produced a shorter effective UB system time delay in the current study compared to the model of spinal stability. For example, the representation of the UB intrinsic mechanism did not include the complex musculature surrounding the UB, pelvis, and lesser trochanters all of which would be expected to influence intrinsic mechanisms and reflexive responses differently when the LB is fixed in space (as in the previous spinal stability study) compared to freestanding conditions.

*Influence of stance width on mechanisms of balance control*

The model was used to characterize the effect of stance width on intrinsic and active control mechanisms. Relative to total stiffness contributions to LB and UB systems, the LB intrinsic stiffness greatly increased and the UB intrinsic stiffness slightly

increased with stance width (Fig. 5.6). In the UB system, the relative increase in intrinsic stiffness ($K_{U4}$) was due to a decreased contribution from active mechanisms with increasing stance width. In the LB system, the increased LB intrinsic stiffness with increasing stance width could be directly related to the changes in biomechanics of LB motion with stance width (Scrivens et al. 2009; Day et al. 1993). Specifically, muscles and tendons that span the hip joints are initially stretched to a greater length in wide compared to narrow stance. Because muscles and tendons have nonlinear spring-like properties (Loeb and Ghez 2000), the increased length results in a larger spring constant and thus larger force generation in muscles and tendons per unit of LB sway. This larger force generation is further amplified in wide stance because the hip joint rotates through a larger angle in wide compared to narrow stance for a given LB displacement. This larger hip joint rotation results in muscles and tendons that span the hip joint being stretched to a greater extent and therefore generating a larger restoring force in wide compared to narrow stance.

Results showed that $K_{L3}$ increased and $K_{L4}$ decreased with increasing stance width. Effectively, the active stiffness control was being partially replaced by the intrinsic stiffness. Because long time delays in feedback control are associated with unstable systems, the relative increase in intrinsic stiffness with stance width enhanced the LB system stability. The enhanced stability in wide compared to narrower stances could have reduced the need to use mechanisms of balance control based on sensory integration and sensory reweighting.

With respect to sensory reweighting, modeling results imply that the LB control system becomes more linear in wider stance conditions and thus exhibits less sensory reweighting across stimulus amplitude in both EO and EC conditions. This conclusion was based on the fact that in medium stance conditions, LB gains varied less across stimulus amplitude than in narrow or parallel; and in wide stance conditions, a linear LB system could be assumed without loosing model accuracy (Fig. 5.5 and 4.7). A more linear LB system in medium and wide stance conditions is consistent with the smaller variations in experimental FRFs and IRFs across stimulus amplitude in medium and wide stance compared to narrow and parallel stance widths.

In contrast to the LB system, modeling results indicated that UB control is nonlinear across stimulus amplitude at all stance widths, consistent with experimental UB

FRFs and IRFs which showed stimulus amplitude-dependency across all stance widths. In narrow stance, nonlinear UB control was caused by a decrease in magnitude of active UB stiffness (Fig. 5.5 and 4.7) and a sensory reweighting of stiffness gains in EO conditions (Fig. 5.4). At all other stance widths, variation in active UB damping gains indicated that UB system damping from inter-segmental proprioceptive and vestibular/visual inputs increased as stimulus amplitude increased (Fig. 5.5 and 4.7).

*State variable feedback*

The model in Fig. 5.2 was developed to help understand the biomechanical and physiological systems contributing to frontal plane balance control. Therefore, input signals to intrinsic mechanisms were selected so that gains provided an approximate representation of the contribution of intrinsic biomechanical systems to torque generation. Similarly, input signals to active mechanisms were selected so that active mechanism gains could provide insight into the contribution of specific sensory systems to torque generation. However, a model structure could have been developed where input signals were based on sensory representations of state variable estimates *SS*, *LBS*, and *UBS* and their derivatives. This type of model, which is similar to many previous sagittal plane models (Alexandrov et al. 2005; Barin 1989; Kuo 1995; Park et al. 2004) is not able to represent intrinsic and active mechanisms with separate time delays and many important kinematic signals are distributed across state variables. For example, it was previously shown that *ps-ubs* was an important proprioceptive signal for UB control. A gain on this signal, $K_{U3}$ in the current study, represents the pelvis-orienting proprioceptive contribution to UB torque. To equivalently represent this proprioceptive contribution in a model with state variable feedback, three gains would be required, a $P_R * K_{U3}$ gain that is multiplied by *ss*, a $(1-P_R)*K_{U3}$ gain that is multiplied by *lbs*, and a $-K_{U3}$ gain that is multiplied by *ubs*.

Nevertheless, certain control features could be seen more easily when the model was restructured such that gains were on state variables and their derivatives. This restructuring is shown in Fig. 5.9 for the narrow stance system where gains in intrinsic and active mechanisms were represented as gains on *SS*, *LBS*, and *UBS* and their derivatives. The transformation to state variable form in Fig. 5.9 did not influence $G_t$, $\tau_t$,

$\tau_{LB}$, and $\tau_{UB}$, and therefore results are not completely analogous to previous sagittal plane models where separate time delays and torque feedback were not represented.

Fig. 5.9 shows that a positive *SS* and *SS* velocity results in positive torque (represented as x's in Fig. 5.9, left column), positive *LBS* and *LBS* velocity results in negative torque (squares), and positive *UBS* and *UBS* velocity results in negative torque (diamonds) about LB joints. As stimulus amplitude increases, gains on *SS*, *SS* velocity, *UBS*, and *UBS* velocity decreased while gains on *LBS* and *LBS* velocity increased in magnitude. In EO compared to EC, stiffness gains of *SS* and *LBS* decreased while gains on *UBS* increased in magnitude. Overall stiffness and damping was defined as the sum of the magnitude of all gains. Overall stiffness (but not damping) decreased across stimulus amplitude in EC conditions (but not EO conditions). There were no consistent differences in overall stiffness or damping between EO and EC.

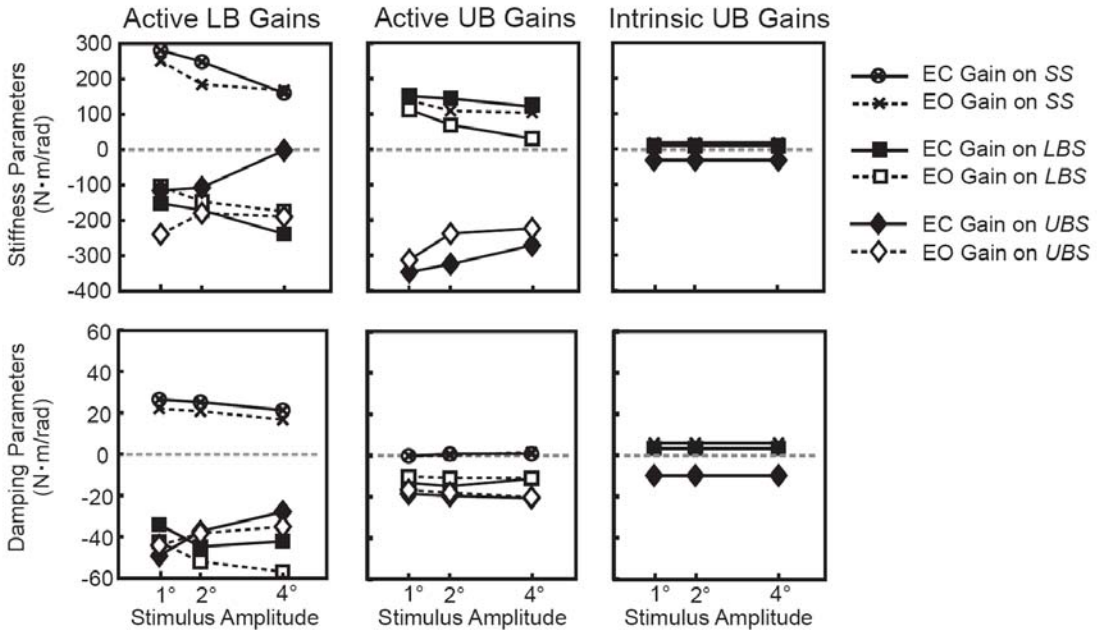


**FIG. 5.9.** *The narrow stance control system represented with the gains in Fig. 5.3 and 4.4 transformed into gains on state variables, SS, LBS, and UBS and their derivatives. Values of $G_t$, $\tau_t$, $\tau_{LB}$, and $\tau_{UB}$ were not changed and are displayed in Table 5.1. Intrinsic UB gains were the same for eyes closed and open.*

For the active UB narrow stance system (middle column in Fig. 5.9), positive *SS* and *SS* velocity results in positive UB torque (x's), positive *UBS* and *UBS* velocity results in negative UB torque (diamonds), positive *LBS* results in positive UB torque, and

positive *LBS* velocity results in negative UB torque. As stimulus amplitude increases and in EO compared to EC, all stiffness-related gains decrease, thus reducing the overall stiffness in the UB system. Changes in damping parameters were minimal across stimulus amplitude and between EO/EC. All intrinsic UB gains were relatively low compared to active UB gains.

*Other model structures*

The model structure itself represents a quantitative hypothesis about how the LB and UB control systems are organized. We explored numerous other model structures in addition to the one presented in the current study. Three examples are given below.

One simple control hypothesis is that the LB and UB system is based entirely on intrinsic mechanisms. That is, LB control is based on intrinsic stiffness and damping that orients the LB toward the surface with no time delay and UB control is based on intrinsic stiffness and damping that orients the UB toward the pelvis with no time delay. Results from a model based on intrinsic mechanisms were only able to account for some general features of experimental FRF gains in narrow and wide stance conditions (Fig. 5.10, black curves). Phase curves were poorly described. Only with a large decrease in damping could phases be better accounted for, but a decrease in damping also produced high resonance in gain curves and therefore no overall improvement. Thus, the intrinsic mechanism model was rejected as a reasonable hypothesis about how the LB and UB systems are controlled.

A model structure was also explored where control was based only on feedback from local segment dynamics. That is, LB control consisted of an intrinsic mechanism based on *LBS* relative to *SS* and a time-delayed mechanism based on *lbs* and *lbs* relative to *ss*; while UB control consisted of an intrinsic mechanism based on *UBS* relative to *PS* and a time-delayed mechanism based on *ubs* and *ubs* relative to *ps*. Results from this model structure were able to account for most of features of experimental FRFs in both narrow and wide stance conditions (Fig. 5.10, red curves). However, this model was unable to account for detailed features such as the LB peak or plateau of gain and phase around 3 Hz, LB gains between 0.1 and 0.8 Hz in wide stance, UB gains below 0.l Hz and between 1 Hz and 3 Hz in wide stance, and UB phases around 0.1 Hz in wide stance. Therefore, with only feedback from local segment dynamics, the system is stable and

able to describe general sway patterns but cannot account for detailed experimental FRFs. This finding is in agreement with Barin (1989) who found that a model based only on local segment kinematics was also stable and able to account for general sway patterns, but improvement in model fits were obtained when feedback from segments across the body were used to control each joint. Although a control scheme where feedback is only from local segment dynamics may appear "simple," sensorimotor transformations across body segments still must take place. For example, an estimate of *lbs* is assumed to arise from the transformation of visual and/or vestibular information, encoding head-in-space orientation, through inter-segmental proprioceptive signals (Mergner and Rosemeier 1998).

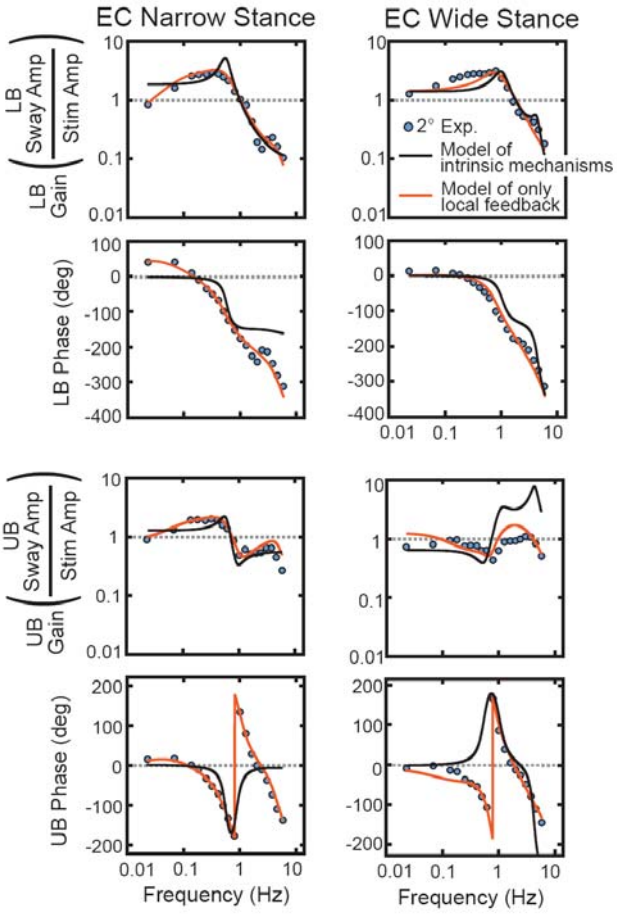


**FIG. 5.10.** *Alternative LB and UB model structures. Intrinsic mechanisms (solid black curves) alone could not account for experimental FRFs (blue circles). A model with only local feedback (red curves) could account for general experimental FRFs features, but many details could not be described without the inclusion of feedback across body segments.*

*Conclusions*

The proposed model indicates that LB control differs from UB control during freestanding responses to continuous surface rotations at all stance widths. In narrow stance, LB control was primarily based on active mechanisms. Changes in the LB active mechanism across stimulus amplitude suggested sensory reweighting contributed to nonlinear LB dynamics whereby subject shifted away from reliance on surface-orienting proprioceptive cues and shifted toward reliance on vestibular/visual cues to control the LB system as stimulus amplitude increased in both EO and EC conditions. In contrast, the model indicated that the UB nonlinearity was due a reduction in active stiffness (lower contributions from all sensory systems to UB control) as stimulus amplitude increased and in EO compared to EC. As stance width increased, overall UB stiffness and damping decreased while LB intrinsic stiffness increased making the LB system more stable. This increase in LB stability was also accompanied by active LB control that was more linear across stimulus amplitude.

# CHAPTER VI.
# FUTURE WORK

*Manipulation of control mechanisms*

Future experiments can be performed that manipulate various control mechanisms to better understand the frontal plane balance system. In the chapters two and three, LB sway was prevented and UB control was investigated. It would be possible to reverse this experimental paradigm by using a stiff pelvis/torso corset or backboard assembly that enforced UB orientation perpendicular to the pelvis. This set up would essentially remove the UB control system because UB tilt in space would be completely determined by the pelvis tilt angle. Thus, UB torque would have no impact on UB motion. With this paradigm, the linearized LB equation of motion no longer has an interaction torque from UB motion, but instead exhibits a much larger than normal interaction torque from the surface because surface rotations directly produce UB tilts. Although the biomechanics are somewhat artificial, this experimental paradigm would enable a close investigation of LB control mechanisms independent of UB control.

Another future study could be to further investigate the inter-segmental proprioceptive contribution. Medium-latency inter-segmental proprioceptive cues provided major contributions to UB system damping in conditions where LB sway was prevented. Similarly, in freestanding conditions, an inter-segmental proprioceptive signal was also found to be an important contributor to the UB and LB system. In previous studies, this sensory cue has received little attention compared to other sensory inputs to balance control. Future experiments could be carried out with a backboard assembly that enforced LB and UB alignment, which would make the inter-segmental proprioceptive input approximately zero (Cenciarini and Peterka 2006). The model developed in chapter five could be used to predict the stance-width dependent effects of this altered biomechanical condition on stability. It is anticipated that in eyes closed (EC) conditions,

normal subjects would be able to compensate via increased reliance on vestibular inputs. However, EC subjects with a bilateral vestibular loss (BVL) should have a more difficult time maintaining stability when the LB and UB are aligned.

Finally, the role of surface-orienting proprioception could be investigated. The majority of LB system stiffness came through surface-orienting proprioception in narrow stance conditions, which was also found to decrease with increasing stance width. The surface-orienting proprioceptive signal could be made approximately zero with surface sway referencing whereby the surface rotation angle was equal to the LB sway angle at all times. Again, model predictions could be tested and further insight gained into the stance-width dependent mechanisms underlying frontal plane balance control.

*Frontal plane control during visual stimulation*

In Chapter 4, results were presented of subjects' responses to rotations of a visual surround. Relative responsiveness to visual stimuli decreased as the stimulus amplitude increased. Also, responsiveness decreased with increasing stance width. The reduced responsiveness to visual stimuli in wide stance could be related to an increase in LB stability in wide stance because UB responses to visual stimuli were low when LB sway was prevented (see Chapter 2).

It would be beneficial to develop a model that can tie together the stance-dependent and stimulus amplitude-dependent responses to visual stimuli. The mechanism by which visual information is incorporated into balance control is not simple or well understood. Evoked sway from visual stimuli may be triggered by optic flow patterns (Lee and Lishman 1975; Warren et al. 1996) or by an efference copy of eye movements tracking the visual stimuli (Glasauer et al. 2005). Some insight into LB and UB responses to visual stimuli found in Chapter 4 may be found by considering how the LB and UB naturally sway in the frontal plane compared to visual surround rotation. Because the visual surround rotated about the axis midway between the heels at ankle height, LB sway shares the same axis of rotation with the visual surround, but UB sway does not. To model LB and UB sway behavior, many assumptions about how visual information is processed with would need to be further explored. For example, to better understand the relationship between axis of rotation and the LB and UB sway responses to visual

stimuli, it may be helpful to systematically adjust the visual surround axis of rotation height and examine freestanding LB and UB responses to the visual stimuli.

*Influences of cognition and age*

In all experiments presented in this dissertation, healthy young subjects were instructed to respond naturally to external perturbations while listening to a short story. However, it is well documented that cognitive loads can have an impact on balance responses under certain conditions and these impacts can be influenced by a subject's age (Maki and McIlroy 2007). Recent studies used a model structure similar to models proposed in the current dissertation and found the effective time delay and sensory weights to be sensitive to cognitive loads (Mahboobin et al. 2007) and active stiffness and damping gains to be sensitive to age (Cenciarini et al. 2010). Therefore, as a next step, the role of cognition could be investigated as a function of frontal plane stance width. In particular, model parameters could be determined from a dual task/cognitive load experiment and compared to model parameters determined from a control condition where no cognitive load was presented. One hypothesis to test would be that in narrow stance conditions, LB and UB system time delays and active sensory gains will be influenced by the presence of a cognitive task similar to a previous sagittal plane study (Mahboobin et al. 2007). But as stance width increases, the increased contribution of intrinsic stiffness and LB control and the nearly linear LB control system would enable subjects to participate in a dual task/cognitive load without an impact on balance control.

*Nonlinear modeling*

In each test condition, the model was assumed linear time invariant. However, because biological systems are nonlinear, models presented in this dissertation provided a linear approximation to the true nonlinear system. A future experiment could expand the models in this dissertation to include nonlinear equations of motion and/or nonlinear control.

Equations of motion were linearized about upright in this dissertation because subjects swayed symmetrically about the upright position. However, in future experiments, subjects could be asked to maintain a steady sway angle while external perturbations are applied. This type of protocol would enable further model validation by

testing predictions about the voluntary nature of a "set point". However, to model a set point other than upright, it would be necessary to linearize the equations of motion about the set point. In addition, nonlinear equations of motion may be necessary when body sways are much greater than those found in the current dissertation. For example, a study could be carried out to explore control of the spinal column under a wider range of motion representing the distributed control of the spinal column. Experimental data could include measurements at numerous spinal joints during large sagittal and/or frontal plane sway and modeling could be used to infer how each joint is controlled. The spinal column could be modeled as multiple segments connected as an open-chain with nonlinear equations of motion.

Nonlinear control schemes could be another important area for future research. In the current dissertation, a linear model could not be assumed across different peak-to-peak stimulus amplitudes. However, within a particular test condition, the system was assumed to be in steady-state and model parameters were constant throughout each particular test. Although this assumption provided good predictions of experimental results, it may be more accurate to assume the system was not in completely steady-state conditions throughout each test. For example, it may be that sensory weights varied throughout each test and therefore gains on sensory signals were in fact continuously varying through each test. To incorporate this type of nonlinear control in the model, gains on each sensory signal could be a function of body segment sway. For example, as LB sway increases in amplitude, the gain on $-lbs$ could also increase; this would tend to limit LB excursions to a greater extent as LB sway increased.

*Optimization principles in balance control*

This dissertation identified balance control mechanisms. However, it is not known *why* these control mechanisms were used. Optimization has emerged as a powerful tool to explain sensorimotor control behavior (Todorov 2004). With respect to sensory integration, further modeling could be carried out based on principles of optimal, minimum variance perceptual estimates (Ernst and Banks 2002; van Beers et al. 1999). In the proposed models, noise could be summed with sensory inputs (van der Kooij 1999; van der Kooij 2001) and torque inputs. Then, model predictions could be used to determine if control mechanisms such as sensory reweighting could be predicted from

optimal estimation theory. With respect to motor control, further modeling could be carried out based on optimization principles to understand why certain balance strategies were implemented (Kuo 1995; Goodworth et al. 2007; Qu and Nussbaum 2009). For example, modeling could used to explore possible reasons why subjects did not use counter-phase UB and LB sway in narrow stance conditions even though this strategy would appear to be beneficial for limiting center of mass motion. It is likely that minimizing center of mass sway was not the only variable of interest to subjects.

Finally, optimal control could be used to understand LB torque generation. In narrow stance, ankle torque is more effective than hip torque at producing LB motion, and vice versa in wide stance. Therefore, if subjects wished to use optimal control to minimize the amount of torque needed to produce LB motion, then subjects would apply LB torque primarily about the ankles in narrow stance but as stance width increased subjects would progressively apply a greater percentage of LB torque about the hip joints. This hypothesis could be tested using inverse dynamics to measure torque distributions across joints and compare to optimal predictions. Modeling in combination with impulse-response functions of each of the four LB torques could be used to tease apart the relative contribution of active torque generation to torque generation based on intrinsic biomechanics (see Fig. 2.8). However, instead of minimizing LB torque generation, it may be that a more physiological variable is minimized, such as metabolic energy (Hoyt and Taylor 1981). Some of the difficulties associated with modeling metabolic energy would include the need to specify muscle insertions, muscles sizes, and type of muscle fibers. However, existing computer programs, such as SIMM software (Motion Analysis Corporation, Santa Rosa, CA) could provide a starting point for this type of analysis.

## REFERENCES


Alexandrov AV, Frolov AA, Horak FB, Carlson-Kuhta P, and Park S. Feedback equilibrium control during human standing. *Biol Cybern* 93: 309-322, 2005.

Ali AS, Rowen KA, and Iles JF. Vestibular actions on back and lower limb muscles during postural tasks in man. *J Physiol* 546: 615-624, 2003.

Allison LK, Kiemel T, and Jeka JJ. Multisensory reweighting of vision and touch is intact in healthy and fall-prone older adults. *Exp Brain Res* 175: 342-352, 2006

Allum JH. Organization of stabilizing reflex responses in tibialis anterior muscles following ankle flexion perturbations of standing man. *Brain Res* 264: 297-301, 1983.

Angelaki DE, McHenry MQ, Dickman JD, Newlands SD, and Hess BJ. Computation of inertial motion: neural strategies to resolve ambiguous otolith information. *J Neurosci* 19: 316-327, 1999.

Barin K. Evaluation of a generalized model of human postural dynamics and control in the sagittal plane. *Biol Cybern* 61:34-50, 1989.

Bendat JS and Piersol AG. *Random Data: Analysis and Measurement Procedures*. New York: Wiley, 2000.

Berthoz A, Lacour M, Soechting JF, and Vidal PP. The role of vision in the control of posture during linear motion. *Prog Brain Res* 50: 197-209, 1979.

Blouin J, Teasdale N, and Mouchnino L. Vestibular signal processing in a subject with somatosensory deafferentation: the case of sitting posture. *BMC Neurology* 7: 25, 2007.

Bronstein AM. Suppression of visually evoked postural responses. *Exp Brain Res* 63: 655-658, 1986

Brown SH and McGill SM. The intrinsic stiffness of the in vivo lumbar spine in response to quick releases: Implications for reflexive requirements. *J Electromyogr Kinesiol* 19: 727-736, 2009.

Carpenter MG, Allum JH, and Honegger F. Vestibular influences on human postural control in combinations of pitch and roll planes reveal differences in spatiotemporal processing. *Exp Brain Res* 140: 95-111, 2001.

Casadio M, Morasso PG, and Sanguineti V. Direct measurement of ankle stiffness during quiet standing: implications for control modelling and clinical application. *Gait Posture* 21: 410-424, 2005.

Cenciarini M, Loughlin PJ, Sparto PJ, and Redfern MS. Stiffness and damping in postural control increase with age. *IEEE Trans Biomed Eng* 57: 267-275, 2010.

Cenciarini M and Peterka RJ. Stimulus-dependent changes in the vestibular contribution to human postural control. *J Neurophysiol* 95: 2733-2750, 2006.

Cholewicki J, Juluru K, Radebold A, Panjabi MM, and McGill SM. Lumbar spine stability can be augmented with an abdominal belt and/or increased intra-abdominal pressure. *Eur Spine J* 8: 388-395, 1999.

Cholewicki J, Polzhofer GK, and Radebold A. Postural control of trunk during unstable sitting. *J Biomech* 33: 1733-1737, 2000a.

Cholewicki J, Simons AP, and Radebold A. Effects of external trunk loads on lumbar spine stability. *J Biomech* 33: 1377-1385, 2000b.

Cordo PJ and Nashner LM. Properties of postural adjustments associated with rapid arm movements. *J Neurophysiol* 47: 287-302, 1982.

Crago PE. *Neuroprostheses, in: Biomechanics and neural control of posture and movement, Section IX*, Editors Winters JM andP.E. Crago PE, New York, Springer, 2000.

Creath R, Kiemel T, Horak F, and Jeka JJ. The role of vestibular and somatosensory systems in intersegmental control of upright stance. *J Vestib Res* 18: 39-49, 2008.

Creath R, Kiemel T, Horak F, Peterka R, and Jeka J. A unified view of quiet and perturbed stance: simultaneous co-existing excitable modes. *Neurosci Lett* 377: 75-80, 2005.

Cresswell AG, Oddsson L, and Thorstensson A. The influence of sudden perturbations on trunk muscle activity and intra-abdominal pressure while standing. *Exp Brain Res* 98: 336-341, 1994.

Davies WDT. *System Identification for Self-adaptive Control*. London, New York,: Wiley-Interscience, 1970.

Day BL and Cole J. Vestibular-evoked postural responses in the absence of somatosensory information. *Brain* 125: 2081-2088, 2002.

Day BL, Severac Cauquil A, Bartolomei L, Pastor MA, and Lyon IN. Human body-segment tilts induced by galvanic stimulation: a vestibularly driven balance protection mechanism. *J Physiol* 500: 661-672, 1997.

Day BL, Steiger MJ, Thompson PD, and Marsden CD. Effect of vision and stance width on human body motion when standing: implications for afferent control of lateral sway. *J Physiol* 469: 479-499, 1993.

Ebenbichler GR, Oddsson LI, Kollmitzer J, and Erim Z. Sensory-motor control of the lower back: implications for rehabilitation. *Med Sci Sports Exerc* 33: 1889-1898, 2001.

Erdmann WS. Geometric and inertial data of the trunk in adult males. *J Biomech* 30: 679-688, 1997.

Ernst MO and Banks MS. Humans integrate visual and haptic information in a statistically optimal fashion. *Nature* 415: 429-433, 2002.

Gardner-Morse MG and Stokes IA. Trunk stiffness increases with steady-state effort. *J Biomech* 34: 457-463, 2001.

Genthon N and Rougier P. Does the capacity to appropriately stabilize trunk movements facilitate the control of upright standing? *Motor control* 10: 232-243, 2006.

Ghez C and Krakauer J. The Organization of Movement. In: *Principles of Neuroscience* (4th ed.), edited by Kandel E, Schwartz J and Jessel T. New York: McGraw-Hill, p. 653-673, 2000.

Glasauer S, Schneider E, Jahn K, Strupp M, Brandt T. How the eyes move the body. *Neurology* 65:1291-1293, 2005.

Goodworth AD and Peterka RJ. Contribution of sensorimotor integration to spinal stabilization in humans. *J Neurophysiol* 102: 496-512, 2009.

Goodworth and Peterka RJ. Influence of Bilateral Vestibular Loss on Spinal Stabilization in Humans. *Journal of Neurophysiology*, in press, 2010.

Goodworth AD and Peterka RJ. Influence of Frontal Plane Stance Width on Sensory Reweighting and Coordination in Human Balance Control. *Journal of Neurophysiology*, in revision, 2010.

Goodworth AD, Wall III C, and Peterka RJ, "Application of optimization methods to predict performance of a vibrotactile balance prosthesis," *Proc of the IEEE EMBS Conf Neural Eng,* pp. 510-513, 2007.

Goodworth AD, Wall III C, and Peterka RJ. Influence of Feedback Parameters on Performance of a Vibrotactile Balance Prosthesis, *IEEE Trans. Neural Systems & Rehabilitation Eng*, 17: 397-409, 2009.

Granata KP, Slota GP, and Bennett BC. Paraspinal muscle reflex dynamics. *J Biomech* 37: 241-247, 2004.

Gurfinkel VS, Ivanenko YP, Levik YS, Babakova IA. Kinesthetic reference for human orthograde posture. *Neuroscience* 68: 229-243, 1995.

Hogan N. Mechanical Impedance of Single- and Multi-Articular Systems. In: *Multiple Muscle Systems: Biomechanics and Movement Organization*, edited by Winters JM and Woo SL-Y. New York: Springer-Verlag, 1990, p. 149-164.

Henry SH, Fung J and Horak FB. Effect of stance width on multidirectional postural responses, *J Neurophysiol* 85, 559-570, 2001.

Horak FB. Postural compensation for vestibular loss. *Basic and Clinical Aspects of Vertigo and Dizziness: Ann NY Acad Sci* 1164: 76-81, 2009.

Horak FB. Postural orientation and equilibrium: what do we need to know about neural control of balance to prevent falls? *Age Ageing* 35: 7-11, 2006

Horak FB, Frank J, and Nutt J. Effects of dopamine on postural control in parkinsonian subjects: scaling, set, and tone. *J Neurophysiology* 75:2380-2396, 1996.

Horak FB, Henry SM, and Shumway-Cook A. Postural perturbations: new insights for treatment of balance disorders. *Phys Ther* 77: 517-33. 1997

Horak FB and Macpherson JM. *Postural Orientation and Equilibrium, in Handbook of Physiology: Section 12, Exercise Regulation and Integration of Multiple Systems*. New York: Oxford University Press, 1996.

Horak FB, Nashner LM, and Diener HC. Postural strategies associated with somatosensory and vestibular loss. *Exp Brain Res* 82:167-77, 1990.

Horlings CG, Küng UM, Honegger F, Van Engelen BG, Van Alfen N, Bloem BR, and Allum JH. Vestibular and proprioceptive influences on trunk movements during quiet standing. *Neuroscience* 161:904-14, 2009.

Hoyt DF and Taylor CR. Gait and the energetics of locomotion in horses. *Nature* 292:239-240, 1981.

Ishida A and Imai S. Responses of the posture-control system to pseudorandom acceleration disturbances. *Med Biol Eng Comput* 18: 433-438, 1980.

Jeka J, Oie K, Schöner G, Dijkstra T, and Henson E. Position and velocity coupling of postural sway to somatosensory drive. *J Neurophysiol* 79:1661-74, 1998.

Johansson R and Magnusson M. Human postural dynamics, *Crit Rev Biomed Eng* 18: 413-437, 1991.

Johansson R, Magnusson M, and Akesson M. Identification of human postural dynamics. *IEEE Trans Biomed Eng* 35: 858-869, 1988.

Kajita S, Yokoi K, Saigo M and Tanie K. Balancing a Humanoid Robot Using Backdrive Concerned Torque Control and Direct Angular Momentum Feedback. *Proceedings of the IEEE Conf on Robotics & Automation* Seoul, Korea, May 21-26, 2001.

Kiemel T, Elahi AJ, and Jeka JJ. Identification of the plant for upright stance in humans: multiple movement patterns from a single neural strategy. *J Neurophysiol* 100: 3394-3406, 2008.

Kim JY, Popovic MR, and Mills JK, Dynamic modeling and torque estimation of FES-assisted arm-free standing for paraplegics, *IEEE Trans Neural Syst Rehabil Eng* 14: 46-54, 2006.

Kim S, Horak FB, Patricia C, and Park S. Postural Feedback Scaling Deficits in Parkinson's Disease. *J Neurophysiol* 102: 2910-2920, 2009.

Kirby RL, Price NA, and MacLeod DA. The influence of foot position on standing balance. *J Biomech* 20: 423-427, 1987.

Koeller W, Meier W, and Hartmann F. Biomechanical properties of human intervertebral discs subjected to axial dynamic compression. A comparison of lumbar and thoracic discs. *Spine* 9: 725-733, 1984.

Koozekanani SH, Stockwell CW, McGhee RB, and Firoozmand F. On the role of dynamic models in quantitative posturography. *IEEE Trans Biomed Eng* 27: 605-609, 1980.

Kuo AD. An optimal control model for analyzing human postural balance. *IEEE Trans Biomed Eng* 42: 87-101, 1995.

Kung UM, Horlings CG, Honegger F, Kremer HP, Bloem BR, van De Warrenburg BP, and Allum JH. Postural instability in cerebellar ataxia: correlations of knee, arm and trunk movements to center of mass velocity. *Neuroscience* 159: 390-404, 2009.

Lackner JR and Levine MS. Changes in apparent body orientation and sensory localization induced by vibration of postural muscles: vibratory myesthetic illusions. *Aviat Space Environ Med* 50: 346-54. 1979.

Roll JP, Vedel JP, and Roll R. Eye, head and skeletal muscle spindle feedback in the elaboration of body references. *Prog Brain Res* 80: 113-23, 1989

Lee DN and Lishman JR. Visual proprioceptive control of stance. *J Hum Move Studies* 1: 87-95, 1975.

Loeb G and Ghez C. The Motor Unit and Muscle Action. In: Principles of Neuroscience (4th ed.), edited by Kandel E, Schwartz J and Jessel T. New York: McGraw-Hill, p.674-694, 2000.

Loram ID and Lakie M. Direct measurement of human ankle stiffness during quiet standing: the intrinsic mechanical stiffness is insufficient for stability. *J Physiol.* 545:1041-1053, 2002.

Maki BE and McIlroy WE. Cognitive demands and cortical control of human balance-recovery reactions. *J Neural Transm* 114: 1279-1296, 2007.

Maki BE, McIlroy WE, and Fernie GR. Change-in-support reactions for balance recovery. *IEEE Eng Med Biol Mag*. April/March, 20-26, 2003.

Maki BE, Holliday PJ, and Fernie GR. Aging and postural control. A comparison of spontaneous- and induced-sway balance tests. *J Am Geriatr Soc.*38:1-9, 1990.

Mahboobin A, Loughlin PJ, and Redfern MS. A model-based approach to attention and sensory integration in postural control of older adults. *Neurosci Lett* 429: 147-151, 2007.

Mahboobin A, Loughlin PJ, Redfern MS, Anderson SO, Atkeson CG, and Hodgins JK. Adaptation in Human Balance Control: Lessons for Biomimetic Robotic Bipeds. *Neural Netw* 21: 621–627, 2008.

Marsden CD, Merton PA, and Morton HB. Human postural responses. *Brain* 104: 513-534, 1981.

Maurer C, Mergner T, and Peterka RJ. Multisensory control of human upright stance. *Exp Brain Res* 171: 231-250, 2006.

Mergner, T. Huethe, F., Maurer, C., and Ament, C. Human equilibrium control principles implemented into a biped robot. In: Robot Design, Dynamics, and Control. *Proceedings of*

*the sixteenth CISM-IFToMM Symposium*. Editors Zielinska T and Zielinski C, 487: 271-279, 2006.

Mergner T, Huber W, and Becker W. Vestibular-neck interaction and transformation of sensory coordinates. *J Vestib Res* 7: 347-367, 1997.

Mergner T and Rosemeier. Interaction of vestibular, somatosensory and visual signals for postural control and motion perception under terrestrial and microgravity conditions- a conceptual model. *Brain Res Rev*. 28: 118-135, 1998.

McGill S, Seguin J, and Bennett G. Passive stiffness of the lumbar torso in flexion, extension, lateral bending, and axial rotation. Effect of belt wearing and breath holding. *Spine* 19: 696-704, 1994.

McIlroy WE and Maki BE. Preferred placement of the feet during quiet stance: Development of a standardized foot placement for balance testing. *Clin Biomech* 12: 66-70, 1997

Merfeld DM and Zupan LH. Neural processing of gravitoinertial cues in humans. III. Modeling tilt and translation responses. *J Neurophysiol* 87: 819-833, 2002.

Moorhouse KM and Granata KP. Role of reflex dynamics in spinal stability: intrinsic muscle stiffness alone is insufficient for stability. *J Biomech* 40: 1058-1065, 2007.

Nashner LM. Adapting reflexes controlling the human posture. *Exp Brain Res*. 26: 59-72, 1976.

Nashner LM. Fixed patterns of rapid postural responses among leg muscles during stance *Exp Brain Res*. 30: 13-24, 1977.

Nashner LM, Black FO, and Wall C. 3rd. Adaptation to altered support and visual conditions during stance: patients with vestibular deficits. *J Neurosci* 2: 536-544, 1982.

Nashner LM and Wolfson P. Influence of head position and proprioceptive cues on short latency postural reflexes evoked by galvanic stimulation of the human labyrinth. *Brain Res* 67:255-268, 1974.

Oie KS, Kiemel T, and Jeka JJ. Multisensory fusion: simultaneous re-weighting of vision and touch for the control of human posture. *Cognitive Brain Res* 14: 164-176, 2002.

Otnes RK and Enochson LD. *Digital Time Series Analysis*. New York,: Wiley, 1972.

Pai YC, Maki BE, Iqbal K, McIlroy WE, and Perry SD. Thresholds for step initiation induced by support-surface translation: a dynamic center-of-mass model provides much better prediction than a static model. *J Biomech* 33: 387-92. 2000.

Park S. *Human standing postural control adjusts to biomechanical constraints* (PhD thesis), University of Michigan, Ann Arbor, 2002.

Park S, Horak FB, and Kuo AD. Postural feedback responses scale with biomechanical constraints in human standing. *Exp Brain Res*. 154: 417-427, 2004.

Perreault EJ, Crago PE, and Kirsch RF. Estimation of intrinsic and reflex contributions to muscle dynamics: a modeling study. *Trans Biomed Eng* 47: 1413-1421, 2000.

Peterka RJ. Sensorimotor integration in human postural control. *J Neurophysiol* 88: 1097-1118, 2002.

Peterka RJ. Simplifying the complexities of maintaining balance. *IEEE Eng Med Biol Mag* 22: 63-68, 2003.

Peterka RJ, Black FO, and Schoenhoff MB. Age-related changes in human vestibulo-ocular reflexes: Sinusoidal rotation and caloric tests. *J Vestib Res* 1: 49-59, 1990.

Pierrot-Deseilligny E and Burke D. *The Circuitry of the Human Spinal Cord*. Cambridge: Cambridge University Press, 2005.

Piirtola M and Era P, Force platform measurements as predictors of falls among older people, *Gerontology* 2:1-16, 2006.

Pintelon R and Schoukens J. *System Identification: A Frequency Domain Approach*. Piscataway, NJ: IEEE Press, 2001.

Platt JR. Strong Inference: Certain systematic methods of scientific thinking may produce much more rapid progress than others. *Science* 146: 347-353. 1964

Preuss R and Fung J. Musculature and biomechanics of the trunk in the maintenance of upright posture. *J Electromyogr Kinesiol* 18: 815-828, 2008.

Preuss RA, Grenier SG, and McGill SM. Postural control of the lumbar spine in unstable sitting. *Arch Phys Med Rehabil* 86: 2309-2315, 2005.

Prochazka A. Sensorimotor gain control: a basic strategy of motor systems? *Prog Neurobiol* 33: 281-307, 1989.

Qu X, Nussbaum MA. Evaluation of the roles of passive and active control of balance using a balance control model. *J Biomech* 42: 1850-5. Jul 29, 2009.

Radebold A, Cholewicki J, Panjabi MM, and Patel TC. Muscle response pattern to sudden trunk loading in healthy individuals and in patients with chronic low back pain. *Spine* 25: 947-954, 2000.

Radebold A, Cholewicki J, Polzhofer GK, and Greene HS. Impaired postural control of the lumbar spine is associated with delayed muscle response times in patients with chronic idiopathic low back pain. *Spine* 26: 724-730, 2001.

Reeves NP, Everding VQ, Cholewicki J, and Morrisette DC. The effects of trunk stiffness on postural control during unstable seated balance. *Exp Brain Res* 174: 694-700, 2006.

Reeves NP, Narendra KS, and Cholewicki J. Spine stability: the six blind men and the elephant. *Clin Biomech* 22: 266–274, 2007.

Reynolds RF and Day BL. Rapid visuo-motor processes drive the leg regardless of balance constraints. *Curr Biol* 15: R48-49, 2005.

Scrivens JE, Deweerth SP, and Ting LH. A robotic device for understanding neuromechanical interactions during standing balance control [Online]. *Bioinsp Biomim* 3: http://www.iop.org/EJ/journal/1748-3190, 2008.

Seidel GK, Marchinda DM, Dijkers M, and Soutas-Little RW. Hip joint center location from palpable bony landmarks--a cadaver study. *J Biomech* 28: 995-998, 1995.

Skotte J, Hjortskov N, Essendrop M, Schibye B, and Fallentin N. Short latency stretch reflex in human lumbar paraspinal muscles. *J Neurosci Methods* 145: 145-150, 2005.

Skotte JH. Estimation of low back loading on nurses during patient handling tasks: the importance of bedside reaction force measurement. *J Biomech* 34: 273-276, 2001.

Soechting JF and Lacquaniti F. Modification of trajectory of a pointing movement in response to a change in target location. *J Neurophysiol* 49: 548-564, 1983.

Solomonow M, Zhou BH, Harris M, Lu Y, and Baratta RV. The ligamento-muscular stabilizing system of the spine. *Spine* 23: 2552-2562, 1998.

Todorov E. Optimality principles in sensorimotor control. *Nat Neurosci* 7: 907-915, 2004

van Beers RJ, Sittig AC, and van der Gon JJD. Integration of proprioceptive and visual position-information: An experimentally supported model. *J Neurophysiol* 81: 1355-1364, 1999.

van der Kooij H, Jacobs R, Koopman B, and van der Helm F. An adaptive model of sensory integration in a dynamic environment applied to human stance control. *Biol Cybern* 84: 103-115, 2001.

van der Kooij H, Jacobs R, Koopman B, and Grootenboer H. A multisensory integration model of human stance control. *Biol Cybern* 80: 299-308, 1999.

Warren WH, Kay BA, and Yilmaz EM. Visual control of posture during walking: functional specificity. *J Exp Psychol: Human Percep Perfor* 22:818-838, 1996.

Welch TD and Ting LH. A feedback model reproduces muscle activity during human postural responses to support-surface translations. *J Neurophysiol* 99: 1032-1038, 2008.

Welgampola MS and Colebatch JG. Vestibulospinal reflexes: quantitative effects of sensory feedback and postural task. *Exp Brain Res* 139: 345-345, 2001.

Westwick DT and Kearney RE. *Identification of Nonlinear Physiological Systems*. Piscataway, N.J.: IEEE Press; Wiley-Interscience, 2003.

Winter DA. *Biomechanics and Motor Control of Human Movement*. Hoboken, N.J.: John Wiley & Sons, 2005.

Zajac FE and Gordon ME. Determining muscle's force and action in multi-articular movement. *Exerc Sport Sci Rev* 17: 187-230, 1989.

Zhao G, Ren L, Ren, L, Hutchinson J, Tian L, and Dai J. Segmental kinematic coupling of the human spinal column during locomotion. *J Bionic Eng* 5: 328-334, 2008.

Zhang Y, Kiemel T, and Jeka J. The influence of sensory information on two-component coordination during quiet stance. *Gait Posture* 26: 263-271, 2007.

Zoubir AM and Boashash B. The Bootstrap and its Application in Signal Processing. *IEEE Signal Processing Magazine* 15: 56-76, 1998.